Spring 2004

# Fatigue of drill pipes used in horizontal directional drilling

Feibai Ma
*Louisiana Tech University*

# FATIGUE OF DRILL PIPES USED IN HORIZONTAL DIRECTIONAL DRILLING

by

Feibai Ma, B.S.

A Dissertation Presented in Partial Fulfillment
Of the Requirement for the Degree
Doctor of Philosophy

COLLEGE OF ENGINEERING AND SCIENCE
LOUISIANA TECH UNIVERSITY

MAY 2004

LOUISIANA TECH UNIVERSITY

**THE GRADUATE SCHOOL**

May, 1, 2004
Date

We hereby recommend that the dissertation prepared under our supervision by Feibai Ma entitled Fatigue of Drill Pipe Used in Horizontal Directional Drilling be accepted in partial fulfillment of the requirements for the Degree of Doctor of Philosophy in Engineering

Ray F Sterling
Supervisor of Dissertation Research

Ray F Sterling
Head of Department

Ph.D. in Engineering
Department

Recommendation concurred in:

Advisory Committee

**Approved:**
Director of Graduate Studies

Dean of the College

**Approved:**
Dean of the Graduate School

GS Form 13
(5/03)

# ABSTRACT

Fatigue is the most common cause of mini-HDD drill rod failure. It can occur at stress levels far below the normal operating stress in most drill stem components. Fatigue failures occur because the drill rod, after it has been forced into a curved path, undergoes a cyclic bending stress oscillating from tension to compression in concert with the other stress components caused by torque, thrust, or pullback.

When a rod breaks underground, there is considerable extra cost caused by the delay in "fishing" out the broken rod as well as the cost of replacing the rod. On the other hand, it is expensive to replace drill strings before the end of their useful life as the drill rod is often the most expensive consumable used in the mini-HDD process.

In order to analyze the fatigue life of mini-HDD rod, a fatigue test machine was built in the laboratory of the Trenchless Technology Center. Twelve fatigue tests were conducted in this laboratory on the drill pipes donated by Drilltube, Inc. and Texas Pup, Inc. The pipes donated by Texas Pup were used as the preliminary tests to gain experience in the testing methodology. The pipes donated by Drilltube, Inc. were used to construct an S-N curve for this type of drill pipe. Those two kinds of pipes did show a difference in fatigue life behavior.

During the five preliminary tests, the strong effect of make up torque and joint lubrication was observed. In the later seven tests, six failures occurred. Five of these failures occurred at the joint area, and one failure occurred in the body area. This is

consistent with the reports of field failure: the joint area is the weakest area in the whole pipe. From the test results of the second series of seven tests, an S-N curve for that type of pipe was made. The fatigue limit for this pipe (based on a simple bending stress approximation) is less than 22 ksi. Since the "Atlas of Fatigue Curves" indicates a value in the range of 55 ksi to 65 ksi for similar steels, mini-HDD drill rod fails at considerably less than the normally accepted values. The reason for this was assumed to be due to stress concentration in the joint area.

Since the stress in the joint area is very complex, numerical analysis was used to simulate the stress concentration. An ANSYS model was constructed and run for bending, tension, and thrust conditions.

After applying the stress concentration factor observed within the joint area (approximately 3.0), the fatigue limit did fall within the expected range.

In addition to the experimental and simulation results, the research investigated the theoretical stress condition in different phases of the drilling process compared to the normal stress assumptions used in practice. The S-N curve results were also used to provide an indication of the cost of drill rod fatigue using some illustrative assumptions about curved drilling and drill rod usage.

## APPROVAL FOR SCHOLARLY DISSEMINATION

The author grants to the Prescott Memorial Library of Louisiana Tech University the right to reproduce, by appropriate methods, upon request, any or all portions of this Dissertation. It is understood that "proper request" consists of the agreement, on the part of the requesting party, that said reproduction is for his personal use and that subsequent reproduction will not occur without written approval of the author of this Dissertation. Further, any portions of the Dissertation used in books, papers, and other works must be appropriately referenced to this Dissertation.

Finally, the author of this Dissertation reserves the right to publish freely, in the literature, at any time, any or all portions of this Dissertation.

Author _____

Date 5/12/04

GS Form 14
(5/03)

## TABLE OF CONTENTS

**LIST OF TABLES** ..... xi

**LIST OF FIGURES** ..... xiii

**ACKNOWLEDGMENTS** ..... xvi

**CHAPTER 1 INTRODUCTION** ..... 1

1.1 General Description of Mini-Horizontal Directional Drilling ..... 1
1.1.1 Pilot Hole Boring ..... 3
1.1.2 Reaming Operation ..... 5

1.2 Background and Research Need ..... 8

1.3 Objective and Scope ..... 8

**CHAPTER 2 LITERATURE REVIEW** ..... 10

2.1 Fatigue ..... 10
2.1.1 Cyclic Stresses in Mini-HDD Practice ..... 12
2.1.2 Repeated Stress Cycles ..... 13
2.1.3 Random Stress Cycle ..... 13
2.1.4 Parameters Used to Characterize a Given Cyclic Loading History ..... 14
2.1.4.1 Key Parameters ..... 14
2.1.4.2 Other Parameters ..... 14
2.1.5 The S-N Curve ..... 15
2.1.6 Crack Initiation and Propagation ..... 17
2.1.7 Types of Fatigue ..... 18
2.1.8 Benchmark and Striations ..... 19
2.1.9 Propagation Rate ..... 20

2.2 Factors That Affect Fatigue Life and Behavior Predictions ..... 21
2.2.1 Fatigue Life in Relation to Mean Stress and Stress Amplitude ..... 21
2.2.2 Effect of Surface Treatment ..... 22
2.2.3 Chemical Attack ..... 23
2.2.4 Miner's Rule ..... 23

2.3 Fatigue Research Method ..... 24
2.3.1 Fatigue Failure Models ..... 24

2.3.2 Fatigue Regimes ..... 24
2.3.3 The Stress-Life Approach ..... 25
2.3.4 The Strain-Life Approach ..... 25
2.3.5 The LEFM Approach ..... 25

2.4 Fatigue Research in the Oil Industry ..... 26
2.4.1 Fatigue Study of Drill Pipe in the Oil Industry for a Non Corrosive Environment ..... 27
2.4.2 Research and Guidelines for Operation in a Corrosive Environment.. 31
2.4.3 The Analysis of the Internal Upset Geometry of Drill Pipe for Longer Fatigue Life in the Oil Industry: Finite Element Analysis Approach. 32
2.4.4 Joint Failure Research in the Oil Industry and API Regulations ..... 33
2.4.4.1 API Regulation and Gregory Fehr's research ..... 33
2.4.4.2 I.P. Gnyp's Approach ..... .36
2.4.4.3 The Finite Element Analysis Approach ..... .....36

2.5 Mini-HDD Drilling Pipes ..... 37
2.5.1 Two Basic Types of Drill Pipe are in Use Today ..... 37
2.5.2 The Three Most Common Methods for Manufacturing HDD Pipe ..... 37

**CHAPTER 3 STRESS ANALYSIS OF MINI-HDD DRILL PIPE** ..... 40

3.1 Forces on the HDD Drill String in Operation ..... 40

3.2 Types of Mini-HDD Drill Pipe Investigated in this Research ..... 41

3.3 Stresses Caused by Bending ..... 41
3.3.1 Standard Bending Theory ..... 42
3.3.2 Curvature Due to an Applied Bending Moment ..... 42
3.3.3 Curvature Caused by an Applied Force at the End of the Drill Rod ... 43
3.3.4 Curvature Caused by Uniformly Distributed Load ..... 45
3.3.5 Curvature Caused by a Triangularly Varying Load ..... 46

3.4 Determining the Most Appropriate Model ..... 47
3.4.1 Comparison of the Four Conditions ..... 47
3.4.2 Comparison with HDD Practice ..... 47

3.5 Stresses Caused by Axial Forces ..... 52
3.5.1 Tensile Axial Loading ..... 52
3.5.2 Compressive Axial Loading ..... 52
3.5.3 Stress Computation ..... 52

3.6 Shear Stresses Caused by Torque ..... 54

**CHAPTER 4 FACTORS THAT DOMINATE FATIGUE FAILURE** ..... 55

4.1 Data from Controlled Field Tests ..... 55

4.2 Stress Comparison ..... 56
4.2.1 Thrust/Pull Force ..... 56
4.2.2 Torsion ..... 57
4.2.3 Bending ..... 60
4.2.4 Comparison of the Fatigue Effects from the Various Stress Cycles ..... 60

**CHAPTER 5 FATIGUE TEST EXPERIMENT SETUP** ..... 64

5.1 Setup of Fatigue Test Apparatus ..... 64
5.1.1 Motor Selection ..... 67
5.1.2 Gear Speed Reducer ..... 67
5.1.3 Support System ..... 68
5.1.4 Deformed Shape Control ..... 70
5.1.5 Control System ..... 74

5.2 The Fatigue Test Process ..... 75
5.2.1 Make Up Torque ..... 75
5.2.2 Lubrication ..... 76
5.2.3 Operation and Maintenance ..... 77
5.2.3.1 The Bending of Pipes ..... 77
5.2.3.2 Adjust Reflection Mirror ..... 78
5.2.3.3 Sound Sensor ..... 79
5.2.3.4 Daily Maintenance ..... 80
5.2.3.5 Oil Brake ..... 80

**CHAPTER 6 FATIGUE TEST RESULTS FOR MINI-HDD DRILL RODS** ..... 82

6.1 Fatigue Test Results ..... 83
6.1.1 Pipe Donated by Texas Pup ..... 83
6.1.2 Pipe Donated by Drilltube ..... 83

6.2 Analysis of Results ..... 84
6.2.1 Preliminary Tests ..... 84
6.2.2 S-N Curve Development Tests ..... 86
6.2.3 Comparison of the Test Result with the Fatigue Formula Used in the Oil Industry ..... 87
6.2.4 Comparison of the Regression for the Current Tests with Grondin's Result ..... 89
6.2.5 Radius of Curvature versus Fatigue Life of Drill Rod ..... 93
6.2.6 Relationship of Curvature and Fatigue Life Including Field Conditions ..... 94

6.2.7 Illustrative Estimate of Drill Pipe Cost per Foot Advance under Different Curvature ..... 95
6.2.8 Other Issues Affecting Fatigue Life ..... 97

**CHAPTER 7 SIZE EFFECT AND COMPARISON OF THE FATIGUE LIFE OF DIFFERENT PIPES ..... 99**

7.1 The Fatigue Formula Provided by Grondin ..... 99

7.2 Consideration of Size Effect ..... 100

7.2.1 Geometrical Size Effect ..... 100
7.2.2 Statistical Size Effect ..... 101
7.2.3 Technological Size Effect ..... 103

7.3 Consideration of Steel Grade ..... 104

7.4 Consideration of the Drill Rod Manufacturing Method ..... 106

**CHAPTER 8 PIPE JOINTS AND NUMERICAL ANALYSIS ..... 108**

8.1 The Failure of Pipe Joints ..... 108

8.2 ANSYS Software and Contact Mechanics Analysis ..... 109

8.2.1 Basic Contact Analysis Approach ..... 109
8.2.2 Contact Algorithm ..... 110

8.3 Stress Concentration Factor for Push and Pull Conditions ..... 111
8.3.1 Computation Model for Push and Pull Conditions ..... 111
8.3.2 Elements Used for Mesh of 2-D Model ..... 112
8.3.3 Analysis Result for 2-D Model ..... 114

8.4 Stress Concentration Factor for Bending Conditions ..... 117
8.4.1 Computational Model for Bending ..... 117
8.4.2 Elements Used for Mesh of 3-D Model ..... 119
8.4.3. Analysis Result for 3-D Model ..... 121

8.5 Comparison of Simulation Results with Test Results ..... 123

8.6 Comparison of Test Results with Guidance Provided in the Atlas of Fatigue Curves ..... 124

**CHAPTER 9 SUMMARY AND CONCLUSIONS** ..... 125

9.1 Summary ..... 125

9.2 Conclusions ..... 126

9.3 Recommendations ..... 127

**APPENDIX SAS PROGRAM** ..... 129

**REFERENCES AND BIBLIOGRAPHY** ..... 131

# LIST OF TABLES

Table 1.1 Commonly Used HDD Machines..... 7

Table 2.1 Suggested Ratios for Different Connections.....35

Table 3.1 Comparison of Stress Condition under Two Models.....51

Table 4.1 Peak Count of Thrust Variance .....57

Table 4.2 Peak Count of Torque Variance.....59

Table 4.3 Comparison of the Influence of Stresses Caused by Thrust,Torque, and Bending.....61

Table 4.4 The Dimensions and Force Capabilities of HDD Drill Pipe from Drilltube, Inc.....62

Table 5.1 Gauge Placement.....71

Table 5.2 Strain Gauge Readouts.....73

Table 5.3 Nominal Radius at Each Gauge Point.....73

Table 6.1 Test Result for Texas Pup Drill Pipe.....83

Table 6.2 Test Results for Drilltube Drill Pipes.....84

Table 6.3 Comparison of Test Data and Predicted Results by Grondin.....89

Table 6.4 Relationship between Radius of Curvature and Fatigue Life.....93

Table 6.5 Relationship between Radius of Curvature and Fatigue Life under the Worst Stress Assumptions.....95

Table 6.6 Cost Drill Pipe Cost per Foot Advance under Different Curvature.....96

Table 7.1 Hardness and Other Mechanical Properties for Different Types of Steel.....105

Table 7.2 Mechanical Properties of ANSI Grade 4130 Steel with Varying Tempering Temperature.....106

Table 7.3 Mechanical Properties of ANSI Grade 4130 Steel with Varying Heat Treatment.....106

Table 8.1 ANSYS Contact Capabilities (Point to Surface and Surface to Surface).....110

Table 8.2 Simulation Result for Stress Concentration.....123

# LIST OF FIGURES

Figure 1.1 Process of Mini-Horizontal Directional Drilling....2

Figure 1.2 Steering Face/Drill Bit for Mini-HDD....4

Figure 1.3 Tracking Instrumentation House....5

Figure 1.4 Reamer....6

Figure 1.5 Swivel....6

Figure 2.1 Loading Conditions Causing Axial, Torsion, and Flexural Stresses....12

Figure 2.2 Key Parameters in a Cyclic Loading History....14

Figure 2.3 A Typical S-N Curve....16

Figure 2.4 Surface of a Fatigue Fracture of Mini-HDD Drill String....19

Figure 2.5 An Example of Beach Marks....20

Figure 2.6 The Goodman, Soderberg and Gerber Lines to Account for the Effect of Mean Stress on Fatigue Strength....22

Figure 2.7 Stress Reversals which Can Use Miner's Rule....23

Figure 2.8 Collar Joint Modeling....36

Figure 3.1 External Flush Joint Mini-HDD Drill Pipe Used in this Research....41

Figure 3.2 Simplified Model of Mini-HDD Drill Pipe....41

Figure 3.3 Curvature Caused by an Applied Bending Moment....42

Figure 3.4 Curvature Caused by an Applied Force at the End of the Drill Rod....44

Figure 3.5 Curvature Caused by Uniformly Distributed Load....45

Figure 3.6 Curvature Caused by a Triangularly Varying Load....46

Figure 3.7 Best Fit Situation....48

Figure 3.8 Pipe Placement Change....49

Figure 3.9 Distribution of Earth Force after Pipe Placement Change....49

Figure 3.10 Pipe Load at the Situation of Pipe Displacement Change....50

Figure 3.11 Model 2 Used in FEA....51

Figure 4.1 Thrust Variation in Silty Sand Soil for DitchWitch 4/40 A JT & Bor-Mor 750....56

Figure 4.2 Drilling Torque Variation in Silty Sand for Ditch Witch 4/40 A JT & Bor-Mor 750....58

Figure 5.1 Fatigue Test Machine Design Concept....66

Figure 5.2 Induction Motor to Provide Torque and Rotation....67

Figure 5.3: Gear Speed Reducer....68

Figure 5.4: A Steel Support Table, Pillow Block and Drill Rod....69

Figure 5.5 Pillow Block....70

Figure 5.6 Strain Gauge Readout Configuration....72

Figure 5.7 Attachment of the Gauge....72

Figure 5.8 Control Computer....74

Figure 5.9 PLC Control System....75

Figure 5.10 Extended Pipe Wrench....76

Figure 5.11 Drill Rod Held in a Curved Profile....77

Figure 5.12 Laser Beam Generator and Reflection Mirror....78

Figure 5.13: Reflection Mirror Installed in the Speed Reducer....79

Figure 5.14 Oil Brake....81

Figure 6.1 S-N Curve Regression for the Drilltube Drill Pipes Using SAS.....87

Figure 6.2 Comparison of Grondin's Oil Industry Regression Equation and the Mini-HDD Regression Equation from the Current Research.....90

Figure 6.3 Fatigue Life of Steel 4135 and 4140 from the Fatigue Atlas.....92

Figure 7.1 Stress Gradients versus Diameter for Bending.....101

Figure 7.2 Cross-section of Drill Pipe.....102

Figure 8.1 Broken Joint Caused by Fatigue Failure Tested in the TTC Lab.....108

Figure 8.2 Drill Pipe.....111

Figure 8.3 Computation Model of the Pipe Joint.....111

Figure 8.4 Computational Model of the Drill Pipe Joint for Pull and Push Condition....111

Figure 8.5 Computational Model for Thrust under a Pressure of 100lb/in.....112

Figure 8.6 Computational Model for Pull under a Pressure of 100lb/in.....112

Figure 8.7 ANSYS Analysis Result of Push under Stress of 100 lb/in.....115

Figure 8.8 ANSYS Analysis Result of Pull under Stress of 100 lb/in.....116

Figure 8.9 Three-Dimensional Model for Drill Pipe Joint.....117

Figure 8.10 Simplified Computational Model for Drill Pipe Joint.....118

Figure 8.11 Boundary Condition of the Simplified Model.....119

Figure 8.12 ANSYS Analysis Result of Bending Stress Simulation.....122

# ACKNOWLEDGMENTS

I would like to express my sincere gratitude and appreciation to those who provided me guidance and assistance in the preparation of this dissertation. My heartfelt thanks go to Dr. Raymond Sterling for his guidance in every step in this research, for his encouragement every time I was facing difficulties, and for his kindness to be a good friend.

I wish to express my gratitude especially to Max Tejeda,Tejas Tubular Products, Inc.; without his funding support, this research work would also not have been finished.

I would like to thank to Dr. Raja Nassar for his help. Also, I would like to show my appreciation to Dr. William Jordan, Dr. Jay Wang, and Dr. Jerold Stegeman for their support, encouragement, and service on my advisory committee. Sincere acknowledgement is also extended to Dr. David Hall and Dr. Abdelkader Tayebi for their kindness in helping me in this research.

I wish to express my gratitude to Texas Pup, Inc. and Drilltube, Inc. Their donated drill tube made this research work possible.

I wish to express my gratitude to Dr. Paul Hadala, Dr. Robert McKim, and Dr. Aziz Saber. Their hard work in the development of the fatigue testing machine helped this research very much. Dr. James Eads helped rebuild the control software for the fatigue machine. I also want to say thanks to him sincerely.

I also wish to express my gratitude to the professors and staff at the Trenchless Technology Center and the College of Engineering and Science. Their teaching, support, and encouragement were very important in my graduate studies.

I also want to say thank you to all my friends and fellow students. Your help made this work easier and more enjoyable. Finally, I would like to thank my parents and brothers in China; your love is with me everyday.

# CHAPTER 1

# INTRODUCTION

## 1.1 General Description of Mini-Horizontal Directional Drilling

When constructing underground utilities such as fiber optic cables, telephone lines, electric lines, and gas lines, the conventional open-cut installation method normally causes great surface disruption because of the need for trenches in which to bury the lines. Where these lines run under a public way such as a street or highway, these open trenches delay traffic and cause serious public inconvenience. Fortunately, for those utilities that do not require precise control of alignment or elevation, horizontal directional drilling (HDD) has been developed to install such utilities without serious surface disruption. According to the power of the machine used and the size and length of the utility to be installed, horizontal directional drilling machines are typically divided into three main sizes: mini, midi, and maxi. Mini-HDD refers to a system used to install small diameter pipelines and cables typically less than 10 inches in diameter and up to 600 feet in length. The characteristics of other size ranges of HDD equipment can be found in Table 1.1.

Figure 1.1 shows a schematic drawing of a mini-horizontal directional drilling (mini-HDD) operation. The process is described by Khan et al. 1994. The drill is setup to permit the drilling head and following alloy steel drill rod to enter the ground at an angle

which may range from 5 to 30 degrees above the horizontal. The drill bit is rotated as the rod is advanced by a hydraulic jack which applies thrust to the drill rod.

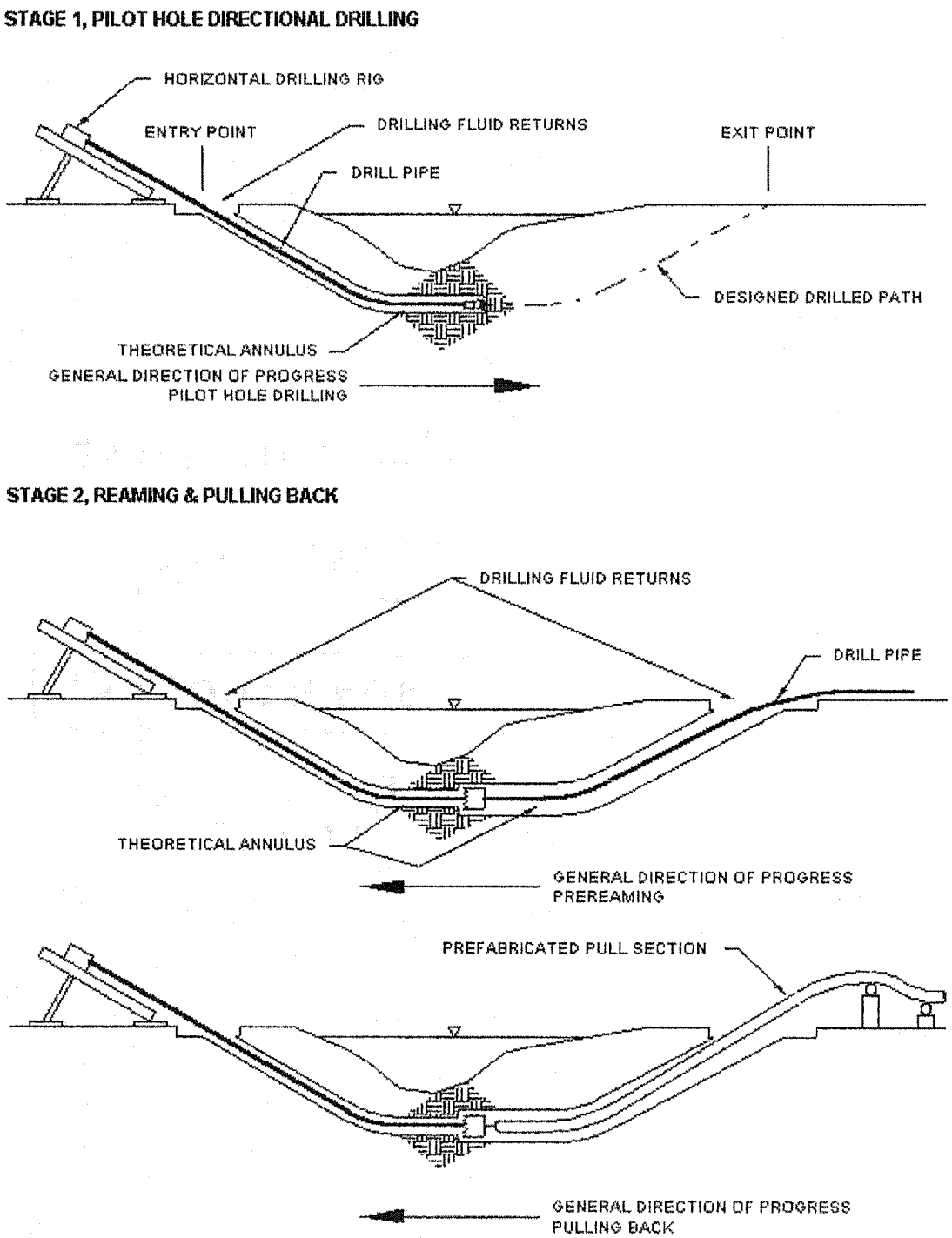


**Figure 1.1: Process of Mini-Horizontal Directional Drilling (after J.D.Hair & Associates, Inc)**

Mini-HDD is normally a two-stage process:

a. Pilot hole boring

b. Product pipe pullback

The two stages are described below.

### 1.1.1 Pilot Hole Boring

The pilot hole (typically from 2 to 4 inches in diameter) is drilled from the starting point to the ending point along the proposed design route.

After the drill is setup to allow the angled entry of the drill bit into the soil, the drill bit is rotated at the same time as the rod is advanced by a hydraulic system that applies thrust to the drill rod. When it is desired to advance along a curved path (either a horizontal or vertical curve), rotation of the bit is stopped, and thrust alone is used to advance the bit. Because of the wedge shape of the bit, the bit is deviated from a straight path, and hence the borehole can be curved in the desired direction.

With a "wet" mini-HDD system (known as fluid-assisted mechanical cutting), drilling fluid is pumped through the drill string when the pilot hole is being drilled. The drilling process is assisted by the use of this drilling fluid (water or drilling mud) that serves to remove cuttings, stabilize the borehole, reduce friction, clean the cutting bits, and cool the downhole electronics used to guide the drilling process. The fluid is pumped to the bit through the drill rod string.

In "dry" mini-HDD, the pilot hole is drilled by rotation and applying thrust to the drill string without using any drill fluid or using air.

In either case, the process is monitored by a walkover locator system which has two parts: a downhole beaconing or transmitting device which is in the tracking

instrumentation housing in the head of the drill string, and a surface receiver unit which is operated by a person who monitors the process.

By alternately advancing the bit by rotating and pushing, a complex underground path composed of a mixture of straight and curved segments can be obtained, and one can steer a path under a highway or a stream or make a 90-degree turn so that the path goes underneath a series of intersecting city streets. Steering is controlled by adjusting the position of the wedge shaped bit.

The drill bit typically consists of a wedge-shaped slanted face with a jet opening with a tracking instrumentation housing located behind the drill bit and connected to the leading end of the drill string. One type of steering face is shown in the Fig.1.2.

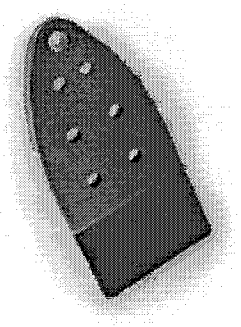

**Figure 1.2 Steering Face/Drill Bit for Mini-HDD**
**(Picture courtesy of Drill's Supply, Inc.)**

Behind the bit is a small radio transmitter or sonde that continuously emits a signal. A receiver can be moved about on the ground surface to locate the horizontal coordinates of drilling head and its depth below ground. Runs up to 600 ft are common, and at the end of a run, the drill bit is either steered to the ground surface or a receiving pit.

Fig.1.3 shows a tracking instrumentation housing together with the attachment point for the steering face/drill bit.

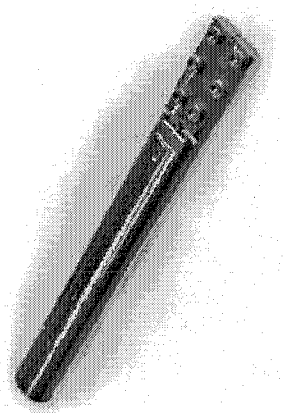

**Figure 1.3 Tracking Instrumentation House**
**(Picture courtesy of Drill's Supply, Inc.)**

In this drilling process, by nature of the curved drill path followed and forces required to advance the drill rod, the drill rod has been subjected to cyclic bending and periods of continuous compression and continuous torsion, sometimes individually but often in combination. The continual subjection of the drill rod to these cyclical forces leads to fatigue type failure in the drill rod and, hence, to the topic of this dissertation.

### 1.1.2 Reaming Operation

When the pilot hole is completed, the second stage of widening the hole and/or installing the pipe or cable is begun. Under normal circumstances, only pipe or cable that can withstand tension and that is flexible enough to follow the curved underground path of the hole can be used. For pipe installation using mini-HDD equipment, this usually means the use of fused or coiled lengths of High Density Polyethylene (HDPE) Pipe.

To begin the second stage process, a reamer and the product pipe are attached to the far end of the drill rod and are pulled back toward the drilling unit using the hydraulic

cylinders on the drill. The reamer is rotated and enlarges and/or cleans the hole for the installation of the product pipe or cable(s).

Figure 1.4 shows one type of reamer.

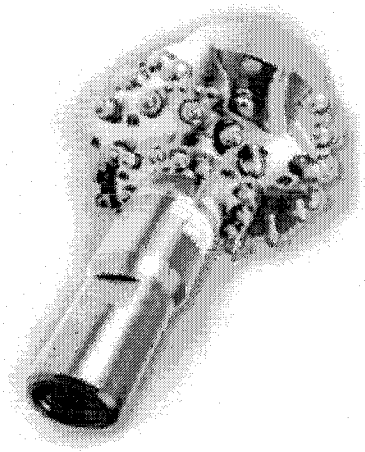

**Figure 1.4 Reamer (Picture courtesy of Drill's Supply, Inc.)**

The product pipe (or cable(s)) is attached to the rod behind the reamer by a swivel (see Fig.1.5) so that it is not subject to undue twisting as it is installed. Product pipes up to 10 inches in diameter can be installed by the mini-HDD process.

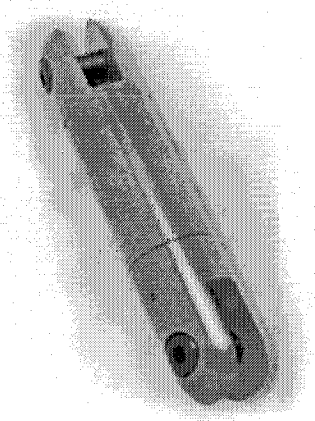

**Figure 1.5 Swivel (Picture courtesy of Drill's Supply, Inc.)**

During the pullback process, the drill rod is again subject to cyclic bending and periods of continuous torsion and continuous tension, sometimes individually but often all at once. Since both the tensile (axial) forces and the torque applied during pullback are typically greater than the thrust forces and torque applied during pilot hole drilling, this phase of the HDD process usually provides the greatest combined stress condition for the HDD drill rod.

Table 1.1 shows a commonly used classification system describing the differences between mini-HDD systems and larger directional drilling machines. Several manufacturers make the drilling machines and/or drilling rods used in the mini-HDD process. Most mini-HDD machines can exert more force on pullback than on thrust, and a typical machine might be considered to be one capable of 1,000 lb thrust, 10,000 lb pullback, and 750 ft-lb of torque.

**Table 1.1 Commonly Used HDD Machines**

| Description | Product Pipe Diameter (in) | Depth Range (ft) | Bore Length (ft) | Torque (ft-lb) | Thrust /Pull back (lb) | Machine Weight Including Truck (ton) | Applications |
|---|---|---|---|---|---|---|---|
| Mini | 2-10 | Up to 15 | Up to 600 | Up to 950 | Up to 20,000 | Up to 9 | Telecommunications and power cables; polyethylene gas lines |
| Midi | 10-24 | Up to 75 | Up to 900 | 900-7000 | 20,000-100,000 | Up to 18 | Under rivers, environmentally sensitive areas, and roadways |
| Maxi | 24-48 | Up to 200 | Up to 5,000 | Up to 80,000 | Exceeds 1,000,000 | Up to 30 | Pipeline crossings under rivers, highways and runways |

## 1.2 Background and Research Need

Fatigue is the most common cause of mini-HDD drill rod failure. It can occur at stress levels far below the normal operating stress in most drill stem components. Fatigue failures occur because the drill rod, after it has been forced into a curved path, undergoes a cyclic bending stress oscillating from tension to compression in concert with the other stress components caused by torque, thrust, or pullback.

When a rod breaks underground, there is considerable extra cost caused by the delay in "fishing" out the broken rod as well as the cost of replacing the rod. On the other hand, it is expensive to replace drill strings before the end of their useful life as the drill rod is often the most expensive consumable used in the mini-HDD process.

Contractors should replace their drill rods with new rods periodically to minimize the likelihood of this type of accident, and they can use inspection of the used rod to check for early warning signs of fatigue damage or for other defects that may hasten fatigue failure. This process may include a visual inspection for surface defects or an expensive set of magnetic particle, ultrasonic or electromagnetic inspection tests. However, none of these approaches is foolproof, and contractors have little guidance on the expected fatigue life of the drill string when drilling under different conditions of hole curvature, thrust, torque, pullback, etc.

## 1.3 Objective and Scope

The objective of this research is to better understand the fatigue behavior of drill rods used in mini-HDD practice and to provide improved guidelines for the use of such drill rods in HDD projects.

For this research, a fatigue test machine was constructed to study the effects of fatigue under different stress conditions. The experimental work was coupled with theoretical analysis and finite element modeling of the stress conditions in the drill rod under different drilling conditions, and the experimental data was compared with fatigue models for drill rod types used in the oil drilling industry.

The research program specifically consists of the following activities:

- A literature review of the drill string fatigue problem in the oil industry and the application of mini-HDD to utility installations.
- The design, specification, purchase, and commissioning of the equipment and instrumentation necessary for the experimental drill string test facility.
- Investigation of the stress conditions in the drill rod in a curved hole under simplified configurations.
- Testing of drill rod fatigue failure under varying conditions of curvature sufficient to construct an S-N curve (stress level versus number of cycles to failure) for one type of HDD drill rod.
- Finite element analysis of the stress conditions in the HDD drill rod joint under simplified loading conditions and comparison with the failure locations observed in the experimental tests.

Use of the S-N curve derived to provide guidance about fatigue failure in mini-HDD drill rods and to examine the potential cost of drill rod usage in holes of different curvature and with simplified assumptions about drill rod usage.

# CHAPTER 2

# LITERATURE REVIEW

## 2.1 Fatigue

Fatigue is defined by Boresi et al. (1993) as "the progressive localized structural changes that occur in a material subjected to repeated or fluctuating strains at stresses having a maximum value less than the tensile strength of the material."

The fatigue life of a structure is defined as the number of cycles of load (N) which is required to cause failure by fracture at a given cyclic stress or a cyclic load level.

The research of fatigue has a long history. The first major fatigue failure occurred in the railway industry in the 1840s. It was recognized that railroad axles failed regularly at shoulders (Peterson, 1950). The word "fatigue" was introduced in the 1840s to 1850s to describe failures occurring from repeated stresses.

During the 1850s, August Wohler performed many laboratory fatigue tests under repeated stresses and first portrayed fatigue in terms of an S-N curve. (*Engineering*, 1967). These experiments were concerned with railway axle failures and are considered to be the first systematic investigation of fatigue. He also introduced the concept of fatigue limit.

During the 1870s and 1890s, Gerber investigated the influence of mean stresses. Goodman proposed a simplified method concerning mean stresses. Their method is still used today.

In the 1900s, the optical microscope provided the method to study fatigue mechanics. Localized slip lines and slip bands leading to the formation of micro cracks were observed. In the 1920s, Gough made great improvement in the understanding of fatigue mechanisms. He also studied the combined effects of bending and torsion.

Since 1927 when Moore and Kommers published the first a book on fatigue of metal in America, there has been a great improvement in understanding fatigue. (Moore, 1927). From 1929 to 1937, efforts were made to explain in the difference in the response of metal when notches are present (Neuber, 1946). Notches under different conditions, such as high tensile strength steel and mild steel, were studied. Neuber introduced the idea of stress gradient effect at notches and pointed out that the average stress over a small volume at the root of the notch is more important than the peak stress at the notch.

In 1945, Miner formulated a linear cumulative damage criterion (Miner 1945), which is still an important tool in fatigue life prediction. In the 1950s, the introduction of electron microscopy opened a new area for understanding fatigue. Irwin introduced the stress intensity factor which has been accepted as the basis of linear elastic fracture mechanics and of fatigue crack growth life predictions (Irwin, 1957).

In the 1960s, Manson and Coffin introduced the well known Mason-Coffin relationship between plastic strain amplitude and fatigue life. It deals with low-cycle strain controlled fatigue behavior (Mason, 1962). In 1963, Paris provided the Paris

formula to show how crack growth rate could be described using the stress intensity factor range (Paris, 1963).

In 1968, the Society of Automotive Engineers published the Fatigue Design Handbook: A Guide for Product Design and Development Engineers. In 1974, the US Air Force issued Mil A-83444 which defines damage tolerance requirements for the design of new military aircraft. The standards of fatigue design were then well established.

The standards for fatigue tests now are available in ASTM. In order to save expenses on fatigue tests using the ASTM standard, the Atlas of Fatigue Curve was published in 1986. It collected many of the important and frequently referenced S-N curves but it is still not complete.

### 2.1.1 Cyclic Stresses in Mini-HDD Practice

There are three common ways in which stresses are applied to drill rods in HDD practice: axial loads, torsion loads, and flexural loads. Examples of these are seen in Fig. 2.1.

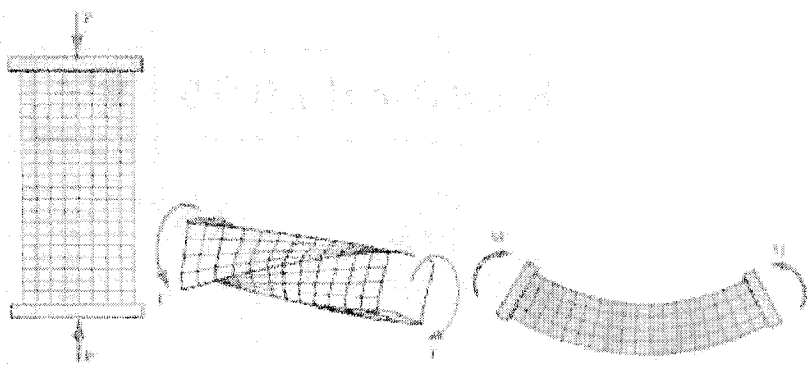

**Figure 2.1 Loading Conditions Causing Axial, Torsion and Flexural Stresses (Beer 1992)**

All three kinds of loads when applied in a cyclical fashion can cause fatigue failure, and the presence of one or both of the other stress conditions can exacerbate

fatigue failure in the primary stress condition. For HDD conditions, the drill pipe experiences axial forces from the compressive thrust during drilling and the tensile load during pullback. It undergoes flexural stress when it is forced into a curved path below ground and a torsion stress is present caused by the torque necessary to rotate the drill bit during pilot hole drilling or the reamer during pullback.

### 2.1.2 Repeated Stress Cycles

The most common type of cycle found in engineering applications is where the stress variation follows a sine wave but the maximum stress ($s_{max}$) and the minimum stress ($s_{min}$) are asymmetric rather than equal and opposite (see Fig. 2.2). This type of stress cycle is called a repeated stress cycle. The standard test reference for this practice is in ASTM E466-96(2002). The mini-HDD drill rods are subjected to such a stress cycle when bent into a curve and rotated while also in the presence of an axial thrust or tension. The axial stress causes the asymmetric cyclical stress conditions.

### 2.1.3 Random Stress Cycle

Another type of cyclical stress condition is where the stress and frequency of stress change vary randomly. An example of this would be the stresses experienced by automobile shock absorbers, where the frequency and magnitude of imperfections in the road surface will produce varying minimum and maximum stresses and changing frequency of stress variations. In mini-HDD practice, the axial torsion loads will contain elements of several types of cycles: a fairly constant torsion load required for drill bit or reamer cutting of the ground, a random torsion component caused by variations in the ground resistance to excavation, and a steadily increasing torsion load due to the friction of the drill rod against the walls of the borehole.

## 2.1.4 Parameters Used to Characterize a Given Cyclic Loading History

**2.1.4.1 Key Parameters.** In Fig 2.2, several key parameters are defined.

- Stress Range: $\Delta\sigma = \sigma_{max} - \sigma_{min}$
- Stress amplitude: $\sigma_a = \frac{1}{2}(\sigma_{max} - \sigma_{min})$
- Mean stress: $\sigma_m = \frac{1}{2}(\sigma_{max} + \sigma_{min})$
- Load ratio: $R = \frac{\sigma_{min}}{\sigma_{max}}$

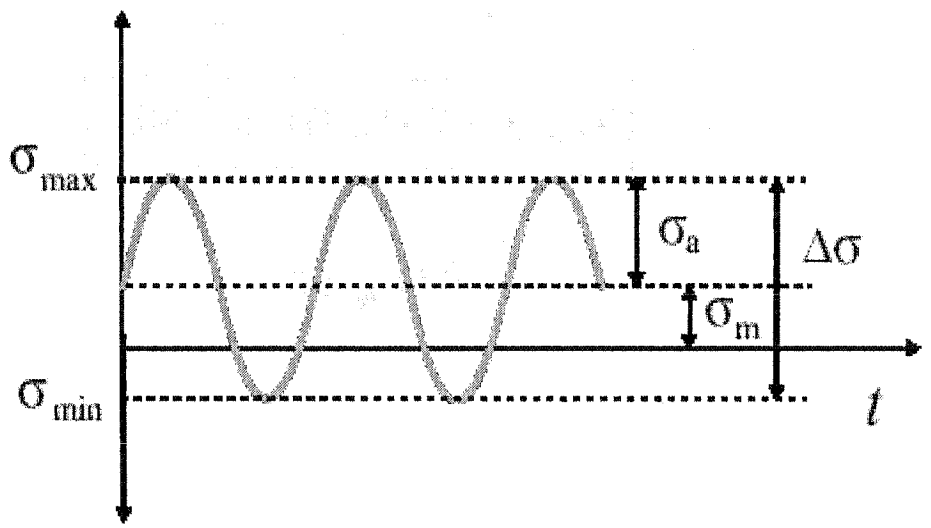


**Figure 2.2 Key Parameters in a Cyclic Loading History (Beer, 1992)**

**2.1.4.2 Other Parameters. Frequency:** in units of Hz. For example, for machinery rotating at 3000 rpm, f = 50 Hz. In general, frequency only influences fatigue if there are environmental effects present (X. J. Wu, 1994). Otherwise, fatigue is controlled by the number of cycles rather than the rate at which they are accumulated. In mini-HDD practice, the frequency is determined by the rate of rotation used in the HDD machine. Typical rotation speeds used for mini-HDD drilling are up to 60 RPM.

**Waveform:** In addition to a sine wave, a stress may follow another waveform pattern such as a square wave. When failure occurs by corrosion fatigue, stress wave shape will affect the cracking process (Howard, 1986).

**Environmental effects:** The main environmental effect is sulfide attack: salt and oxygen corrosion are also environmental effects. (Severinchik, 1977)

Environmental effects for mini-HDD applications are typically not expected to be as strong as they are in the oilfield applications of directional drilling.

Although environmentals effect are not considered in this research, They are still a factor to consider in the mini-HDD field. To prevent premature corrosion damage, use corrosion inhibitors, and perform post bore flushes with clean fluid should be used (Bingham, 2001).

### 2.1.5 The S-N Curve

A very useful way to visualize time to failure for a specific material under different stress scenarios is with the S-N curve. The term "S-N" denotes stress versus number of cycles to failure. It is plotted with maximum stress, minimum stress, or stress amplitude, $\sigma_a$ plotted on the vertical axis and the logarithm of the number of cycles to failure plotted on the horizontal axis. An important characteristic to this plot as seen in Fig. 2.3, is the fatigue limit which can be seen as the horizontal asymptote to the S-N curve.

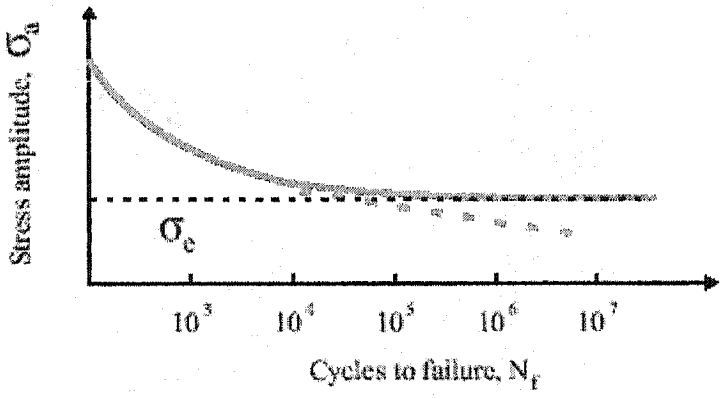


**Figure 2.3 A Typical S-N Curve**

The significance of the fatigue limit is that, if the material is loaded below this stress, it will not fail, regardless of the number of times it is loaded. Steel is an example of a material that typically exhibits a fatigue limit. However, materials such as aluminum, copper, and magnesium do not show a fatigue limit, and, therefore, they will eventually fail after a large enough number of cycles even if the applied stress is reduced to low levels (e.g. dotted line in Figure 2.3.).

Other important terms in describing fatigue behavior are fatigue strength and fatigue life. The applied stress for which failure occurs after a given number of cycles is the fatigue strength. The number of cycles required for a material to fail at a certain stress is the fatigue life.

If the stress is below $\sigma_e$ (the endurance limit or fatigue limit), the component has effectively an infinite life. The $\sigma_e$ is equal to 0.35-0.5 $\sigma_{ts}$ (ultimate tensile strength (UTS)) for most steels and copper alloys.

If the material does not have a well-defined $\sigma_e$, often $\sigma_e$ is arbitrarily defined as the stress that gives a fatigue life $N_f = 10^7$ cycles.

If a plot is prepared of log (a) versus log ($2N_f$) (where $2N_f$ represents the number of reversals to failure, one cycle equals two reversals), a linear relationship is commonly observed. The following relationship between stress amplitude and lifetime (Basquin, 1910) has been proposed:

$$\frac{\Delta\sigma}{2} = \sigma_a = \sigma'_f (2N_f)^b \qquad (2.1)$$

Where $\sigma'_f$ is the fatigue strength coefficient (for most metals this is $\sigma_f$, the true fracture strength)

b is the fatigue strength exponent or Basquin's exponent (from –0.05 to –0.12),

$2N_f$ is the number of reversals to failure.

**2.1.6 Crack Initiation and Propagation**

Failure of a material because of fatigue may be viewed on a microscopic level in three steps:

**Crack Initiation:** The initial crack occurs in this stage. The crack may be caused by surface scratches caused by handling or tooling of the material; threads (as in a screw or bolt); slip bands or dislocations intersecting the surface as a result of previous cyclic loading or work hardening.

**Crack Propagation:** The crack continues to grow during this stage as a result of continually applied (varying) stresses.

**Failure:** Failure occurs when the material that has not yet been affected by the crack growth cannot withstand the applied stress. This stage happens very quickly.

### 2.1.7 Types of Fatigue

Fatigue can also be divided into two broad classes of fatigue failure based on the speed of progression to fatigue failure.

High-cycle fatigue is characterized by

1.many cycles to failure

2.life described by S-N curve data if no flaws are present initially

3.most of the performance life is spent in the crack initiation phase

In mini-HDD practice, most fatigue problems are high-cycle problems, since there are guidelines for the operator to avoid overload of the machine and drill rod.

Low-cycle fatigue is characterized by:

1.failure in a small number of cycles

2.plastic deformation to a significant degree with each cycle

3.strain versus number of cycles describes the behavior in fatigue

4.separate power-law correlations are used for the elastic and plastic parts of the strain

When mini-HDD drill machines are used improperly, for example, letting the drill pipe bend into a very sharp curve, this kind of fatigue will occur.

### 2.1.8 Benchmark and Striations

One can determine that a material failed by fatigue by visually examining the fracture surface. A fatigue fracture will have two distinct regions: One being smooth or burnished as a result of the rubbing of the bottom and top of the crack (steps 1 & 2); the second is granular, caused by the rapid failure of the material (Reed-Hill 1994). These

visual clues may be seen in Fig. 4 which is a photograph of one of the HDD drill rods tested as part of this research.

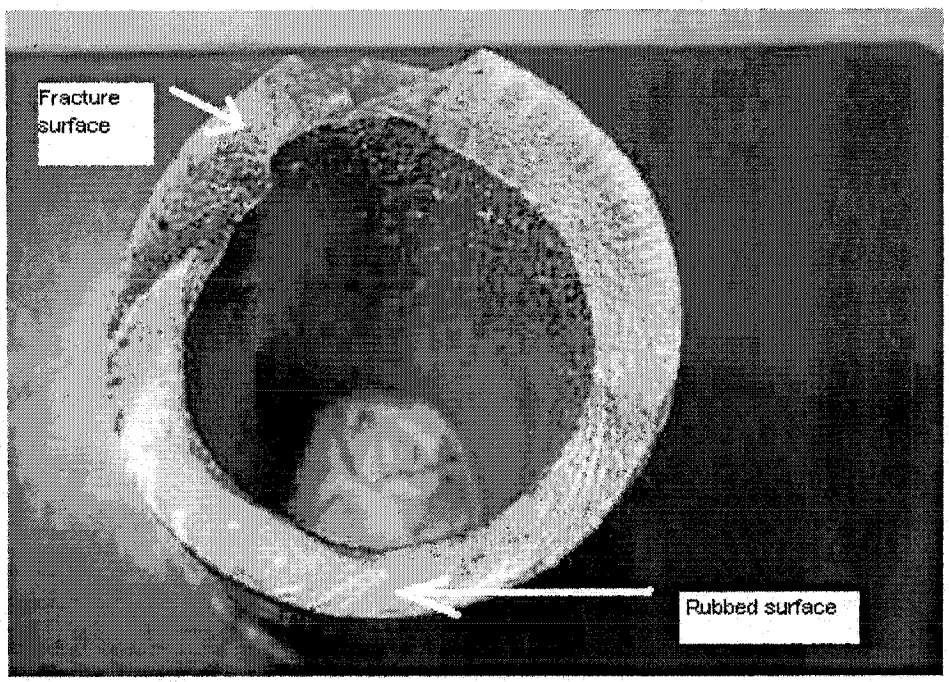


**Figure 2.4 Surface of a Fatigue Fracture of Mini-HDD Drill String**

Other features of a fatigue fracture are beach marks and striations. Beach marks, or clamshell marks, may be seen in fatigue failures of materials that are used for a period of time, allowed to rest for an equivalent time period, and then loaded again as in factory usage. Striations are thought to be steps in crack propagation, where the distance depends on the stress range. Beach marks may contain thousands of striations (Reed-Hill, 1994) Visual examples of beach marks and striations are seen below in Figures 2.5.

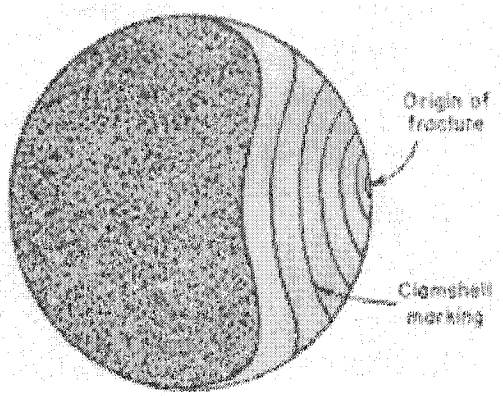


**Figure 2.5 An Example of Beach Marks (Reed Hill, 1994)**

### 2.1.9 Propagation Rate

The rate at which a crack grows has considerable importance in determining the life of a material. The propagation of a crack occurs during the second step of fatigue failure. As a crack begins to propagate, the overall size of the crack also begins to grow. The rate at which the crack continues to grow depends on the stress level applied. The rate at which a crack grows can be seen mathematically as proposed by Paris (1963) using the following equation:

$$\frac{da}{dN} = A(\Delta K)^m \tag{2.2}$$

The variables A and m are properties of the material, *da* is the change in crack length, and *dN* is the change in the number of cycles. K is the change in the stress intensity factor given by

$$\Delta K = K_{max} - K_{min} = Y\Delta\sigma\sqrt{\pi a} \tag{2.3}$$

Rearrangement and integration of Equation 2.2 gives us the relation of the number of cycles of failure, $N_f$, to the size of the initial flaw length, $a_o$ , and the critical crack length, $a_c$, as shown in Equation 2:

$$N_f = \int_0^{N_f} dN = \int_{a_o}^{a_c} \frac{da}{A(Y\Delta\sigma\sqrt{\pi a})^m} = \frac{1}{A\pi^{m/2}(\Delta\sigma)^m} \int_{a_o}^{a_c} \frac{da}{Y^m a^{m/2}} \tag{2.4}$$

where $N_f$ is the estimate of the number of cycles to failure.

$a_o$ is the size of the initial flaw length

$a_c$ is the critical crack length

## 2.2 Factors That Affect Fatigue Life and Behavior Predictions

### 2.2.1 Fatigue Life in Relation to Mean Stress and Stress Amplitude

The mean stress is defined as

$$\sigma_m = \frac{\sigma_{max} + \sigma_{min}}{2} \tag{2.5}$$

As the mean stress is increased, the fatigue life decreases.

The stress amplitude ($\sigma_a$) is defined as

$$\sigma_a = \frac{\sigma_{max} - \sigma_{min}}{2} \tag{2.6}$$

Figure 2.6 shows the variation of fatigue life with stress amplitude and with main stress based on research by Goodman, Gerber and Soderberg (Forrest, 1962).

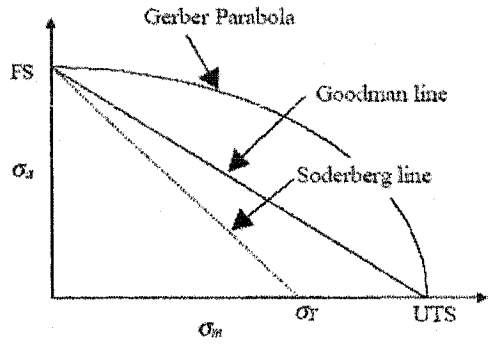


**Figure 2.6. The Goodman, Soderberg, and Gerber Lines to Account for the Effect of Mean Stress on Fatigue Strength (Forrest, 1962)**

$$\sigma_a = \sigma_a|_{\sigma_m=0}\left\{1 - \frac{\sigma_m}{\sigma_y}\right\} \text{ (Soderberg)}$$

$$\sigma_a = \sigma_a|_{\sigma_m=0}\left\{1 - \frac{\sigma_m}{\sigma_{TS}}\right\} \text{ (Goodman)}$$

$$\sigma_a = \sigma_a|_{\sigma_m=0}\left\{1 - \left(\frac{\sigma_m}{\sigma_{TS}}\right)^2\right\} \text{ (Gerber)} \qquad (2.7)$$

where $\sigma_a$ is the stress amplitude denoting the fatigue strength for a nonzero mean stress

$\sigma_a|\sigma_m=0$ is the stress amplitude (for a fixed life) for fully reversed loading

($\sigma_m = 0$ and $R = -1$)

$\sigma_y$ is the yield strength and

$\sigma_{TS}$ is the tensile strength

## 2.2.2 Effect of Surface Treatment

Scratches and other imperfections on the surface will cause a decrease in the fatigue life of a material. Therefore, making an effort to reduce these imperfections by reducing sharp corners, eliminating unnecessary drilling and stamping, shot peening, and, most of all, careful fabrication and handling of the material.

Another surface treatment is called case hardening, which increases surface hardness and fatigue life. This is achieved by exposing the component to a carbon-rich atmosphere at high temperatures. Carbon diffuses into the material -- filling interstices and other vacancies in the material up to 1 mm in depth.

### 2.2.3 Chemical Attack

Another environmental affect on a material is chemical attack, or corrosion. Small pits may form on the surface of the material, similar to the effect etching has when trying to find dislocations. Drilling mud and the borehole environment have an influence in the fatigue of mini-HDD drill pipe. The immersion in flowing drilling mud will tend to reduce the fatigue life of drill pipes (Bingham, 2001).

### 2.2.4 Miner's Rule

Because in mini-HDD practice the rod will be bent into a different curvature and be subjected to different axial and torsion stress for each use, it is difficult to provide a straightforward analysis of the expected fatigue life.

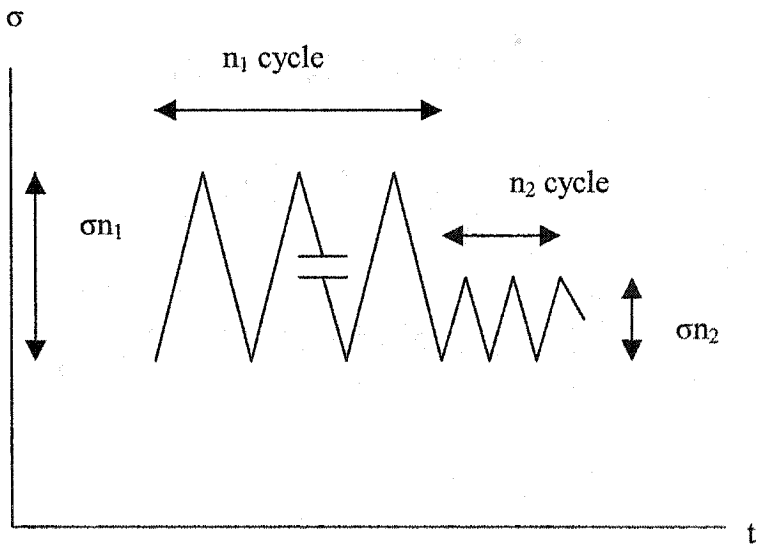


**Figure 2.7 Stress Reversals which Can Use Miner's Rule**

A very common approach to dealing with varying cyclical stress conditions is the Palmgren-Miner linear damage summation rule in Fig 2.7(Miner 1945).

If we define $2N_{fi}$ as the number of reversals to failure at $\sigma_{ai}$, then the partial damage d for each different loading $\sigma_{ai}$ is

$$d = \frac{2n_i}{2N_{fi}} = \frac{\text{Reversals at } \sigma_{ai}}{\text{Reversals to failure at } \sigma_{ai}} \tag{2.8}$$

$$\sum_i \frac{n_i}{N_{fi}} = 1 \tag{2.9}$$

It is assumed in the summation rule that the **sequence** in which the loads are applied has no influence on the lifetime of the component. In fact, the sequence of loads can have a large influence on the lifetime of the component.

## 2.3 Fatigue Research Method

### 2.3.1 Fatigue Failure Models

There are three fatigue failure models in current use, and each has a place and a purpose. They are the stress-life (S-N) approach, the strain-life approach, and the linear elastic fracture-mechanics (LEFM) approach.

### 2.3.2 Fatigue Regimes

Based on the number of stress or strain cycles that a part is expected to undergo in its lifetime, the fatigue condition is defined as a **low-cycle fatigue (LCF)** regime or a **high-cycle fatigue (HCF)** regime. There is no sharp dividing line between the two regimes. Generally it is assumed that $N = 10^3$ cycles is a reasonable approximation of the dividing line between LCF and HCF.

### 2.3.3 The Stress-Life Approach

The stress-life approach is the model most often used for high-cycle fatigue (HCF) applications, where the number of stress cycles is expected to be more than 1000 cycles. It works best when the load and stress amplitudes are predictable and consistent over the life of a part. It is a stress-based model which seeks to determine a fatigue strength and/or an endurance limit (analogous to yield limit) for the material so that cyclic stresses can be kept below that level and fatigue failure avoided for the required number of cycles. The part is designed such that the significant stress never exceeds the material's fatigue strength (or endurance strength). In this approach, the designer attempts to keep local stresses in any notches so low that the crack-initiation stage never begins. The stresses and strains everywhere remain in the elastic region such that no local yielding occurs to initiate a crack.

### 2.3.4 The Strain-Life Approach

This is a strain-based model. Since the crack initiation involves local yielding, the strain-life approach gives a reasonable estimation about the crack-initiation stage. It can also account for cumulative damage caused by variations in the cyclic load over the life of the part. This method is most often applied to LCF and finite life problems where cyclic stresses are high enough to cause yielding.

### 2.3.5 The LEFM Approach

Fracture mechanics theory provides the best model of the crack propagation stage of the process. This method is applied to LCF and finite life problems in predicting the remaining life of cracked components.

The **stress-life** approach described is applicable for situations involving primarily elastic deformation. Under these conditions, the component is expected to have a long lifetime. For situations involving high stresses, high temperatures, or stress concentrations such as notches, where significant plasticity can be involved, the approach is not appropriate. Since the stress in mini-HDD drill rod is normally in the elastic region, high-cycle fatigue (HCF) is the normal condition and the stress life approach will be suitable.

## 2.4 Fatigue Research in the Oil Industry

Very little research about the fatigue of mini-HDD pipe can be found in the literature related to trenchless technology. The oil industry, however, has carried out a great deal of research in this area. Although the drill pipes used in the oil industry are substantially different in size and joint design when compared with mini-HDD drill pipes, there are very useful information and research results that can be adapted to the mini-HDD drill rod fatigue problem.

Oil company records indicate that accumulated fatigue is the most frequent means of failure in drill pipe used for directional drilling wells. Much research has been carried out and valuable results obtained. Lubinski point out the relationship between dogleg severities and fatigue life of drill rod (Lubinski, 1961); until now, the oil industry is still using this method to predict fatigue life of drill pipe. Based on the data collected on the North Sea oil field, M.W. Joost points out how to predict accumulated drill pipe fatigue in directional drilling well (Joost, 1985). Amro used similar methods to investigate tubular failure in the middle East area (Amro, 2000). Those works form the basis of research into the fatigue life of shallow horizontal directional drilling (HDD) rods.

### 2.4.1 Fatigue Study of Drill Pipe in the Oil Industry for a Non Corrosive Environment

As early as 1951, Bachman presented the result of a 15-year investigation performed at the Hughes Tool Company. These results represent a major contribution to the understanding of the fatigue strength of drill pipe. The size of the test specimen and its geometry were recognized as important factors affecting fatigue life. For this reason, the tests were performed on full-size specimens of 114 mm diameter drill pipe. Furthermore, these tests were performed to assess the fatigue resistance of different types of tool joints. Consequently, the test specimens took the form of cantilever beams tested in rotating bending. The tool joint was located at the fixed end of the cantilever. The scatter band of the test results, representing the difference in fatigue strength between the best and the worst specimens, was wide. The surface pits, mill scale, and hardness of the test specimens were believed to contribute to the scatter. Among all the various kinds of tool joints investigated, the integral joint with a flash weld was found to be able to develop the fatigue life of the drill pipe body. And, it was also found that the regular API threaded connections all failed at the last engaged thread. All the tests presented by Bachman were obtained from tests performed in air without the presence of a superimposed axial load.

In 1961, the first guidelines towards establishing quantitative values for fatigue damage in curved holes resulted from early work by Lubinski. The theoretical analysis performed by Lubinski to evaluate bending stresses in a pipe rotating in a dogleg of constant curvature also considered the effect of axial tension and the lateral component of the submerged weight of the drill pipe. In this way, dogleg severity was converted to

stress range. The theoretical stress range was then compared to the endurance limit for the drill pipe to determine whether fatigue failure damage would occur (Lubinski 1961). To account for the effect of axial load on the endurance limit, a modified Goodman diagram was used. The endurance limit used, 250 Mpa, was obtained from laboratory tests conducted in air on drill pipe under no axial load.

In 1964 and 1966, Hansford and Lubinski extended the earlier work of Lubinski (1961) in an effort to account for cumulative fatigue damage if the dogleg severity limits presented by Lubinski (1961) were exceeded. In order to estimate fatigue damage, a stress range versus number of cycles to failure (S-N) curve, representing a lower bound of laboratory test results presented by Bachman (1951), was used in conjunction with Miner's Law to account for cumulative fatigue. The results were presented in the form of a chart that could be used to predict the percentage of the total fatigue life expended in a dogleg interval as a function of dogleg severity and tension in drill pipe at the dogleg. The work of Hansford and Lubinski was intended to be applied to Grade E drill pipes and aluminum drill pipes. The guidelines for aluminum drill pipe were derived using fatigue test data presented by Boice and Dalrymple (1963).

In 1966, Rollins reported the experimental work presented by the Battelle Memorial Institute. In this experiment, the effect of surface finish on fatigue resistance of drill pipe steels was investigated using notched and unnotched specimens. It was found that notched specimens could tolerate 138 Mpa alternating stress while the unnotched specimens could tolerate a stress range of 586 Mpa at 5 million cycles.

In the 1970s, Nicholson (1974) generalized Lubinski's (1961) findings to Grade S-135 drill pipe. Guidelines presented for S-135 drill pipe are based on an endurance limit of 276 Mpa.

In 1984, the American Petroleum Institute published recommended practices. The findings of Lubiski (1961), Hansford and Lubinski (1964, 1966), and Nicholson (1974) were adopted as part of API's findings.

In 1987, the Chinese Petroleum Standardization Committee presented the results of an investigation of the effect of geometry of the transition zone between the pipe upset and the pipe body. Full-sized drill pipes with a transition zone of varying lengths and radius were tested in air as cantilever rotating beams under no axial load. It was found that the fatigue resistance improved with an increase in length of the transition zone. The minimum length of the transition zone recommended was 80 mm, with a taper radius of at least 300 mm.

In 1988, Dale presented another approach to this problem. He used a fracture mechanics model, verified by extensive full-scale testing, to predict fatigue crack growth behavior in both the pipe body and connections of drill collars. The Paris model (Paris, 1963) for crack growth prediction was used. Stress intensity factors were based on a modified solution for an edge crack in a semi-infinite sheet under combinations of tension and bending loads. The research work resulted in recommendations for determining the inspection intervals for drill collars.

In 1991, Grondin and Kulak conducted a study of fatigue in oil well drill pipe in combined axial tension and bending. Their report describes the manufacturing processes used in making drill rod, finite element analyses of upset ends, fatigue tests, and failure

mechanisms. The fatigue data on API Grade E drill pipe with an outside diameter of 4.5 in and a yield strength of 500 Mpa (72,000psi) best fit the relationship:

$$LogN = 14.8 - 3.46 \log S_r - 1.65 \times 10^{-5} (S_m)^2 \qquad (2.10)$$

where $S_r$ is the stress range in Mpa, $S_m$ is the mean stress in Mpa, and N is the fatigue life in cycles. For a probability of survival of 95 %, this equation is modified by changing the constant from 14.8 to 13.8.

Almost none of the failures in the test series occurred in the upset ends. Nearly one half of the failures occurred at surface grinding marks. The finite element analyses for tension only and bending only that did not model connection threads indicated that the highest stress occurred at the junction between the ordinary rod and the internal or external upset but the failures, in general, did not occur there. The stress concentration factors were 1.2 or less at this transaction point.

In 1991, T.H. Hill and his associates unified the methodology to treat fatigue problems in drill pipe. Their paper draws upon failure prediction models, failure investigation results, drill pipe FEA analysis, and the API/IADC Drill String Failure Database to construct a unified approach to failure prevention.

In 2000, Mohammed M. Amro presented a field case study of drill string failure during drilling of a medium radius horizontal well. Investigations as well as a metallurgical evaluation were conducted in an attempt to establish the possible causes of the drill string failures. Other possible reasons for drill string failures and suggestions to minimize the bending stress in drill pipes are discussed. The principal idea was to use Lubinski's modified equations to predict the drill pipe fatigue damage in horizontal and directional drilling wells. The relationship between the maximum permissible dogleg

severity and the maximum stress was created for different pipe geometries. Cracks were analyzed by photomicrograph.

### 2.4.2 Research and Guidelines for Operation in a Corrosive Environment

The first attempt to quantify the effect of the corrosiveness of an environment on the fatigue life of drill pipe was presented in 1941 by Grant and Texter. A number of bending fatigue tests were performed on small samples of drill pipe, all cut from the same pipe and stressed to the same degree. The only variation in conditions was the medium in which the specimens were stressed.

The test results showed a reduction of fatigue life of 35 % as the environment changed from distilled water to salt water, and a reduction of more than 90 % was reported for drill pipe steel tested in dilute hydrochloric acid.

In 1964, Lubinski suggested the fatigue curve obtained from tests conducted in air be lowered by 40 % to account for the detrimental effect of a corrosive environment on fatigue life.

In 1979, experiments by Azar showed a decrease in life expectancy as the amount of $O_2$, $CO_2$, and chlorides in the mud increased.

In the 1980s, Joosten presented data collected during drilling of 20 wells that enabled a comparison to be made between field observations and a fatigue damage analysis.

In 1987, Helbig and Vogt presented the results of more than 10 years of investigations on fatigue of drill pipe. Both full-sized sections of drill pipe body and small bending specimens were tested under conditions encountered in practice. These

tests were conducted with a special emphasis on the loading frequency and the effect of corrosion. Tests on small bending specimens were performed in air, tap water, and a 20% sodium chloride solution. The test results showed that the speed of testing has a significant influence on fatigue life when testing in a corrosive environment. Quenched and tempered steels yielded lower values of fatigue strength than did normalized steels in small bending specimens but showed no difference in full-sized drill pipe. No endurance limit was observed for tests conducted in a corrosive environment.

### 2.4.3 The Analysis of the Internal Upset Geometry of Drill Pipe for Longer Fatigue Life in the Oil Industry: Finite Element Analysis Approach

Yasushi Tsukano and his associate analyzed the fatigue failure of the internal upset in the transition area in 1990. The stress in the transition area of the internal upset under bending load was analyzed by the finite element method to determine the optimum geometry of the internal upset in accordance with the design concept. But since it was extremely difficult to conduct this analysis on all sizes covered by the API specifications, the most popular size was selected as the size of drill pipe for the finite element analysis.

In his research, the pipe geometry was simplified to a two-dimensional cantilever beam and was meshed with the bending moment being applied at one side.

After the finite element analysis, full-sized drill pipe was fatigue tested to validate the optimum internal upset geometry obtained by the finite element analysis. A four point bending fatigue setup was used to conduct the evaluation test, and the test results confirmed the optimum internal upset geometry of drill pipe. The specimens that fractured in the pipe body and those that had upsets of optimum geometry differed little

in fatigue life. The fatigue life of the specimens that fractured in the transition area of the internal upset of less than optimum geometry steeply decreased in fatigue life with the decreasing internal taper length. This obviously was due to the higher stress concentration that occurred in the transition area of the internal upset with a poorer geometry.

Although in mini-HDD practice the fatigue failure does not generally occur at the internal upset location, this approach is very useful in deciding the optimum design of the drill pipe joint by checking for high stress concentrations.

### 2.4.4 Joint Failure Research in the Oil Industry and API Regulations

**2.4.4.1 API Regulation and Gregory Fehr's research.** From T.H. Hill's research on drill pipe failure in the oil industry, 65% failures of pipes are from fatigue failure. Of these, 14% occurred in the pipe tube, and 86% occurred at the tool joint or BHA connection. In those joint failures, pin failures accounted for 89% and box failures only 11%. Because of this, there has been extensive research into joint failure in oilfield drill pipe resulting in guidelines from the American Petroleum Institute (API).

The specification for connections for drilling tools in the petroleum drilling industry is the American Petroleum Institute (API) Spec 7. The guidelines and equations used to determine the values in the API Spec 7 are found in API RP7G. The documents assist the user in choosing connections that will provide maximum fatigue life and optimum tensile and torsional strength for each drilling situation. These guidelines have been developed over many years and include the benefit of the experience of many people who were involved in their development.

In the API guideline, bending strength ratio (BSR) is used to assist the driller in the selection of the best connection for an existing string of drill collars.

The method used to compute the Section Modulus Ratio, which is known as the modified API BSR formula, is as follows:

$$"BSR" = \frac{box\_section\_modulus}{pin\_section\_modulus} = \frac{Z_B}{Z_P}$$
$$Z_B = \left(\frac{D^4 - b^4}{D}\right)\frac{\pi}{16} \qquad (2.11)$$
$$Z_P = \left(\frac{R^4 - d^4}{R}\right)\frac{\pi}{16}$$

where D = outside diameter of joint

b = thread root diameter of box at end of pin nose

R = thread root diameter at last engaged pin thread

D = bore inside diameter of joint

All dimensions are in inches.

In Gregory Fehr's research (1994), he introduced the Moment of Inertia Ratio from box to pin:

$$Moment\_of\_Inertia\_Ratio = \frac{I_{BOX}}{I_{PIN}} \qquad (2.12)$$

$$I_B = \frac{\pi}{64}\left[D^4 - b^4\right]$$
$$I_P = \frac{\pi}{64}\left[R^4 - d^4\right] \qquad (2.13)$$

where D = outside diameter of joint;

b = thread root diameter of box at end of pin nose

R = thread root diameter at last engaged pin thread

D = bore inside diameter of joint

All dimensions are in inches.

In Fehr's Paper (1994), he gave suggested ratios for different connections derived from experience as noted in Table 2.1

**Table 2.1 Suggested Ratios for Different Connections**

| Connection | Section Modulus Ratio Box to Pin | Moment of Inertia Ratio Box to Pin |
|---|---|---|
| Mining Industry Moderate Torque Internal Upset | 1.23 | 1.357 |
| Mining Industry Moderate Torque Straight Wall | 2.377 | 2.750 |
| High Torque Flush Joint Buttress Style | 1.015 | 1.082 |
| Low Torque API EUE Tubing | 1.308 | 1.446 |
| Mining Industry Low Torque | 1.22 | 1.32 |

From Table 2.1, it is clear that the box have a bigger moment of inertia than that of the pin. This explains why the pin is easier to break than the box and to consistent with results in the field that pin failures accounted for 89% and box failures only 11% of total failure. These ratios also can be used to improve the design of joints of mini-HDD drill pipes.

**2.4.4.2 I.P.Gnyp's Approach.** In another approach, I.P.Gnyp, I.S Babyku, and B.O Chernov, in 1990, developed a method of calculation for the lifetime of a fish mouth

collar joint. This method was based on the selection of a model using the criteria of fracture mechanics.

His calculation model is as shown in Fig 2.8.

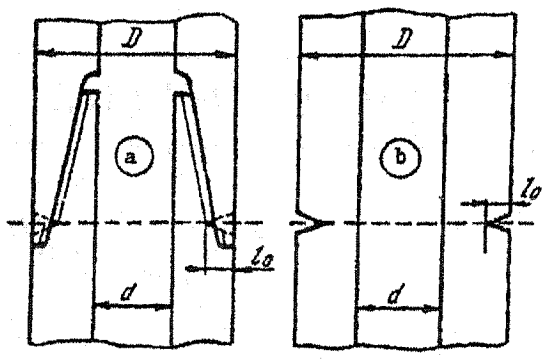


(a) Diagram of collar joint of BDP; (b) calculation model.

**Figure 2.8 Collar Joint Modeling (after Gnyp)**

Using this model, the contact mechanics problem was changed into a fracture mechanics problem. Although this is not strictly an appropriate substitution, it provided a state-of-the-art approach to this problem.

From this research, it is clear that the location of the last engaged thread of drill pipe joint is very important: the higher, the better. The higher the place of the last engaged thread of drill pipe, the bigger the moment of inertia at that point which is always the broken point. Thus, the joint will have a bigger failure resistance.

**2.4.4.3 The Finite Element Analysis Approach.** In 1995, Omesh Malik used finite element analysis to analyze a steel pipe joint for trenchless construction. This steel pipe was not the same type of pipe used in mini-HDD drill pipe but rather a jacking pipe used in auger boring, pipe jacking, and microtunneling. It has a different type of press-fit interlocking joint, but it was also clear from this research that the stress concentrations

resulting from the detailed connection were very important and that the finite element analysis was a very useful means of investigating an optimum configuration.

## 2.5 Mini-HDD Drilling Pipes

From the literature review, it is clear that fatigue life depends not only on the conditions of use of the drill pipe but also on its design and manufacture. Some key manufacturing parameters are

1. the type of steel used and its heat treatment
2. the surface finish of the steel and any in-plant handling damage
3. the joint design including the type and design of upset and the thread configuration

### 2.5.1 Two Basic Types of Drill Pipe are in Use Today

1. The **external flush joint** pipe -- in the external flush joint pipe, the upset area and/or tool joints have the same outside diameter as the pipe body
2. The **elevated shoulder** pipe -- in the elevated shoulder drill pipe, the upset area and/or tool joints have a larger outside diameter than the pipe body.

### 2.5.2 The Three Most Common Methods for Manufacturing HDD Pipe

1. Internal forged

Internal forged drill rod is made solely from one piece of material. This product has the same chemical makeup for the connections and the tube body, and no weld zone exists between the two. The basic rod material ("green" tube) is cut to the required length to ensure the proper final length tolerances are met. The ends of the cut tube are then heated as to produce a workable material for forging.

The forging process creates the desired upset OD, ID, and length configuration required for a given connection. The next step in the manufacturing process is to heat treat the tube to the customer's specified grade, producing a tube with a specified minimum yield strength.

Once the heat treating has been concluded, the connections are then machined on the upsets of each tube, generally one pin and one box. As a result of forging constraints, the upset OD, ID, and length are limited on the integral forged drill rod.

2. Inertia fit welded

Because of connection, OD, ID, and length requirements, inertial welded drill rods are in popular demand. An inertia welded drill rod is similar to an integral drill rod in that the green tube is cut to length, upsets are forged on the ends, and the tube is heat-treated.

The main difference with the inertia welded drill rod is that the tool joints, connections, and tubes are manufactured separately. The tool joints are forged from bar stock, heat treated, inspected, and threaded. The tool joints and the tube are then brought together for welding.

The welding process produces a seamless bond between the tool joint and the tube by using the momentum created by the inertia welding machine. No filler materials are used in this type of welding, so no impurities will be found in the weld.

The welding process begins with the tube being held stationary by a set of fixture clamps in the inertia welder. The tool joints are placed in a set of clamps (collets) and aligned with the turned and bored upset on the tube. The weld cycle begins with the machine rotating the tool joint to a calculated RPM. Once the proper RPM has been

reached, the machine forces the tool joints and the tube together, creating friction and heating the interface to weld the surfaces together. The weld zone is then heat treated and tested to ensure the proper strength has been obtained to provide a quality product to the customer

3. Shrink fit welded

Shrink fit and welded drill rod is manufactured with tubes that may have upset ends or be a parallel wall (or plain end) tube. This process machines the ID of the tube to produce interference fit with the weld tang of the tool joint connection. The weld tang is actually pressed inside the mid body tube, and a fillet weld bonds the tool joints to the tube.

Because of its mass, shrink fit and welded pipe has similar advantages to inertia welded pipe. This process is well accepted in all industries and provides a strong joint. The disadvantage of this method is the filler metal between the two mating parts. If a tool joint is shrink fit to the parallel wall of a plain end tube and any wear is sustained on the outside diameter, then the connection is weakened and subjected to increased fatigue

# CHAPTER 3

# STRESS ANALYSIS OF MINI-HDD DRILL PIPE

Since "high life" fatigue is the principal failure scenario for mini-HDD drill pipe, it is important to understand the potential stresses in the drill pipe during HDD operations.

## 3.1 Forces on the HDD Drill String in Operation

Three basic stress conditions act on the drill string:

1. A bending stress resulting from the curvature of the drill string. The bending stress, which is an axial stress varying across the cross-section, oscillates from tension to compression at a particular point each time the drill rod makes one revolution.
2. The axial stress caused by thrust (compression) or pullback (tension).
3. The shear stress derived from the torque on the drill rod.

The typical range of installation for mini-HDD will be up to 600 ft. The torque of the machine will be in the range of 400~950 ft-lb and the thrust/pullback will be in the range of 6,000~20,000 lb (see Table 1.1)

## 3.2 Types of Mini-HDD Drill Pipe Investigated in this Research

Drill pipe used in the testing and analysis program for this research project were supplied by Texas Pup, Inc. and Drilltube, Inc. The configuration for each of the drill pipes is shown in Figures 3.1. All the rods are forged and heat treated.

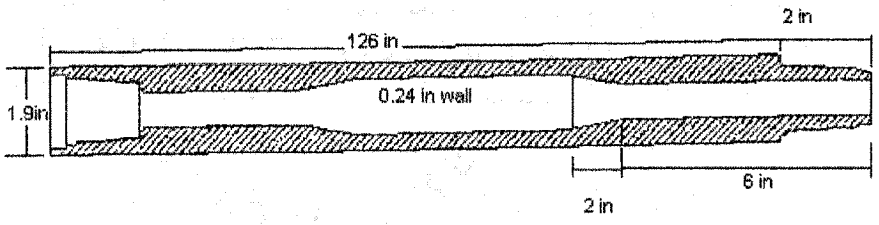


**Figure 3.1 External Flush Joint Mni-HDD Drill Pipe Used in this Research**

For the analysis of the stress condition in a uniform section of mini-HDD drill pipe, the configuration of the drill rod was simplified to that shown in Fig.3.2

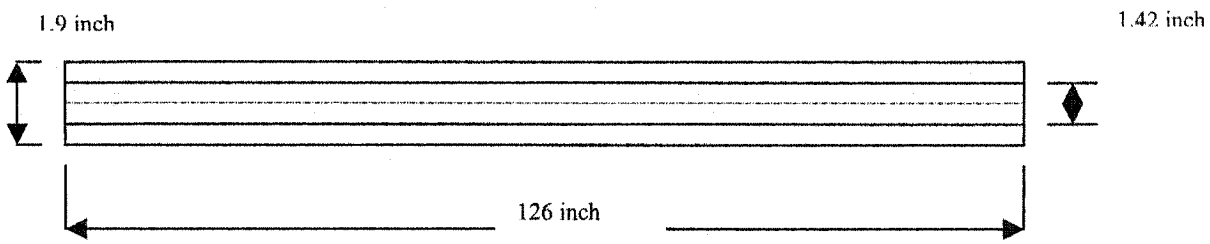


**Figure 3.2 Simplified Model of Mini-HDD Drill Pipe**

## 3.3 Stresses Caused by Bending

Drill pipe bending resulting from following a curved alignment or from over-steering will cause bending stresses. Rotation of the drill string will cause stress cycling leading to fatigue if the stress is above the endurance limit.

### 3.3.1 Standard Bending Theory

Assuming a given radius of curvature for the drill pipe, the bending stresses developed in the drill pipe can be directly estimated by the following:

$$\sigma = \frac{E \times D}{2R} \tag{3.1}$$

where $\sigma$ peak tensile (or compression) stress developed in pipe (psi)

E modulus of elasticity (psi)

R radius of curvature of bends (in)

D pipe outside diameter (in)

However, several different scenarios for drill pipe bending within the borehole can be postulated, and these can result in different curvatures and bending stress conditions. Three scenarios are investigated in the following sections.

### 3.3.2 Curvature Due to an Applied Bending Moment

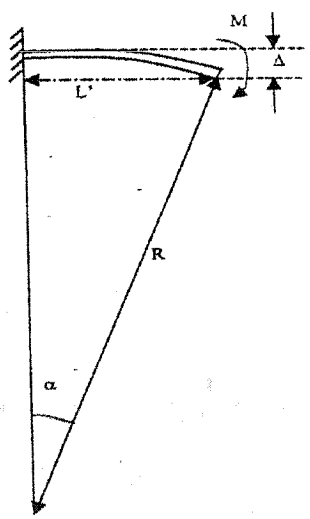


**Figure 3.3 Curvature Caused by an Applied Bending Moment**

In this situation

$$M = \frac{2\Delta EI}{L^2}$$

$$\sigma = \frac{MD}{2I} = \frac{2\Delta EID}{2IL^2} = \frac{\Delta ED}{L^2} \quad \text{(a)}$$

$$L^2 + (R - \Delta)^2 = R^2$$

$$L^2 + R^2 - 2R\Delta + \Delta^2 = R^2$$

$$\frac{L^2}{\Delta} = 2R$$

$$\Delta = \frac{L^2}{2R}$$

Inputting into (a)

$$\sigma = 0.5\frac{ED}{R} \quad (3.2)$$

This is the same as Equation 3.1 confirming that the radius of curvature is a constant with a pure applied moment. This formula is the one normally provided in the literature (McKelve, 1992).

### 3.3.3 Curvature Caused by an AppliedForce at the End of the Drill Rod

This configuration corresponds to the condition where the leading end of the drill rod is deviated to follow a prescribed path.

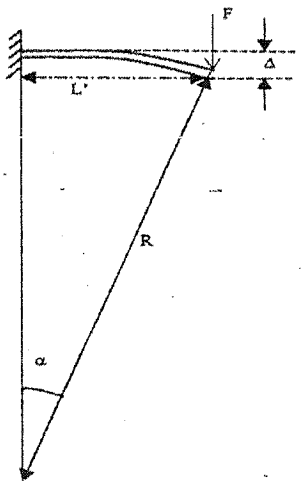


**Figure 3.4 Curvature Caused by an Applied Force at the End of the Drill Rod**

The force and stress can be derived as follows:

$$F = \frac{3\Delta EI}{L^3}$$

$$\sigma = \frac{MD}{2I} = \frac{FLD}{2I} = \frac{3\Delta EILD}{2IL^3} = \frac{ED}{\frac{2L^2}{3\Delta}}$$

The curvature in this case is not constant and varies with the moment and hence the distance from the applied load. However, using the same approximation for curvature based on deviation Δ over the length L provides a comparison of the different maximum stress under the different loading condition.

Thus, $\Delta = \frac{L^2}{2R}$ and substituting for Δ yields

$$\sigma = 0.75\frac{ED}{R} \qquad (3.3)$$

This provides a higher estimate of the stress in the drill rod than the first approximation.

### 3.3.4 Curvature Caused by Uniformly Distributed Load

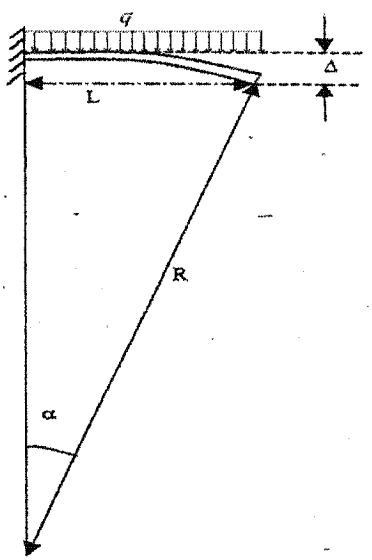


**Figure 3.5 Curvature Caused by Uniformly Distributed Load**

Following the standard derivation of the force/deflection relationships:

$$\Delta = \frac{qL^4}{8EI}$$

Using the same relationship of nominal curvature to deviation

$$\Delta = \frac{L^2}{2R}$$

This leads to

$$\frac{L^2}{2R} = \frac{qL^4}{8EI}$$
$$\frac{1}{2}qL^2 = \frac{2EI}{R}$$

And hence

$$\sigma = \frac{MD}{2I} = \frac{\frac{1}{2}qL^2 D}{2I} = \frac{\frac{2EI}{R}D}{2I} = \frac{ED}{R} \qquad (3.4)$$

### 3.3.5 Curvature Caused by a Triangularly Varying Load

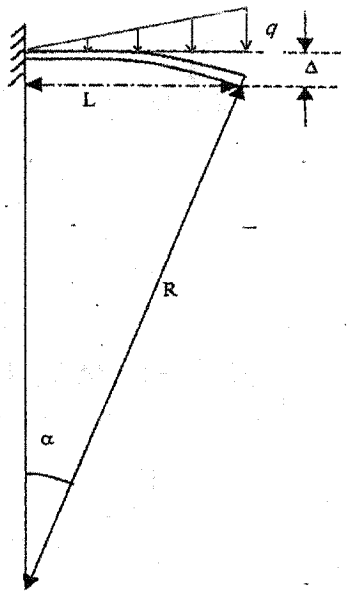


**Figure 3.6 Curvature Caused by a Triangularly Varying Load**

Again, from standard derivations,

$$\Delta = \frac{11qL^4}{120EI}$$

And, as in the first example,

$$\Delta = \frac{L^2}{2R}$$

$$\frac{1}{3}qL^2 = \frac{20EI}{11R}$$

Therefore, in this situation,

$$M_{max} = \frac{1}{3}qL^2$$

$$\sigma = \frac{MD}{2I} = \frac{\frac{20EI}{11R}\frac{D}{2}}{I} = 0.909\frac{ED}{R} \qquad (3.5)$$

## 3.4 Determining the Most Appropriate Model

### 3.4.1 Comparison of the Four Conditions

From these four conditions, we have the same average curvature R over a drill rod section but develop different maximum stresses. The smallest stress is obtained in the approach given in 3.3.1, and the largest is obtained in the approach given in 3.3.4. The difference in stress is very significant – the stress caused by a uniform loading being twice that created by an applied moment at each end.

Although the best representation of the actual condition of the drill string is difficult to determine, it is clear that the common assumption of an applied moment to cause the bending (which corresponds to a uniform curvature) provides a lower-bound estimate of the maximum drill stress.

### 3.4.2 Comparison with HDD Practice

When the drill head is actively being steered, the drill pipe is forced into curvature by a change in the direction of the drill head. In this case, it is reasonable to assume that a point load at the drill head provides the drill string curvature.

In this situation, it can be assumed the best fit is situation analyzed in 3.3.3:

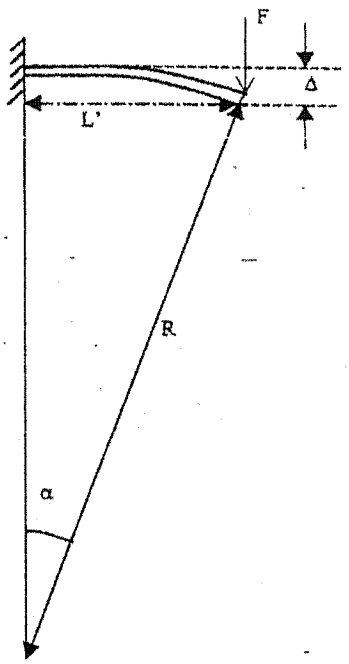


**Figure 3.7 Best Fit Situation**

For this condition, the max stress is

$$\sigma = 0.75\frac{ED}{R}$$

Once the drill head has been steered to the correct alignment, the continuous rotation will start again. The drill head and the first section of drill rod will drill approximately straight, and the following sections of drill rod that are negotiating the curved section will be forced into curvature by pressure against the walls of the borehole. In this condition, the drill pipe will follow the inner wall of the borehole in the central section of the curve and will relax into a slightly larger curvature at the entry and exit points of the curve as shown in Fig. 3.8.

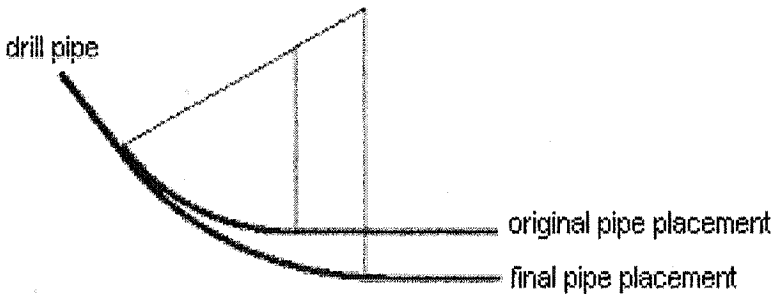


**Figure 3.8 Pipe Placement Change**

If we make the assumption that the earth is elastic material, the force of the earth is linear with the displacement, so we can assume the load distribution in Fig. 3.9.

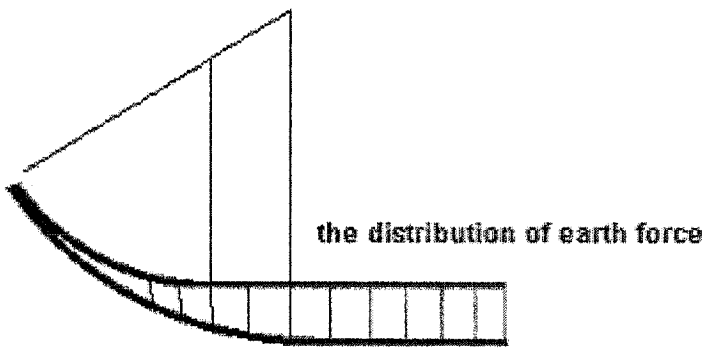


**Figure 3.9 Distribution of Earth Force after Pipe Placement Change**

A simple loading assumption for this section of drill rod that approximates the varying lateral force along the drill rod is the triangular load configuration shown in Fig.3.10.

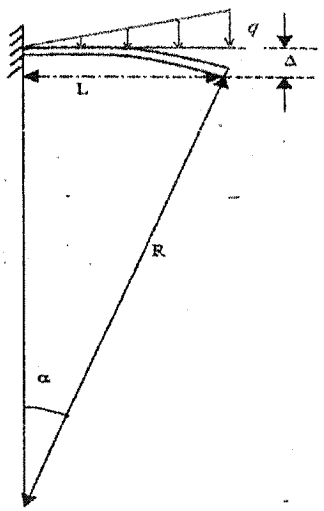


**Figure 3.10 Pipe Load at the Situation of Pipe Displacement Change**

In this condition, the max stress is

$$\sigma = \frac{MD}{2I} = \frac{\frac{20EI}{11R}\frac{D}{2}}{I} = 0.909\frac{ED}{R} \tag{3.6}$$

Thus, as the drill rod passes through the borehole is subjected to different stress conditions according to whether the drill path is straight or curved, the position of the drill rod in the drill string, and the location of a section of drill rod with respect to the entry and exit points of borehole curvature. Furthermore, this simplified approach neglects the influence on drill rod curvature of the changes in cross-section of the pipe at and near the drill pipe joints and effects on curvature due to the thrust within the drill rod during the drilling process (e.g. helical buckling within the borehole). More complex analyses are necessary to evaluate the effect of changes in cross-section, buckling conditions and variable curvature on the fatigue conditions in the drill pipe.

To study the issue of stress change caused by the change of cross-section near the joint area, a Finite Element Analysis was carried out.

The following Table 3.1 provides the comparison of the two models in the FEA model. Model 1 considers the change of cross-section near the joint area and uses 3 sections of drill pipe (Fig.3.1); Model 2 (Fig.3.11) ignores the change of cross-section near the joint area and hence uses a continuous cross-section as shown in Figure 3.11.

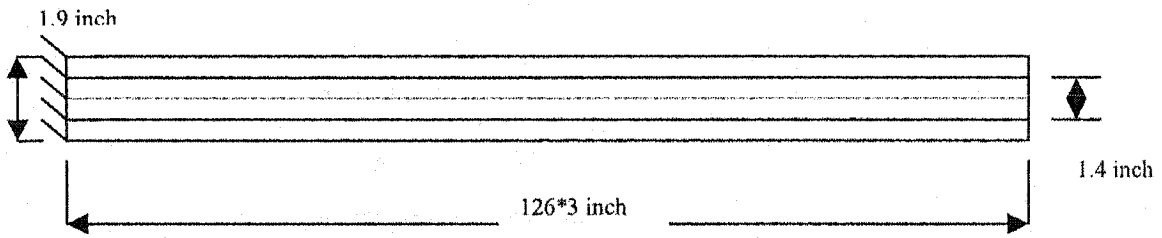


**Figure 3.11 Model 2 Used in FEA**

**Table 3.1 Comparison of Stress Condition under Two Models**

| | Model | Maximum stress |
|---|---|---|
| bending pipe 10 in displacement | model 1 | 48852 psi |
| | model 2 | 48728 psi |
| pulling pipe 0.5 in displacement | model 1 | 19800 psi |
| | model 2 | 20599 psi |

From the results, we can conclude that the cross-section change in a mini-HDD pipe does not have a large effect on the maximum stress caused by varying curvature. In practice, most failure does not happen in the area of change of cross-section, but happens at the joint area.

## 3.5 Stresses Caused by Axial Forces

### 3.5.1 Tensile Axial Loading

Tension in the drill pipe develops mainly during pullback caused by the frictional force on the drill string and product pipe (or utility lines) and the resistive force at the cutting face of the reaming assembly.

### 3.5.2 Compressive Axial Loading

Compression in the drill pipe provides the thrust for the drill bit during the pilot hole boring process. As mentioned above, because the drill pipe is very slender compared to its length, it will try to buckle and will be restrained by the walls of the borehole. Buckling of the drill pipe during drilling typically assumes a helical buckling configuration (Zhou, 1998). The consideration of helical buckling conditions is not attempted in the current research.

### 3.5.3 Stress Computation

If we know the pullback or thrust, the axial stress is given by the standard equation

$$\sigma = \frac{F}{\frac{\pi}{4}(D^2 - d^2)} \tag{3.7}$$

Where D is the outside diameter of the pipe

d is the inside diameter of the pipe

F is the pullback or thrust force

$\sigma$ is the maximum axial stress in the drill string

When a certain drill rig capacity for thrust or pullback is available, it is commonly used by field crews to try to overcome any obstacles or other difficulties. This means that, even when a drill rig is oversized, it is important to match the drill rod not only to the calculated design thrusts and pullback but also to the capability of the rig. Furthermore, in design guidelines for horizontal directional drilling, it is typically suggested that, when checking the adequacy of drill rods against axial stresses, a safety factor be used of at least twice the maximum thrust or pull back capability of the drill rig (e.g.,USCE et al., 1995). This safety factor is used to account for transient loads and other loads that are difficult to estimate.

Thus, for maximum axial stress design in the drill rod, it is appropriate to use

$$\sigma = k\frac{F}{\frac{\pi}{4}(D^2 - d^2)} \tag{3.8}$$

Where D is the outside diameter of the pipe

d is the inside diameter of the pipe

F is the pullback or push force

k is safety factor (between 2~3)

$\sigma$ is the maximum stress in the drill string

This stress, however, would only be appropriate for use in combination with bending and torque stresses in a fatigue analysis under particular conditions. If high-cycle fatigue is expected, this stress would be inappropriate because it does not represent a typical operating stress condition during drill rod rotation. It would only be appropriate if

the temporary stress conditions were so severe as to cause low-cycle fatigue in combination with the bending and torque stresses.

### 3.6 Shear Stresses Caused by Torque

The shear stress is given by the following formula:

$$\sigma = \frac{TD}{\pi (D^4 - d^4)} \tag{3.9}$$

where T is the torque on the drill string

D is the outside diameter of the drill string

d is the inside diameter of the drill string

$\sigma$ is the maximum stress in the drill string

If the torque acting on the drill string is known, this formula can used to compute the shear stress in the pipe caused by the torque. It is more difficult, however, to determine how the combined effect of axial stress, varying bending stress, and torque affect the fatigue life of the drill steel.

# CHAPTER 4

# FACTORS THAT DOMINATE FATIGUE FAILURE

Drill string failure continues to a major concern in HDD practice in the trenchless technology industry. Field drill string failure is mainly caused by fatigue. Among the bending, thrust/pull and torque influences on fatigue failure, it is useful to try to determine which has the greatest impact. This chapter examines this question.

## 4.1 Data from Controlled Field Tests

In 1993, a series test of mini-HDD systems were undertaken at the US Army Corps of Engineers Waterways Experiment Station in Vicksburg, Mississippi. In 1994, a mini-HDD field demonstration was held at the Holiday Inn in the University of Central Florida, Orlando, Florida.

In the above two tests, different types of data were recorded. These data include thrust/pullback force, rotational torque, drilling fluid pressure, etc. In this chapter, the data from these tests are analyzed to help decide which factor would have been the controlling factor in deciding the fatigue failure during this type of drilling.

## 4.2 Stress Comparison

### 4.2.1 Thrust/Pull Force

Figure 4.1 shows the thrust for the Bor-Mor 750 and Ditch Witch 4/40a Jet Trac drill rigs passing through Silty Sand in Orlando (after Abdus, 1995).

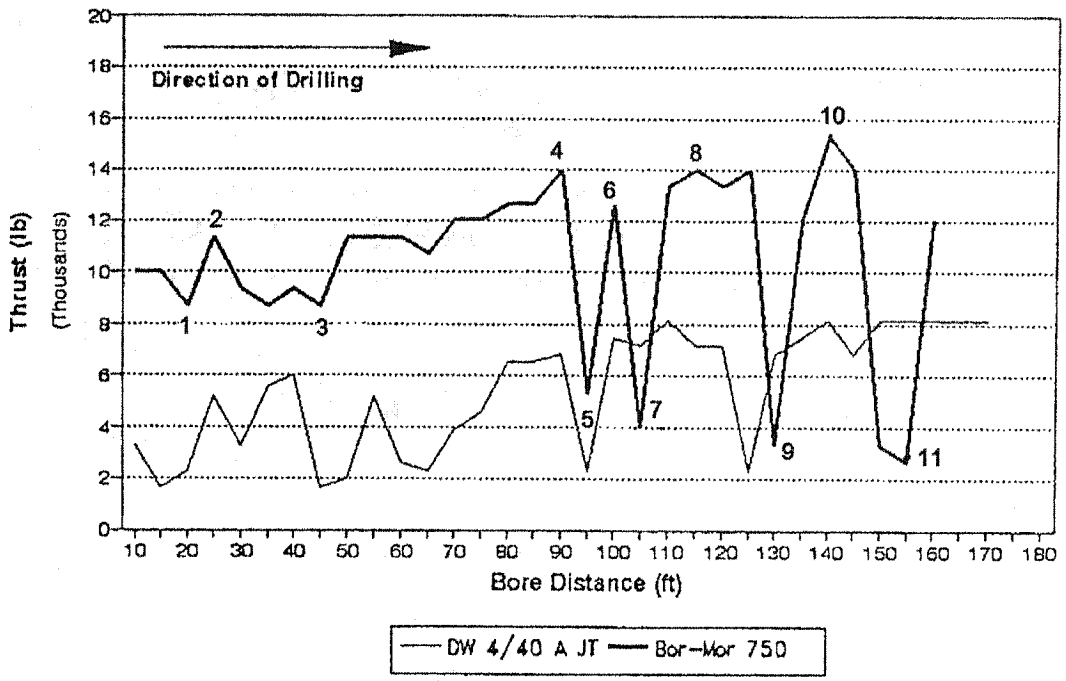


**Figure 4.1 Thrust Variation in Silty Sand Soil for Ditch Witch 4/40 A JT & Bor-Mor 750**

In order to evaluate the fatigue effect, a method called peak counting is used. The Bor-Mor 750 data is used since it yields a larger stress.

**Table 4.1 Peak Count of Thrust Variance**

| Peak | Range (1000 lb) |
|---|---|
| 1—2 | 2 (too small can be ignored) |
| 2—3 | 5 (too small can be ignored) |
| 3—4 | 10 |
| 4—5 | 9 |
| 5—6 | 11 |
| 6—7 | 12 |
| 7—8 | 10 |

The pipe would have been in the range of 1.25 to 1.75 in diameter. For the purposes of calculation, 1.625 OD and 1.245 ID are assumed, so the maximum thrust variation will be

$$\sigma_{trust\_var} = \frac{12000}{A} = 14000 psi$$

From Table 4.1, the average thrust stress is about 12,400 psi, and the number of cycles is 5.

### 4.2.2 Torsion

The following figure is the variation of Maximum Torque for the Bor-Mor 750 and Ditch Witch 4/40a Jet Trac during the pilot hole boring through Silty Sand in Orlando(after Abdus 1995).

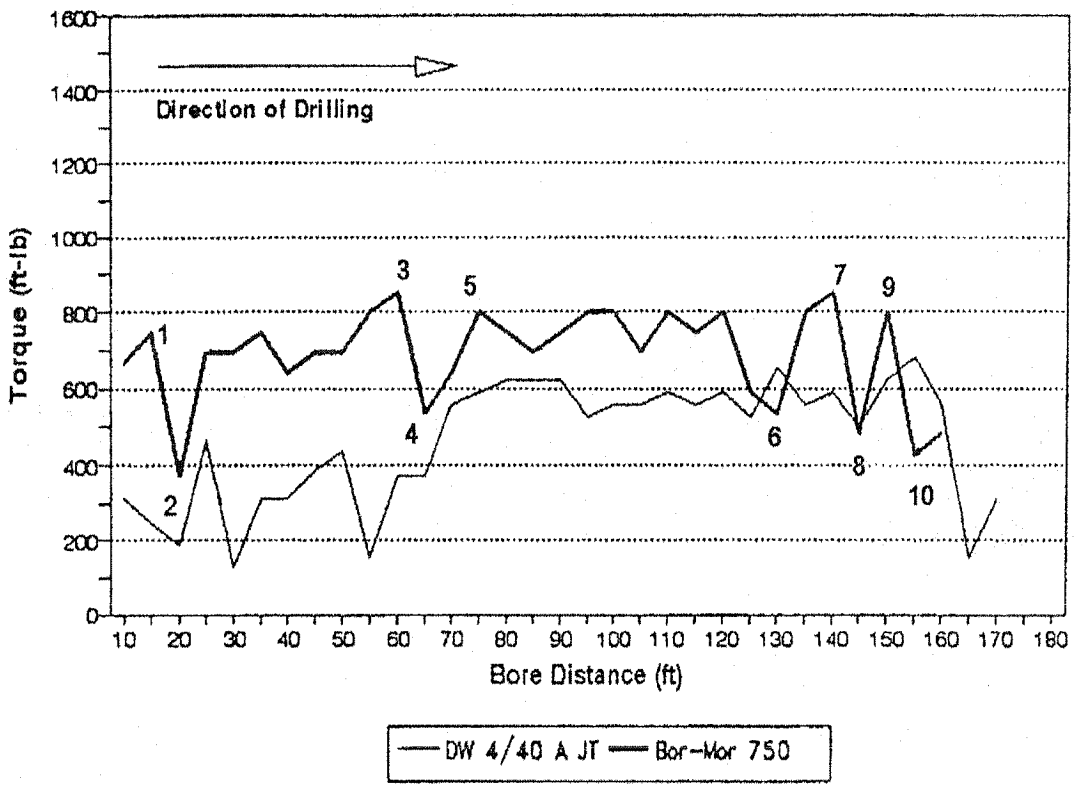


**Figure 4.2 Drilling Torque Variation in Silty Sand for Ditch Witch 4/40 A JT & Bor-Mor 750**

In order to evaluate the fatigue effect, the peak counting method is also used here, and, again, the Bor-Mor 750 data are used as it yields larger stresses.

**Table 4.2 Peak Count of Torque Variance**

| Peak (ft-lb) | Torque variance (ft-lb) |
|---|---|
| 1—2 (800 to 400) | 400 |
| 2—3 (400 to 850) | 450 |
| 3—4 (850 to 500) | 350 |
| 4—5 (500 to 800) | 300 |
| 5—6 (800 to 500) | 300 |
| 6—7 (500 to 850) | 350 |
| 7—8 (850 to 500) | 350 |
| 8—9 (500 to 800) | 300 |
| 9—10 (800 to 450) | 350 |

Stress will be computed by the following equation:

$$\tau_{torque\_var} = \frac{T}{W} \tag{4.1}$$

Where T is torque

$$W = \frac{\pi}{16} D^3 (1 - a^4)$$

D is the outside diameter of drill pipe

a is the ratio of inside diameter of drill pipe to outside diameter of drill pipe

as the drill pipe is assumed to be 1.625 OD, 1.245 ID, the maximum stress variation will be

$$\tau_{torque\_var} = \frac{400 * 12}{\frac{\pi}{16} * D^3 * (1 - a^4)} = 8696 psi$$

From Table 4.2, the average torque is about 600 ft-lb and hence the average shear stress is 13,044 psi. The number of cycles is 10.

### 4.2.3 Bending

In the two tests, the radius of curvature of the drill pipe is 100 ft, so the variation in bending stress can be computed (using the standard formula with R in feet) as

$$\sigma_{bending\_var} = 2 \times \frac{ED}{2R \times 12} = \frac{ED}{12R} \tag{4.2}$$

where R is the bending radius in feet

D is the outside diameter of the drill pipe in inches

E is the Elastic Modulus of Steel in psi

Here R=100 ft

D=1.625 in

$$\sigma_{bending\_var} = \frac{ED}{R \times 12} = \frac{29000000 \times 1.625}{100 \times 12} psi = 39270 psi$$

The number of cycles cannot be calculated without more data on drill rig operations, but it will be in the thousands of cycles.

### 4.2.4 Comparison of the Fatigue Effects from the Various Stress Cycles

When comparing fatigue life influences of torque, bending, and thrust, it is important to consider that each stress does not have the same impact on fatigue life. Prior research on fatigue has addressed this issue, and load factors have been derived to account for the different influences on fatigue life (Robert, 1991). For example, a torque stress will have bigger influence on fatigue life than the same amount of stress as a bending stress. Applying the published load factors to the stresses calculated for the Orlando field trial yields the adjusted stresses shown in Table 4.3

**Table 4.3 Comparison of the Influence of Stresses Caused by Thrust, Torque, and Bending**

| Stress Type | Maximum Stress Variance (psi) | Load Factor | Maximum Stress After Adjustment (psi) |
|---|---|---|---|
| Thrust/Pulling | 14,000 | 1.11 | 15,400 |
| Torque | 8,696 | 1.72 | 14,957 |
| Bending | 19,635 | 1.0 | 19,635 |

For the Orlando field trial, the maximum stresses after adjustment do not have a very large difference. However, when the number of stress cycles is considered and the fact that the stress variation in each rotation for bending stresses is twice the maximum stress, it is clear that bending stress variation with its number of cycles in the thousands is the primary influence on high-cycle fatigue. It must be remembered, however, that the torque and thrust/pullback contribute to the combined stress condition in the drill rod and that very high overall stress levels or high peaks close to the yield stress may cause direct failure of the drill rod or low-cycle fatigue failure.

Table 4.4 provides examples of the tensile and torque resistance of various sizes of drill rod provided by one manufacturer.

**Table 4.4 The Dimensions and Force Capabilities of HDD Drill Pipe from Drilltube, Inc.**

| OD | Wall | Tube ID | Upset | Length | Torsional (ft-lbs) | Tensile (lbs) | Connections | Connection OD | Connection ID |
|---|---|---|---|---|---|---|---|---|---|
| 1.100 | 0.190 | 0.720 | IEU | 4' 11" | 1385 | 73330 | Ditch Witch | 1.750 | 0.310 |
| 1.350 | 0.190 | 0.970 | IEU | 6' 6" | 2300 | 93475 | Ditch Witch | 2.000 | 0.375 |
| 1.625 | 0.190 | 1.245 | IEU | 10' | 3585 | 115635 | Ditch Witch | 2.000 | 0.375 |
| 1.660 | 0.240 | 1.180 | IEU | 6' | 4342 | 144539 | Firestick | 1.875 | 0.750 |
| 1.900 | 0.240 | 1.420 | IEU | 10' | 6015 | 168968 | Case | 2.625 | 0.875 |
| 1.900 | 0.240 | 1.420 | IEU | 10' | 6015 | 168968 | Firestick | 2.125 | 0.875 |
| 2.063 | 0.240 | 1.583 | IEU | 9' 10" | 7311 | 185559 | Ditch Witch | 2.500 | 0.625 |
| 2.063 | 0.240 | 1.583 | IEU | 10' | 7311 | 185559 | Case | 2.625 | 0.875 |
| 2.063 | 0.240 | 1.583 | IEU | 10' | 7311 | 185559 | Firestick | 2.250 | 0.875 |
| 2.210 | 0.270 | 1.670 | IEU | 9' 10" | 9272 | 222152 | Ditch Witch | 2.750 | 0.625 |
| 2.375 | 0.281 | 1.813 | IEU | 10' | 11277 | 249556 | Firestick | 2.625 | 0.875 |
| 2.375 | 0.281 | 1.813 | IEU | 10' | 11277 | 249556 | QD65 | 2.625 | 0.988 |
| 2.375 | 0.281 | 1.813 | IEU | 10' | 11277 | 249556 | 2" IFDS | 2.625 | 0.875 |
| 2.375 | 0.281 | 1.813 | IEU | 15' | 11277 | 249556 | Firestick | 2.625 | 0.875 |
| 2.563 | 0.330 | 1.903 | IEU | 14' 10" | 14930 | 312457 | Ditch Witch | 3.250 | 1.250 |
| 2.875 | 0.362 | 2.151 | IU | 10' | 20798 | 385821 | QD65 | 2.875 | 0.938 |
| 2.875 | 0.362 | 2.151 | IU | 10' | 20798 | 385821 | Mayhew Junior | 2.875 | 1.250 |
| 2.875 | 0.362 | 2.151 | IU | 10' | 20798 | 385821 | PACDS | 2.875 | 1.250 |
| 2.875 | 0.362 | 2.151 | IEU | 15' | 20798 | 385821 | Firestick | 3.250 | 1.150 |
| 3.500 | 0.449 | 2.602 | IEU | 15' | 37954 | 560996 | Firestick | 3.625 | 1.500 |
| 3.500 | 0.449 | 2.602 | IEU | 15' | 37954 | 560996 | 2-7/8 IF | 4.125 | 1.750 |
| 3.625 | 0.330 | 2.965 | IEU | 14' 10" | 33540 | 461163 | Ditch Witch | 4.000 | 1.500 |
| 4.000 | 0.330 | 3.340 | IEU | 15' | 41918 | 513647 | DS38 | 4.750 | 2.438 |
| 4.000 | 0.330 | 3.340 | IU | 20' | 41918 | 513647 | 2-7/8 IF | 4.125 | 1.750 |
| 5.000 | 0.362 | 4.276 | IU | 20' | 74100 | 712072 | 3-1/2 IF | 5.000 | 2.438 |
| 5.000 | 0.362 | 4.276 | IU | 20' | 74100 | 712072 | DS38 | 5.000 | 2.438 |
| 5.500 | 0.362 | 4.276 | IU | 20' | 94161 | 788837 | DS40 | 5.000 | 2.688 |
| 6.625 | 0.362 | 5.901 | IU | 30' | 137331 | 961558 | DS50 | 6.625 | 2.750 |
| 6.625 | 0.362 | 5.901 | IU | 30' | 137331 | 961558 | NC50 | 6.625 | 2.750 |
| 6.625 | 0.362 | 5.901 | IEU | 30' | 137331 | 961558 | DS55 | 8.250 | 4.000 |
| 6.625 | 0.362 | 5.901 | IEU | 30' | 137331 | 961558 | DS65 | 8.500 | 4.250 |

Referencing the Drilltube drill pipe with an O.D of 1.625 in, the torsion capability of the drill rod is 3,585 ft-lb. This compares to a maximum recorded torque in Orlando of 850 ft-lb and an average torque of 600 ft-lb and a torque variation of 400 ft-lb. Thus the maximum torque is less than 25% of the torque capability of the drill string. If the maximum torque for the drill rod were used in practice, the combined stresses could cause a direct or low-cycle fatigue failure very quickly.

Maximum torque stresses should not occur in normal operating conditions in which drilling mud is used. But if the drill suddenly encounters hard earth or even rock and the drill bit is stalled, then the drill rig may apply its maximum torque and, in

addition, transient effects may be present. This reinforces the earlier discussion that the drill rod should be sized with a significant safety factor over the capability of the drill rig.

# CHAPTER 5

# FATIGUE TEST EXPERIMENT SETUP

This chapter describes the experimental apparatus which was developed specifically for this research. The physical test configuration and equipment are described first. The instrumentation and data acquisition are described in the last section of this chapter.

## 5.1 Setup of Fatigue Test Apparatus

A fatigue test apparatus was constructed in a little-used storage building at Louisiana Tech University. The Trenchless Technology Center obtained the use of this building for the fatigue experiments so that the fatigue tests could run unattended and there would be little chance of physical injury to a person or adjacent equipment caused by the fatigue failure of the curved drill string. Sensors and controls (described with the instrumentation) were added to the test setup so that a failure could be detected and the torque motor shut down automatically. The test apparatus was designed so it can apply rotation to a drill string held in a curved configuration. Through the use of a hydraulic brake, it was also possible to apply a resisting torque to the drill rod although this feature was not used during the tests conducted for this research. The initial design and

specification for the test apparatus was carried out by Dr. Paul Hadala, and the author continued the development of the apparatus and test procedures following the retirement of Dr. Hadala.

In order to include both plain drill rod and drill rod joints in the central test region away from end effects at the torque motor and the hydraulic brake, a 30-ft length of drill rod was provided for in the test setup. This allowed for three 10-ft drill rods to be used – with the center drill rod and the two intermediate joints being well away from the motor and brake.

Although it may seem at first sight a simple activity to bend a drill rod into a constant curvature and hold it in that position with pillow blocks (roller bearings through which the drill rod passes). It is not so simple either in theory or in practice. For example, a classic simply supported uniform beam with one-third point loading would maintain a constant bending moment and hence a constant curvature in the center section. However, in the application for the drill rod testing, the curvature required in the testing produces deflections that are far from the small deflections on which the first order bending theory is based. In addition, the application point for forces through the pillow blocks would coincide with the thickened joint region of the drill rod. Finally, the non-uniform cross-section of the drill rod (thickened in the joint regions) means that the curvature changes locally in the region of the joints. In the final design of the test configuration, the 30-ft long rotating drill rod was supported by four pillow blocks to maintain a curved shape with approximately a constant curvature.

The test configuration design adopted is shown in Figure 5.1. It consists of a three-phase AC induction motor, an in-line gear reducer to reduce the shaft speed, a

series of bearings (pillow blocks), support structures for the pillow blocks to keep the drill rod level, and a reaction system to supply torsion resistance (a brake) at the far end.

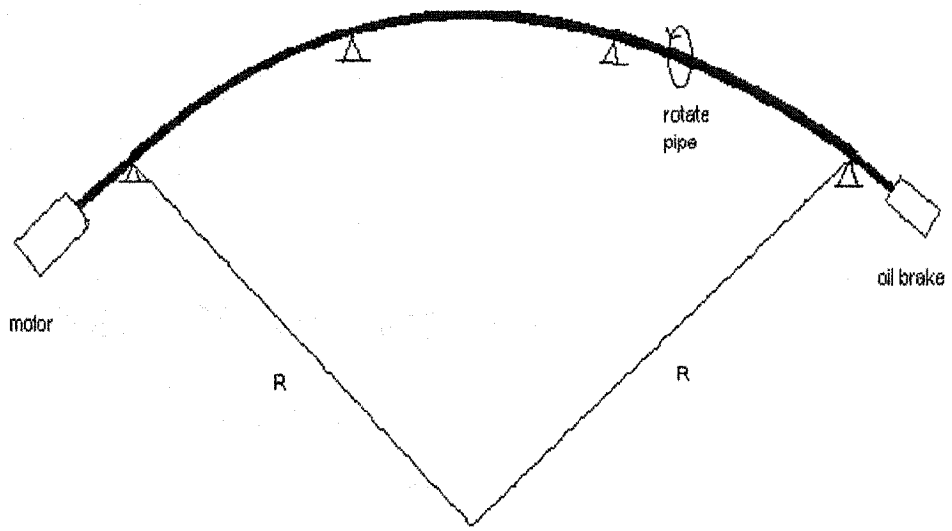


**Figure 5.1 Fatigue Test Machine Design Concept**

When it was first built, the test machine was desired to be able to achieve a bending stress of more than 0.5 of the yield strength of the drill steel. The target stress level was selected as 70,000 psi. A bending radius of about 40 ft is required to achieve this stress. The early tests using the apparatus were run at this curvature, but, after the first several tests, it was found that the fatigue life was very short under this severe curvature. The anchors for the pillow blocks and the placement of the hydraulic brake were then modified to increase the potential bending radius to over 100 ft. This radius corresponds to the bending limit prescribed by some manufacturers for their mini-HDD drill pipes. In order to accommodate the larger curvatures, the support tables had to be extended and provided a curvature test range of up to 110 ft.

### 5.1.1 Motor Selection

The available electrical power in the lab was a 208V, 3-phase 100 amp service. The easiest type of motor to control is an induction motor which has a speed which is nearly constant under varying load. The most common induction motors operate at 1750 RPM under full load. The actual motor used was a Reliance Model P25G 3330 (Fig 5.2).

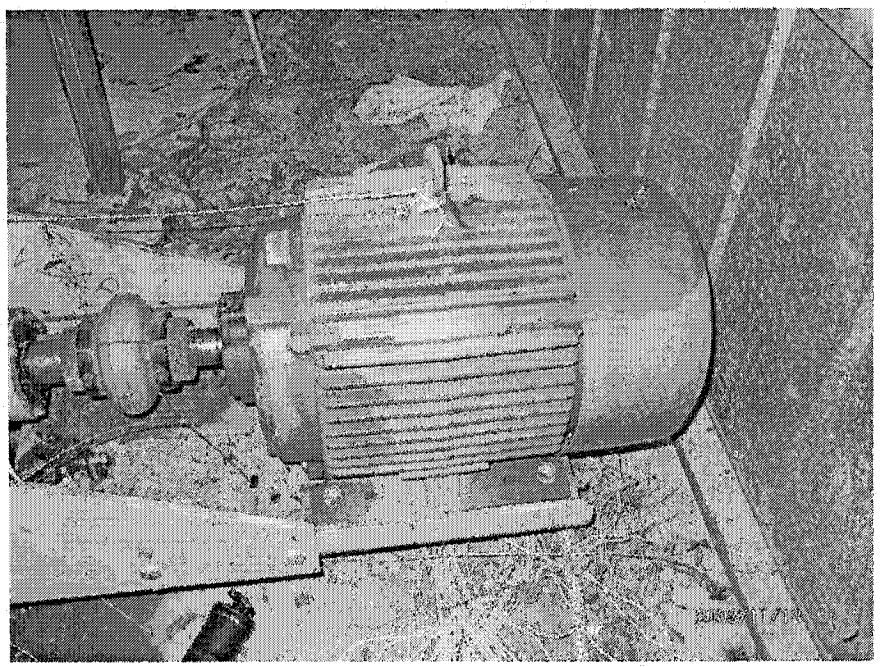

**Figure 5.2 Induction Motor to Provide Torque and Rotation**

### 5.1.2 Gear Speed Reducer

Depending on which operating speed was needed, either a 30:1 or 60:1 speed reducer could be used. It was decided to use an inline speed reducer, and commercial sources were researched extensively until a reducer was found that would operate in this speed and horsepower range. The device procured was a Rex-Atlas Planetary Speed Reducer Model AABA0066 with a gear ratio of 32.94 to 1 and a 15 speed reduction (Fig.

5.3). This system has an available modification kit which when installed yields a 56.18 to 1 speed reduction.

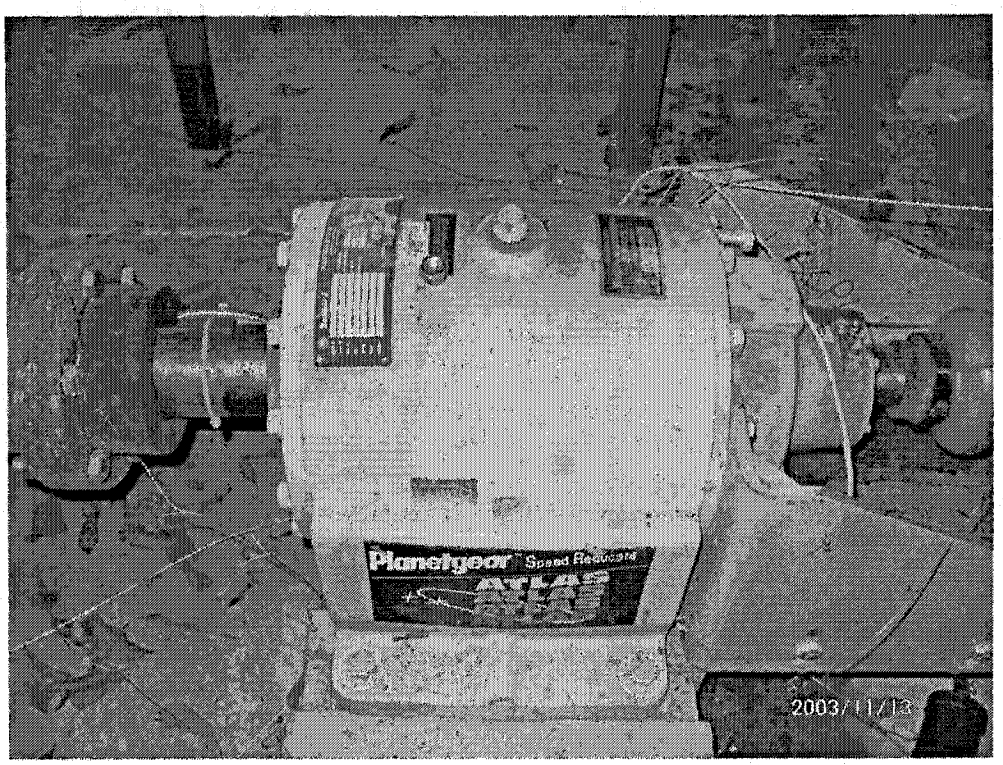


**Figure 5.3: Gear Speed Reducer**

### 5.1.3 Support System

Several steel tables were used at the pillow block locations to allow the curvature of the drill rod to be adjusted without drill holes in the floor at each location and also to place the pillow blocks at the correct height so that the drill rod was maintained in a horizontal plane. In the initial configuration, it was 3 inches high and ranged from 18in*18in to 24in*72in in top surface dimensions.

After the purchase of the oil brake (which had a long delivery time), the height of the steel tables and motor needed adjustment to about 6 inches height to fit the height of the oil brake. As mentioned earlier, after the initial fatigue tests, an increase in test radius

was made and the steel tables had to be extended to change from support of a test curve of 40 ft (low-cycle fatigue) to cover the ability to test curves over 100 ft in radius (high-cycle fatigue).

These steel tables were anchored to the concrete floor with bolts and brought to the same elevation (Fig.5.4).

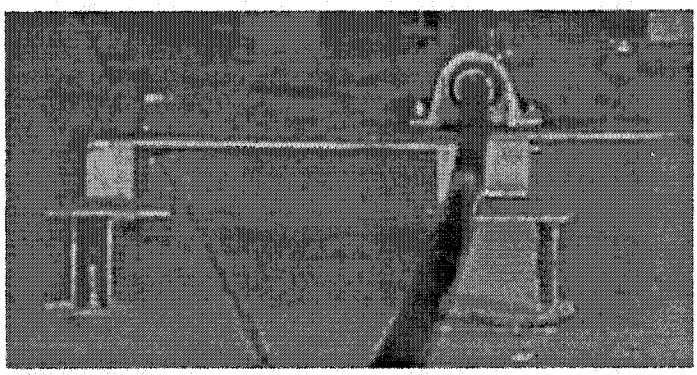

**Figure 5.4: A Steel Support Table, Pillow Block, and Drill Rod**

A pillow block (a bearing which employs internal ball bearings) was placed on each of these tables (Fig. 5.4). The pillow blocks permit the drill rod to rotate and bend while restricting its lateral movement to zero at specific points. They enforce an overall deformed shape of approximately constant radius.

The pillow blocks used here have a diameter of 2.0 inches; this diameter is slightly larger than the maximum diameter (at the joints) of the pipes donated by Drilltube Inc. and the pipes donated by Texas Pup -- both of which have a maximum outside diameter of 1.9 in.

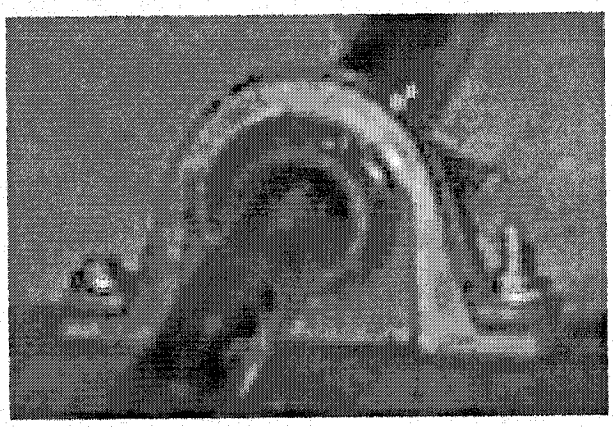

**Figure 5.5 Pillow Block**

### 5.1.4 Deformed Shape Control

It is assumed that the x and y coordinates of the center of each pillow block can be calculated from trigonometry under the assumption that the deformed shape is an arc of a circle. This assumption is not strictly true as the rod is slightly bent between the gear box and the first pillow block, and, in addition as discussed earlier, even the precise positioning of the pillow blocks does not result in a uniform curvature.

To maintain as close as possible to a uniform curvature in the center section of the drill rod, the following procedure was adopted for the experimental setup for each test. After the theoretical computation of required position, the pillow block was set in place at this location. Strain gauges were then applied to the drill rod at 8 locations before the drill rod was inserted and bent into position. The strain gauge readings and the large variation among the gauge readings indicated that the pillow block positions would have to be adjusted to provide a more constant curvature. This was carried out by keeping the strain gauges on the pipes and adjusting the curve by trial and error using the strain gauge

readings to indicate the drill rod curvature at each location. This procedure was continued until an acceptable constant curvature was obtained at each strain gauge location.

The gauges were bonded on the surface of the rod assembly at numerous locations as shown in Table 5.1.

**Table 5.1 Gauge Placement**

| Gauge Number | Distance from the Gear Box (in) | Remarks |
|---|---|---|
| 1 | 104 | |
| 2 | 124 | Joint at 126.5 in |
| 3 | 144 | |
| 4 | 164 | |
| 5 | 184 | |
| 6 | 204 | |
| 7 | 224 | |
| 8 | 250 | Joint at 246.6 in |

The gauges used were 120 ohm temperature compensated foil strain gauges. The surface of the rod was stripped of paint and worked with finer increasingly emery paper. It was then cleaned with alcohol and cotton, and the gauge was glued to the surface using glue recommended by the gauge manufacturer (Measurement Group, Inc.)

The gauges were applied in a cold, damp environment and one gauge showed an abnormal reading which was neglected.

The initial resistance (in ohms) of each gauge was read in the unbent position ($R_0$), the rod was bent to the nominal radius and the resistance $R_i$ was read. Strains were computed as

$$\varepsilon = \frac{R_i - R_0}{2(GF)R_0} \tag{5.1}$$

where GF is the gauge factor (for this gauge, it is 2.055)

The strain data are given in Table 5.2.

Using this method, 5 curves were made. Fig 5.6 is the strain gauge readout configuration. Fig 5.7 is the attachment of gauge.

**Figure 5.6 Strain Gauge Readout Configuration**

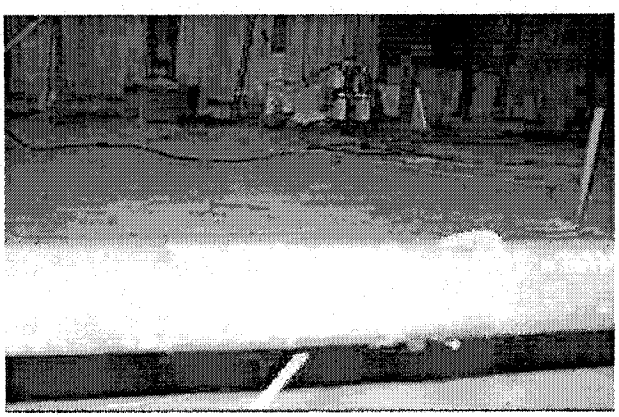

**Figure 5.7 Attachment of the Gauge**

**Table 5.2 Strain Gauge Readouts**

| | Curve 105 | Curve 95 | Curve 73 | Curve 59 | Curve 40 |
|---|---|---|---|---|---|
| Gauge 1 | 0.000757 | 0.000829 | 0.001020 | 0.001339 | 0.000468 |
| Gauge 2 | 0.000804 | 0.000863 | 0.001133 | 0.001421 | 0.000985 |
| Gauge 3 | 0.000749 | 0.000772 | 0.001080 | 0.001517 | 0.001425 |
| Gauge 4 | 0.000733 | 0.000785 | 0.001073 | 0.001330 | 0.001994 |
| Gauge 5 | 0.000838 | Bad reading | Bad reading | Bad reading | 0.001586 |
| Gauge 6 | 0.000727 | 0.000774 | 0.001079 | 0.001294 | 0.002012 |
| Gauge 7 | 0.000754 | 0.000866 | 0.001175 | 0.001329 | 0.001449 |
| Gauge 8 | 0.000680 | 0.000810 | 0.001072 | 0.001127 | 0.002004 |

The stain data were also converted into the nominal radius at each point and these data are provided in Table 5.3.

The nominal curves were computed as:

$$R = \frac{D}{2*12*\varepsilon} \tag{5.2}$$

where ε is the peak strain developed in pipe

E is the modulus of elasticity

R is the radius of curvature of bends (ft)

D is the pipe outside diameter (inch)

**Table 5.3 Nominal Radius at Each Gauge Point**

| Curve | Gauge 1 | Gauge 2 | Gauge 3 | Gauge 4 | Gauge 5 | Gauge 6 | Gauge 7 | Gauge 8 |
|---|---|---|---|---|---|---|---|---|
| 105 ft | 104.58ft | 98.48ft | 105.76ft | 108.01ft | 94.48ft | 108.82ft | 105.0ft | 116.5ft |
| 95ft | 95.5 ft | 91.4ft | 102.54ft | 100.85ft | NA | 102.23ft | 91.40ft | 97.79ft |
| 73ft | 77.62ft | 69.88ft | 73.72ft | 73.84ft | NA | 73.34ft | 67.4ft | 73.84ft |
| 59ft | 59.14ft | 55.7ft | 52.19ft | 59.54ft | NA | 61.20ft | 59.57ft | 70.23ft |
| 40ft | 169.33ft | 80.36ft | 55.53ft | 39.69ft | 48.84ft | 39.54ft | 54.62ft | 39.51ft |

### 5.1.5 Control System

A control system was developed that could stop the machine when the pipe is broken or the machine is overheated. The system also can record the current number of revolutions of the rod, the date and time, and the number of revolutions at shutdown.

This functional control was provided by PLC hardware and software called DirectSOFT32. Visual Basic (VB) software was created with the help of Dr. Eads from the Electrical Engineering program to create the connection between the computer monitor output and the data read from DirectSOFT32 which, in turn, read data from the PLC hardware. Fig 5.8 is the control computer and Fig 5.9 is the PLC control system.

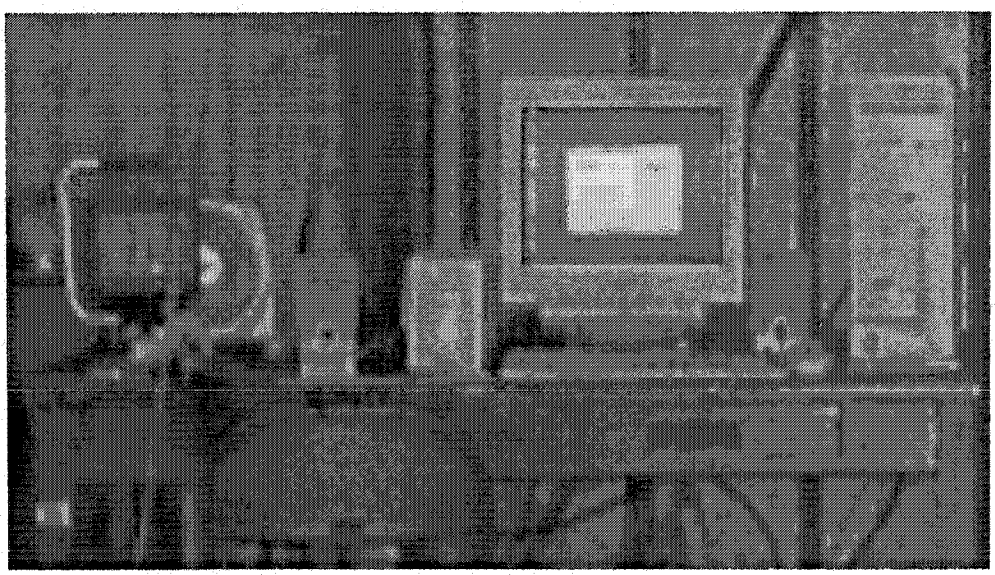

**Figure 5.8 Control Computer**

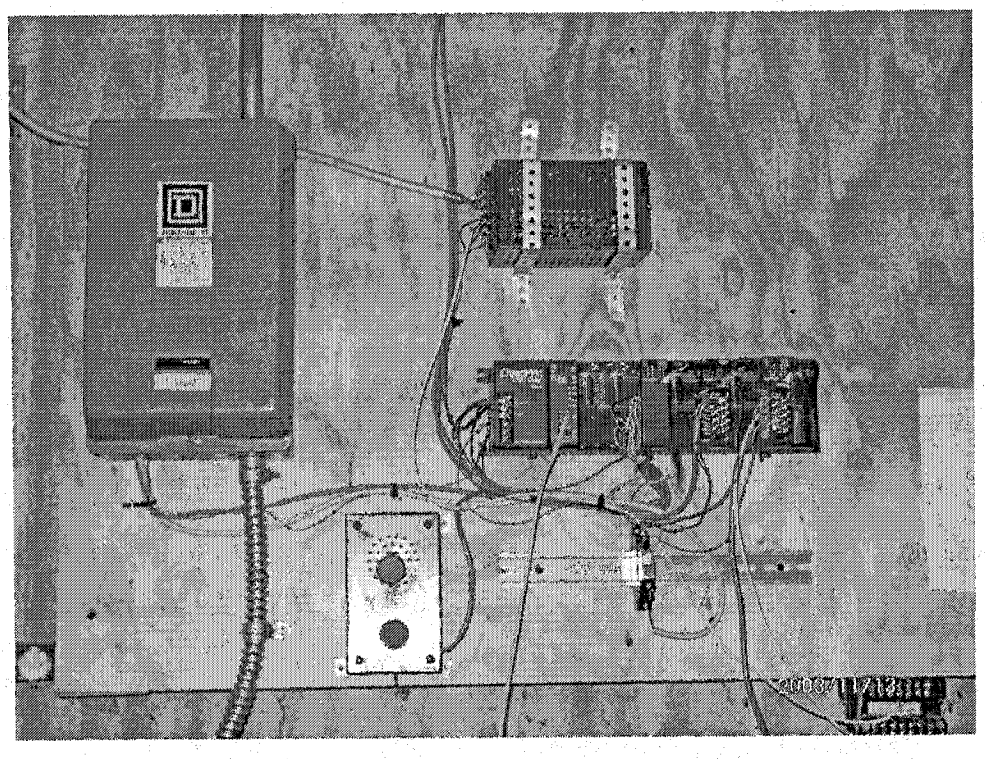

**Figure 5.9 PLC Control System**

## 5.2 The Fatigue Test Process

### 5.2.1 Make Up Torque

In the first group of tests, the pipe donated by Texas Pup, Inc. was used. Those tests were used to adjust the machine and to get some experience with operation of a fatigue test. Not much attention was paid to the correct make up torque because the necessary torque wrenches were not available during the preliminary setup. It was quickly discovered that, as is stressed in drilling practice, the proper make up torque does make a large difference in fatigue performance of drill rods.

In normal practice, the connection is torqued to about 60% of its capacity. In this preliminary test, only about 250 lb-ft torque was applied using a 3-ft long pipe wrench.

This was not enough for the proper make up torque, and failure occurred at only 663 revolutions at the joint location.

After some adjustments and extending the handle of the pipe wrench with a piece of steel pipe (Fig.5.10), it was possible for one person to apply 750 lb-ft torque to make up the joint.

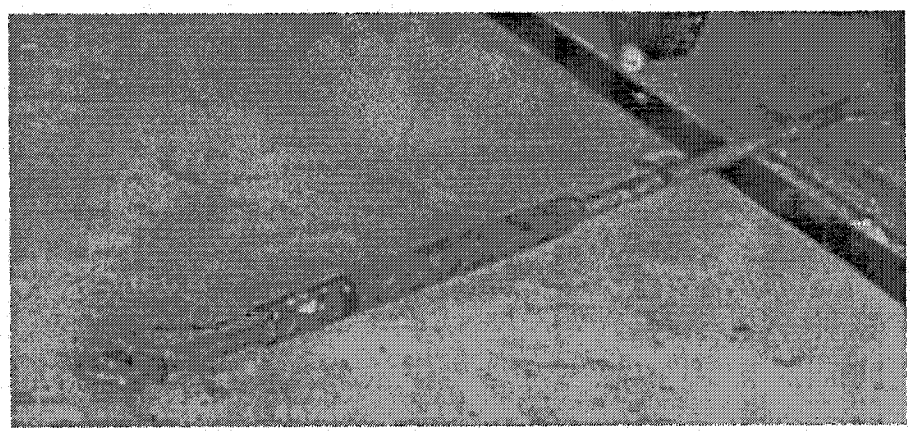

**Figure 5.10 Extended Pipe Wrench**

Use of the right make up torque also shifted the fatigue failure location. For the drill rod made by Texas Pup, Inc., all the failures occurring after the increase in make up torque happened in the pipe body instead of the pipe joint.

### 5.2.2 Lubrication

Lubrication is also very important in the make up process. A joint without lubrication has a large resistance in the make up process, and, even under the right makeup torque, the joint shoulders may still not be in contact because of the friction. For friction between two steel surfaces, the coefficient of friction is 0.74 under the static condition, but, if lubricated, the coefficient of friction is only 0.07 – allowing the make up torque to go into shoulder contact between the joint faces rather than overcoming drill thread friction. If the shoulders are not in contact from poor make up procedures, then

excessive forces are transferred to the threads. This will gall the threads, cause the connection to distort in the hole, and can increase the chance of snapping a pin tool joint. Over-torqueing should also be prevented as this can cause the box end to swell and the connection can lose its shouldering capability.

### 5.2.3 Operation and Maintenance

**5.2.3.1 The Bending of Pipes.** After connecting the three pipes into the machine and using proper make up torque and lubrication, the next step is to bend the pipe into the required curvature. The process was undertaken very carefully, and safety procedures were used to prevent the chance of injury when bending the drill rod into shape and fixing it in position.

After the pipe was bent into the right curvature, the pillow blocks were bolted to the steel table to maintain this alignment (Fig. 5.11).

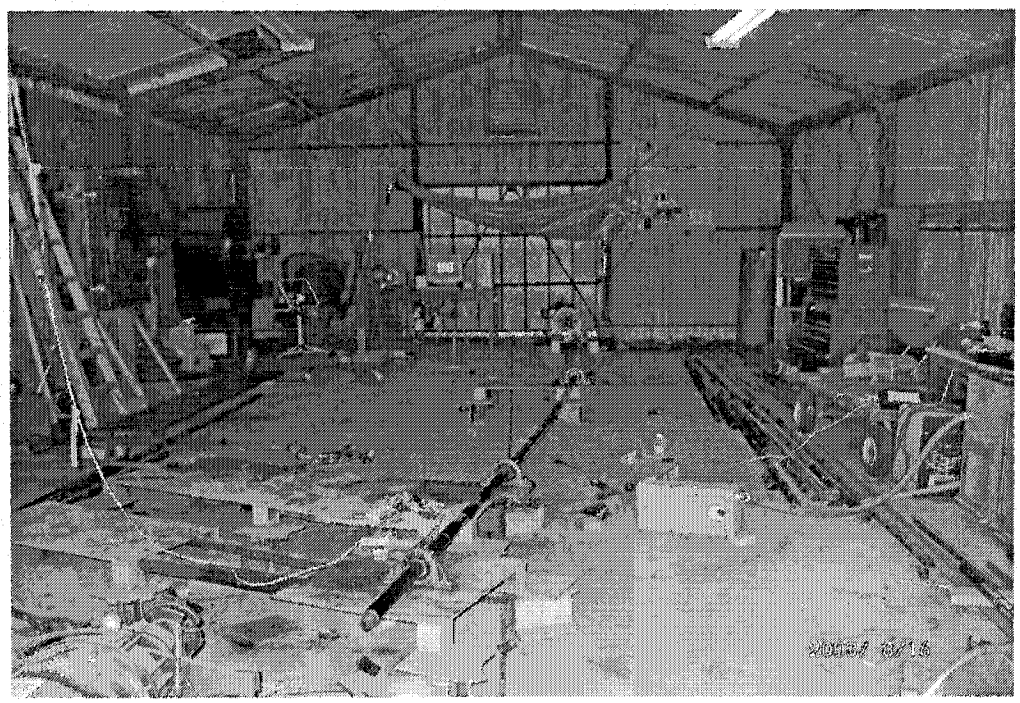

Figure 5.11 Drill Rod Held in a Curved Profile

**5.2.3.2 Adjust Reflection Mirror.** A laser beam generator and reflection mirror were installed at each end of the drill pipe test configuration. These laser beams and mirrors had two functions:

1. To record the number of revolutions: in each revolution, the laser beams are reflected once by the reflection mirror attached at the surface of the pipe. The electrical signal is send to the PLC and finally recorded in the computer.
2. If the pipe snaps, the number recorded by the two different reflection mirrors (Fig.5.12 and Fig 5.13) will be different as one part is broken and stops moving and another part is still moving. This will create the signal to stop the machine.

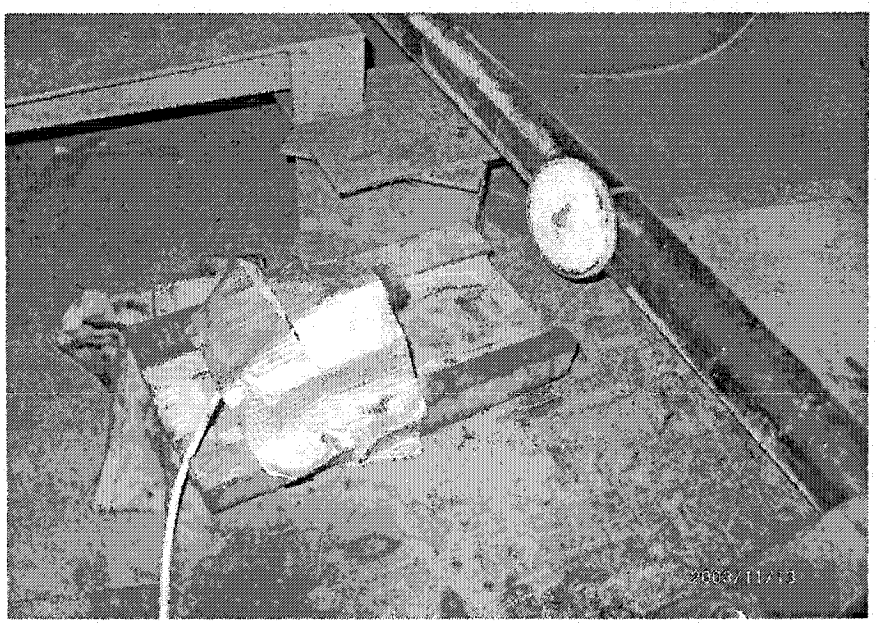

**Figure 5.12 Laser Beam Generator and Reflection Mirror**

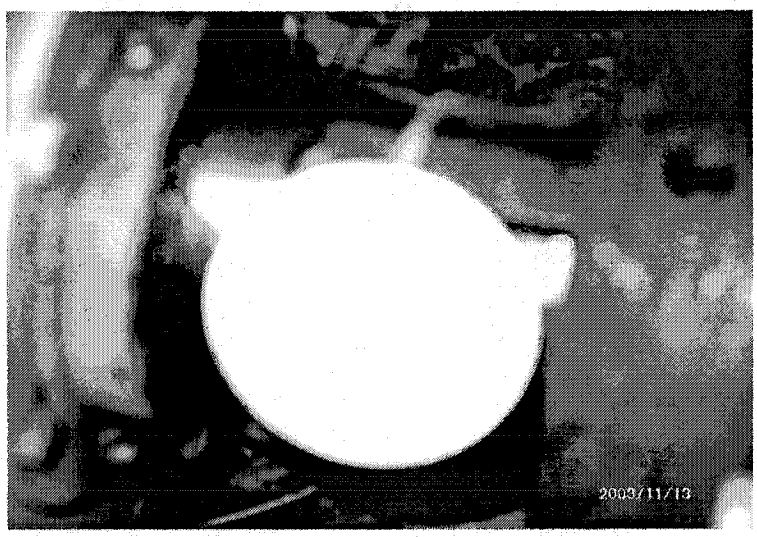


**Figure 5.13 Reflection Mirror Installed in the Speed Reducer**

During the testing, it was found that, if the laser beam generator is too close to the reflection mirror, the equipment records the wrong revolution value and stops the machine. As the drill pipe curvature changes in different tests, fixed laser beam generator and reflection mirrors were found to be not suitable. They needed adjustment every time a new curvature was set.

Another operating difficulty encountered was that, in the test operation, the vibration of the machine sometimes allowed the position or orientation of the reflection mirror to shift thus causing the two beam/mirror setups to record different revolution times and forcing the machine to stop with no other reason. To avoid this, the reflection mirror was checked and adjusted every day during a test run to make sure it was working properly.

**5.2.3.3 Sound Sensor.** An additional failsafe sensor was incorporated in the test setup. This was a sound sensor that would respond to any sound above a certain threshold and thus would respond to the sound of a pipe fracture or other noisy failure of the equipment.

**5.2.3.4 Daily Maintenance.** The facility was visited daily during test operation to see if shutdown had occurred either caused by drill rod failure or some other cause like a power failure or a loud noise. Sometimes, especially in the summer, overheating of the induction motor occurred and this also shut down the machine. If the pipe and pillow blocks were still intact, the machine was restarted. The current data and other relevant information observed were recorded in the test log so that the bulk of the test data would be retained even in the case of computer failure.

On a weekly basis, the pillow blocks and motor bearings were greased as lack of grease would overheat the machine and let it shut down or even break the motor. The software and test record were backed up regularly. As the test facility was in a harsh environment (unheated and non air-conditioned building), the computer operation was troublesome. In the early testing, the hard drive of the computer failed causing a significant delay in reinstalling and configuring the test setup.

**5.2.3.5 Oil Brake.** Since the induction motor was fixed in position and orientation, each time a new curvature was set, the oil brake had to be moved to the required position and anchored in position (Fig.5.14). It had been intended to run tests at different torque levels using the oil brake, but the induction motor was not capable of rotating the drill rod against a torque without overheating and it was decided to concentrate the current testing on bending fatigue only. With a more powerful motor, variable torque could be included in future research.

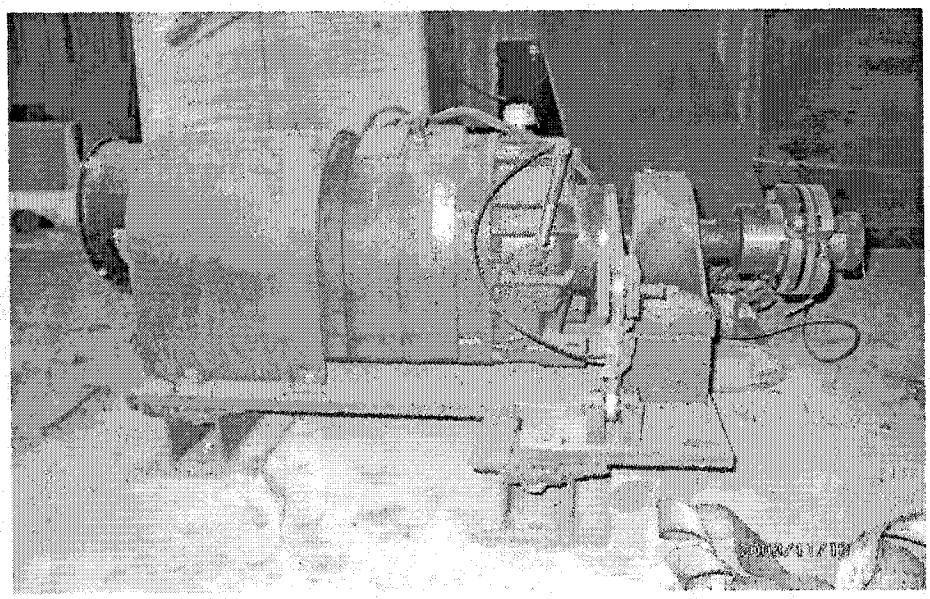

**Figure 5.14 Oil Brake**

# CHAPTER 6

## FATIGUE TEST RESULTS FOR MINI-HDD DRILL RODS

Twelve fatigue tests were conducted on the drill pipes donated by Drilltube, Inc and Texas Pup, Inc. All the tests were conducted a specially setup area in a storage building of the Trenchless Technology Center at Louisiana Tech University. The pipes donated by Texas Pup were used as the preliminary tests because of the numbers and kinds of pipes that exist for the test: there were only 6 external flush joint pipes and 9 elevated shoulder pipes which were not enough to conduct tests to create an S-N curve for this type. These kinds of pipe were assigned as Test Series 1. The pipes donated by Drilltube, Inc. are all elevated shoulder pipes and are used to conduct tests to create an S-N curve for this type of drill pipe. This test was assigned as Test Series 2. Although directly comparable test series were not run for both types of pipe, the two kinds of pipes did show a difference in fatigue life behavior

## 6.1 Fatigue Test Results

### 6.1.1 Pipe Donated by Texas Pup

In the first group of five tests, the pipe donated by Texas Pup, Inc was used. The test results are summarized in Table 3.1. All the tests are under pure bending, and no torque resistance was added.

**Table 6.1 Test Results for Texas Pup Drill Pipe**

| No | OD (in) | ID (in) | Nominal Curve (ft) | Bending Stress (Psi) | Fatigue life (revolutions) | Failure Location | Note |
|---|---|---|---|---|---|---|---|
| 1 | 1.908 | 1.435 | 74.8 | 29,279 | 663 | joint | Improper make up torque |
| 2 | 1.676 | 1.119 | 106.8 | 18,962 | 86,125 | joint | Lack of lubrication |
| 3 | 1.676 | 1.119 | 66.9 | 30,268 | 361,577 | body | N/A |
| 4 | 1.676 | 1.119 | 61.9 | 32,713 | 157,069 | body | N/A |
| 5 | 1.908 | 1.435 | 100 | 23,055 | 411,781 | body | N/A |

### 6.1.2 Pipe Donated by Drilltube

In the second group of seven tests, the pipe donated by Drilltube, Inc. was used. The test results are summarized in Table 3.2. All tests are under pure bending, and no torque resistance was added.

**Table 6.2 Test Results for Drilltube Drill Pipes**

| No. | OD (in) | ID (in) | Nominal Curve (ft) | Bending stress (Psi) | Fatigue life (Revolutions) | Failure location | Note |
|---|---|---|---|---|---|---|---|
| 1 | 1.90 | 1.42 | 104.6 | 21,955 | 2,277,031 | Not broken | N/A |
| 2 | 1.90 | 1.42 | 55.7 | 41,218 | 255,214 | Joint | N/A |
| 3 | 1.90 | 1.42 | 73.8* | 31,092 | 9,140 | Joint | Poor curve |
| 4 | 1.90 | 1.42 | 91.4 | 25,119 | 1,425,460 | Joint | N/A |
| 5 | 1.90 | 1.42 | 91.4 | 25,119 | 1,341,415 | Body | N/A |
| 6 | 1.90 | 1.42 | 39.5 | 58,116 | 70,138 | Joint | N/A |
| 7 | 1.90 | 1.42 | 55.7 | 41,218 | 383,846 | Joint | N/A |

* Due to a mistake after curve make up, one hole at the platform was not marked correctly, which created uneven extremely sharp curvature at some part of the curved pipes.

## 6.2 Analysis of Results

### 6.2.1 Preliminary Tests

Five tests were conducted as preliminary tests using the pipe donated by Texas Pup, Inc.

In the first test, the failure occurred very quickly in the joint area and at only 663 revolutions. This failure was most likely caused by an improperly low make up torque on

the connection. In normal practice, the connections are made up with a torque of about 60% of their capacity. Because the lack of the right equipment in the setup period, only a make up torque of about 250 ft-lb was applied – representing approximately the torque a small person could apply using a 3-ft long pipe wrench.

In the second test, a steel pipe was used to extend the 3-ft long pipe wrench to an effective 9-ft handle. With this extended handle, 750 ft-lb of torque could be applied to the pipe connections. With the right make-up torque and a lesser curvature, the life of the drill pipe extended to 86,125 revolutions, but the location of failure was still in the joint area. Joint lubrication during the joint make up was not used in this case, providing a test of another potential field condition for drill pipe usage.

In the third, fourth, and subsequent tests, proper make-up torque and lubrication were applied to the test pipes. In the third and fourth tests, the failure occurred in the pipe body with a considerably longer life compared to the first two tests despite a tighter test radius of curvature.

In the fifth test, a different kind of drill pipe from Texas Pup, Inc. was used. In this case, the failure occurred in the joint area despite the use of the proper make-up torque and lubrication.

For the drill pipes donated by Texas Pup, it seems that, if the drill pipe is properly used (make-up torque and lubrication), the failure is more likely to occur in the body of the drill pipe than in the joint area. This conclusion is quite different from the failure results reported by the mini-HDD industry. In the field, most fatigue failures are reported to occur in the joint area. This may result from improper handling, but it may also reflect less than

ideal curvature and stress conditions in the boring and reaming operation that are not reflected in the theoretical analysis.

### 6.2.2 S-N Curve Development Tests

Seven tests were conducted in this series. All were conducted with the drill pipe donated by Drilltube, Inc. Overall, six failures were recorded, and five of these failures occurred in the joint area. One failure occurred in the body of the drill rod sections. The first test in the series was conducted with a radius of 104.6 ft and was terminated after 2,277,031 revolutions without failure.

The results for the Drilltube drill pipe are consistent with the result reported from field work that most failures occur in the joint area. This indicates that the joint for the Drilltube pipe is the weakest area in the pipe. Although there may be potential for improved performance by a redesign of the joint, the number of revolutions to failure for the failure in the joint is quite close to that for failure in the body for the same radius of curvature. This indicates a balanced design of body resistance to fatigue versus joint resistance to fatigue.

Of the seven tests conducted, six results produced consistent results when plotted on an S-N curve (see Figure 6.1). However, one result was not consistent with other results. The test conducted with a nominal curve of 73.8 ft, showed an unusually low fatigue life with failure occurring at only 9,140 revolutions. After carefully checking the experimental setup, it appears that this result was due to an error in the experimental setup resulting in the last support point for the curve being marked wrongly and causing an unusually sharp curvature in the last pipe of the three drill pipes configuration. This result is recorded in the results table for completeness but was discarded from the regression analysis.

From the six test results considered valid, a non-linear regression analysis was performed using the commercial SAS software package. The results are quite consistent having an R-Square value of 0.9808 and an adjusted R-Square value of 0.9760. The results and the S-N curve are plotted in Figure 6.1.

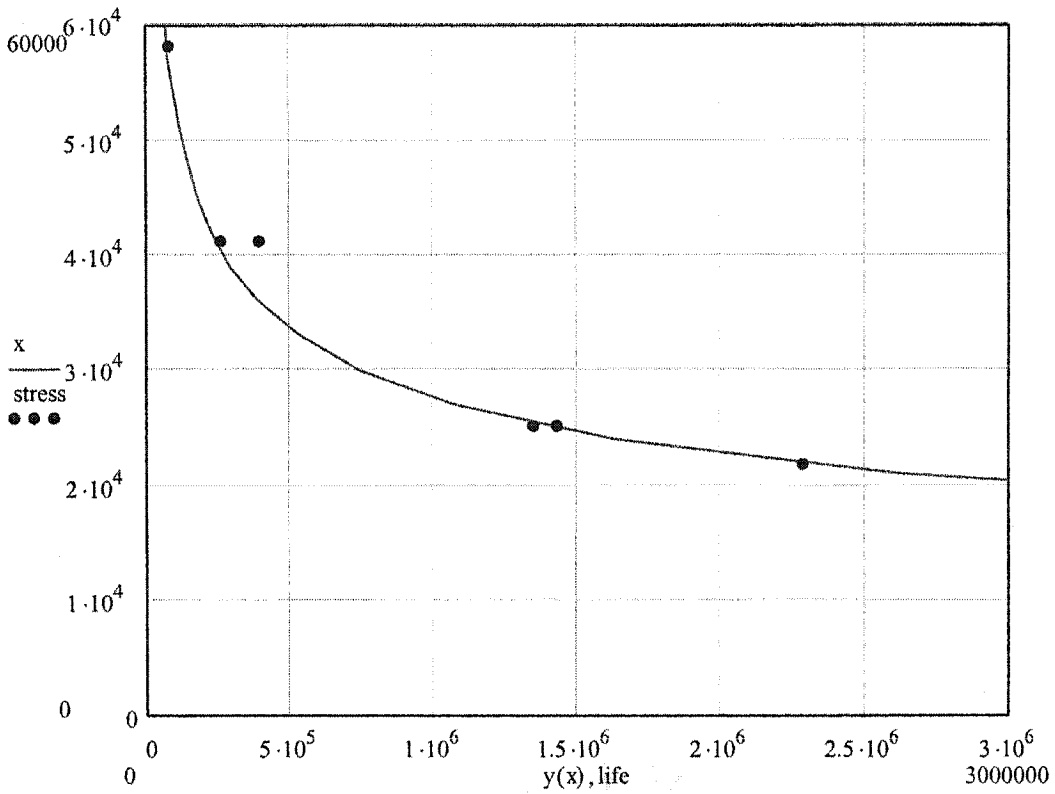


**Figure 6.1 S-N Curve Regression for the Drilltube Drill Pipes Using SAS**

The data in Table 2 and the regression curve indicate that the fatigue limit of the drill pipe from Drilltube, Inc. is about 22,000 psi.

### 6.2.3 Comparison of the Test Result with the Fatigue Formula Used in the Oil Industry

Research on drill tube fatigue in the oil industry (Grondin 1991) has produced a predictive curve for fatigue failure:

$$\log N = 14.8 - 3.46 \log S_r - 1.65 \times 10^{-5} (S_m)^2 \qquad (6.1)$$

where $S_r$ is the stress range in MPa

$S_m$ is the mean stress in MPa

N is the number of revolutions to fatigue failure

If this formula is used to predict the failure for the drill pipes used in the current research on HDD drill pipes, we can find the following results:

For the drill pipe donated by Texas PUP, using a stress of 23055 psi

Sr=23055*2=46110 psi (318 Mpa) Sm=0

logN=6.1416

N=1,385,486

The expected result is far bigger than the test result (Table 6.3), which is only 411,781. But for the drill pipe donated by Drilltube, Inc., the result is a little smaller than the test result.

From the test result (Table 6.3), it is clear that the equation gotten by the oil industry may be used in the mini-HDD industry, but has a some difference which may need correction.

**Table 6.3 Comparison of Test Data and Predicted Results by Grondin**

| No | OD (in) | ID (in) | Nominal Curve (ft) | Bending stress (Psi) | Fatigue life (Revolutions) | Expected Fatigue life by Grondin's Equation | Pipe Manufacture Company |
|---|---|---|---|---|---|---|---|
| **1** | 1.90 | 1.42 | 104.6 | 21,955 | 2,277,031 | 1,642,308 | Drilltube |
| **2** | 1.90 | 1.42 | 55.7 | 41,218 | 255,214 | 185,763 | Drilltube |
| **3** | 1.90 | 1.42 | 91.4 | 25,119 | 1,425,460 | 1,030,747 | Drilltube |
| **4** | 1.90 | 1.42 | 91.4 | 25,119 | 1,341,415 | 1,030,747 | Drilltube |
| **5** | 1.90 | 1.42 | 39.5 | 58,116 | 70,138 | 56,584 | Drilltube |
| **6** | 1.90 | 1.42 | 55.7 | 41,218 | 383,846 | 185,763 | Drilltube |
| **7** | 1.68 | 1.12 | 66.9 | 30,268 | 361,577 | 540,700 | Texas Pup |
| **8** | 1.68 | 1.12 | 61.9 | 32,713 | 157,069 | 413,264 | Texas Pup |
| **9** | 1.90 | 1.44 | 100.0 | 23,055 | 411,781 | 1,385,486 | Texas Pup |

### 6.2.4 Comparison of the Regression for the Current Tests with Grondin's Result

Using the SAS software package, the regression result for the test series 2 data is:

$$\text{Log } N = 22.783 - 3.54 \log Sr \qquad (6.2)$$

where Sr is stress range in psi

This can be compared with the 1992 formula from Grondin which can be simplified for the case of bending (with a mean stress of zero) as

$$\text{LogN}=22.28-3.46\text{logSr} \qquad (6.3)$$

where Sr is stress range in psi

The comparison of the two formulas is shown in Figure 6.2 using Mathcad.

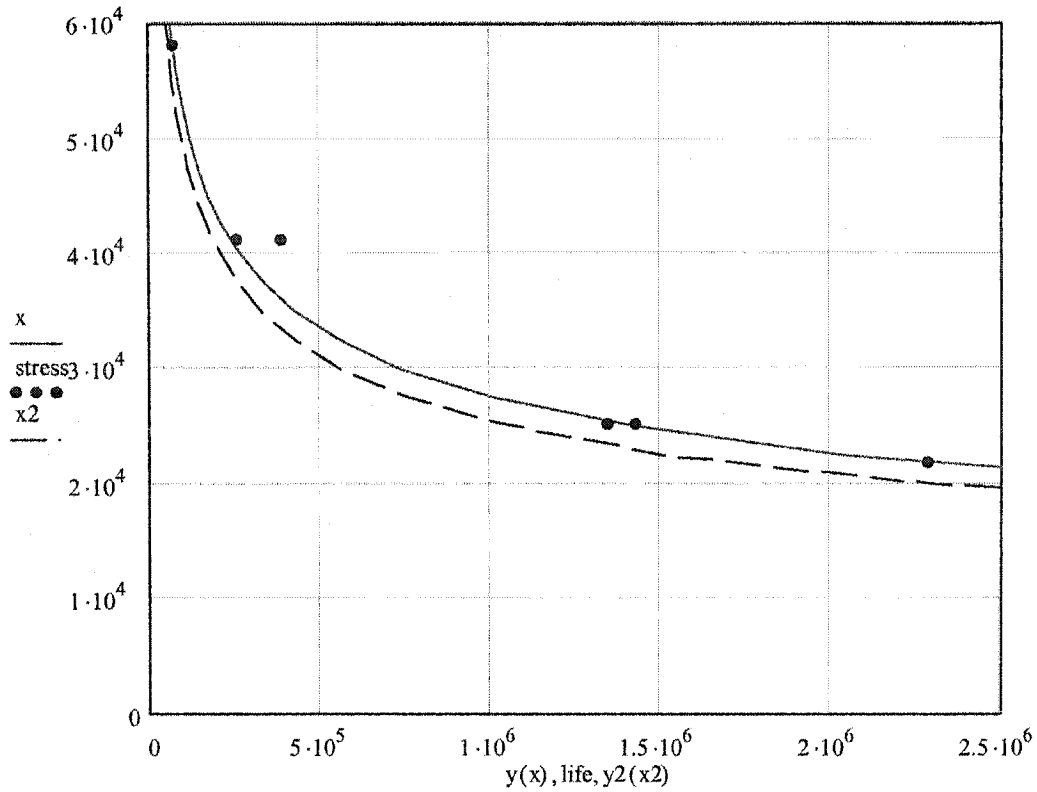


**Figure 6.2 Comparison of Grondin's Oil Industry Regression Equation and the Mini-HDD Regression Equation from the Current Research**

The dashed line is the S-N curve from the results of Grondin's research. The solid line is the S-N curve from the results of the tests at the TTC.

The comparison shows that the two lines are very close, the solid line is above the dashed line, meaning the test results at the TTC show a higher fatigue performance than Grondin's test result.

The fatigue results can also be compared with the Atlas of Fatigue curves (Boyer, 1986) as shown in Figure 6.3.

The Atlas of Fatigue indicates that an un-notched steel specimen should have a fatigue limit of stress amplitude between 53,000 psi and 70,000 psi and that a notched specimen should have a fatigue limit of stress amplitude between 26,000 psi and 50,000 psi. The data from the current research of stress amplitude (slightly below 22,000 psi) indicate a fatigue limit slightly lower than the notched data in the fatigue atlas.

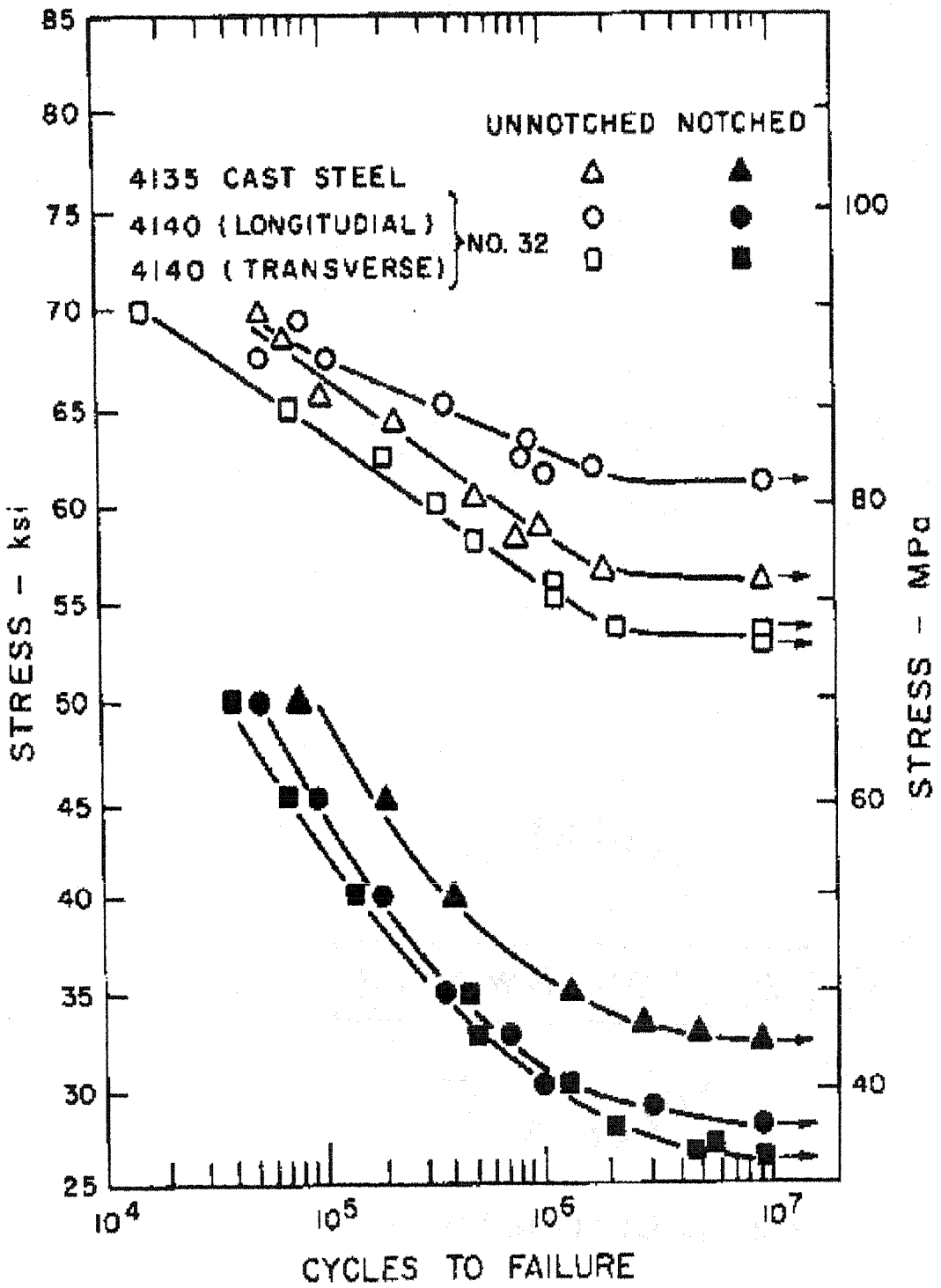


**Figure 6.3 Fatigue Life of Steel 4135 and 4140 from the Fatigue Atlas (Boyer, 1986)**

### 6.2.5 Radius of Curvature versus Fatigue Life of Drill Rod

Using the regression curve from the Series 2 test results and calculating the theoretical maximum bending stress at different radii of curvature produces a relationship between Radius of Curvature and Fatigue Life as shown in Table 6.4. In calculating the bending stresses caused by curvature in this table, the standard practice of using a bending stress based on a constant curvatures and constant moment is used (see discussion in Chapter 3).

**Table 6.4 Relationship between Radius of Curvature and Fatigue Life**

| Fatigue Life (Number of Revolutions) | Maximum Stress (psi) | Curve (feet) |
|---|---|---|
| 1,906,650 | 22,958 | 100 |
| 1,313,075 | 25,509 | 90 |
| 865,385 | 28,698 | 80 |
| 539,409 | 32,798 | 70 |
| 312,555 | 38,264 | 60 |
| 163,917 | 45,917 | 50 |
| 74,398 | 57,396 | 40 |

Table 6.4 shows the clear relationship between the nominal radius of curvature of the drill pipe and its fatigue life.

### 6.2.6 Relationship of Curvature and Fatigue Life Including Field Conditions

As discussed in Chapter 3, the normal relationship between curvature and maximum bending stress follows the relationship

where $\sigma = 0.5\frac{E \times D}{R}$ (6.4)

| | |
|---|---|
| $\sigma$ | peak tensile (or compression) stress developed in pipe (psi) |
| E | modulus of elasticity (psi) |
| R | radius of curvature of bends (in) |
| D | pipe outside diameter (in) |

It is also demonstrated in Chapter 3 that, at various stages of the boring process, this formula may not provide a good estimate of the actual maximum stress in the drill rod. In the other circumstances discussed in Chapter 3, the following conditions can be construed:

During thrust and deviation by a slanted drill head:

$$\sigma = 0.75\frac{ED}{R} \quad (6.5)$$

In another situation with a triangular lateral loading as an approximation:

$$\sigma = \frac{MD}{2I} = \frac{\frac{20EI}{11R}\frac{D}{2}}{I} = 0.91\frac{ED}{R} \quad (6.6)$$

That means the maximum stress should be higher than expected; if the worst situation is used (0.91 ED/R), the data in Table 6.4 would be altered to that shown in Table 6.5.

**Table 6.5 Relationship between Radius of Curvature and Fatigue Life under the Worst Stress Assumptions**

| Fatigue Life (Revolution) | Max stress (psi) | Curve (feet) |
|---|---|---|
| 229,697 | 41,742 | 100 |
| 158,188 | 46,380 | 90 |
| 104,254 | 52,178 | 80 |
| 64,983 | 59,632 | 70 |
| 37,654 | 69,571 | 60 |
| 19,747 | 83,485 | 50 |
| 8,963 | 104,356 | 40 |

Table6.5 gives an indication of the reduction of fatigue life caused by worst case assumptions about the actual curvature/stress conditions within the borehole. However, it does not account for the stress concentrations present in the drill rod and joint design, nor for the effect of combined stresses. Some of these issues are explored further in the next section.

### 6.2.7 Illustrative Estimate of Drill Pipe Cost per Foot Advance under Different Curvatures

The cost of drill pipe per feet advance can be computed from the following equation:

$$C = \frac{P \times \frac{L}{l}}{\frac{N}{S}} = \frac{P \times \frac{0.262R}{l}}{\frac{N}{S}} \qquad (6.7)$$

where C the cost of drill pipe per feet advance (USD per foot advance)

P the price of one piece of drill rod (USD)

L the average curve length (ft), which equal to 0.262R

R the curve radius (ft)

l the length of one piece of drill pipe (ft)

N revolutions to failure at the specified curvature (from equation 6.2)

S revolution per foot advance

The cost analysis in Table 6.6 is the result of the following assumptions:

1. A typical rate of rotation in soil is 2 revolutions per foot
2. The average curve length is based on deviating 15° at the curvature specified (this leads to a curve length of 0.262 R).
3. The price for each drill rod is US$820.

Then we can compute the cost per foot under different curves. For example, under curve with radius of 100 ft, the regression curve gives N=1,906,651. The cost of drill pipe per foot advance is

$$C = \frac{P \times \frac{0.262R}{l}}{\frac{N}{S}} = \frac{820 \times \frac{100 \times 0.262}{10}}{\frac{1906651}{2}} = 0.00225USD$$

**Table 6.6 Cost Drill Pipe Cost per Foot Advance under Different Curvature**

| Curve (ft) | Cost of drill pipe per foot advance during curved drilling only (under assumed usage conditions) |
|---|---|
| 100 | Less than 0.23 cent / foot advance (no failure after 1,906,651 rev) |
| 90 | 0.29 cent / foot |
| 80 | 0.40 cent / foot |
| 70 | 2.47 cent / foot |
| 60 | 3.66 cent / foot |
| 50 | 5.81 cent / foot |
| 40 | $1.02 / foot |

Table 6.6 provides an estimated cost of drilling per foot while actually drilling around a curve of a specified radius and deviating the direction of the drill path by 15 degrees. This cost applies only to the curved portion of the drilling and can be factored to an overall cost of fatigue in HDD practice depending on the proportion of curved drilling within an overall drill path.

From Table 6.6, it is clear that a sharp curve will greatly increase the cost of drill pipe replacement as a function of the total cost of the drilling operations. So, keeping a gentle curve is important in the cost control of mini-HDD practice.

### 6.2.8 Other Issues Affecting Fatigue Life

One additional fatigue life issue will be the effect of combined stresses on the fatigue life of the drill rod. This includes the influence of mean stress (the axial stress during the pull/push process) and the torque applied to the drill pipe.

From the data from the research by Abdus (1995), in mini-HDD practice, a pull back force of 17,000 lb and a thrust of 10,000 lb may be considered average with a normal torque being about 600 lb-ft. Using equation 3.7 and equation 3.9 presented in Chapter 3, this will create a mean stress and torque during pullback of

$$\sigma = \frac{F}{\frac{\pi}{4}(D^2 - d^2)} = \frac{17000}{3.14\frac{1.9^2 - 1.4^2}{4}} = 13124 psi$$

$$\tau = \frac{TD}{\pi(D^4 - d^4)} = \frac{600*1.9*12}{3.14*(1.9^4 - 1.4^4)} = 474 psi$$

Since the shear stress is small, the main effect is the axial stress, which is about 60% of the bending stress of +/- 21,955 psi (43910 psi range) in a 100-ft curve. In the oil

industry , because of the large depths drilled and the weight of the drill pipe, the mean stress is typically a very important issue to consider.

# CHAPTER 7

# SIZE EFFECT AND COMPARISON OF THE FATIGUE LIFE OF DIFFERENT PIPES

## 7.1 The Fatigue Formula Provided by Grondin

As introduced in Section 6.2.5, Grondin's formula for the effect of stress range and mean stress in air is

$$\log N = 14.8 - 3.46 \log S_r - 1.65 \times 10^{-5} (S_m)^2 \qquad (7.1)$$

where $S_m$ is the mean stress in MPa

$S_r$ is the stress range in MPa

This formula was developed by testing at the University of Alberta of the directional drilling pipe used in the oil industry. The dimensions of the pipe tested were 114 mm outside diameter, and the steel used was 4135 alloy steel.

After comparing the test result of mini-HDD drilling pipe at Louisiana Tech University with the formula obtained by Grondin for the oil industry, it seems that this formula also predicts the fatigue life in mini-HDD drill pipes reasonably well and generates a conservative result.

As there are differences in the predictions based on the two regression curves, it needs to be considered whether there are factors that account for the differences in behavior and whether there is a unique formula to measure the fatigue life of all mini-HDD drilling pipes.

In the discussion below, the effect of the following factors is examined in terms of their influence on the fatigue results.

1. size effect
2. steel grade used to create the pipe
3. manufacturing method and design.

## 7.2 Consideration of Size Effect

In tests on similarly shaped specimens, the observed reduction in fatigue strength with increasing size is commonly ascribed to three main sources: the geometrical size effect, the technological size effect, and the statistical size effect (Haagensen 1990).

### 7.2.1 Geometrical Size Effect

This effect is also referred to as an effect of stress gradient. The geometrical size effect is related to the stress gradient at the notch root and to the degree of geometric scaling. The stress gradient influences crack initiation as well as the crack growth stage. In geometrically similar parts with similar micro structural and defect features, the stress gradient is steeper in the smaller part, and a surface grain experiences a lower average strain than a grain at the surface of a thick part at the same surface stress (Fig. 7.1). That means that the small specimen has a longer fatigue life irrespective of whether the major part of the life is spent in initiating a crack or consists of growth of a pre-existing crack like a defect.

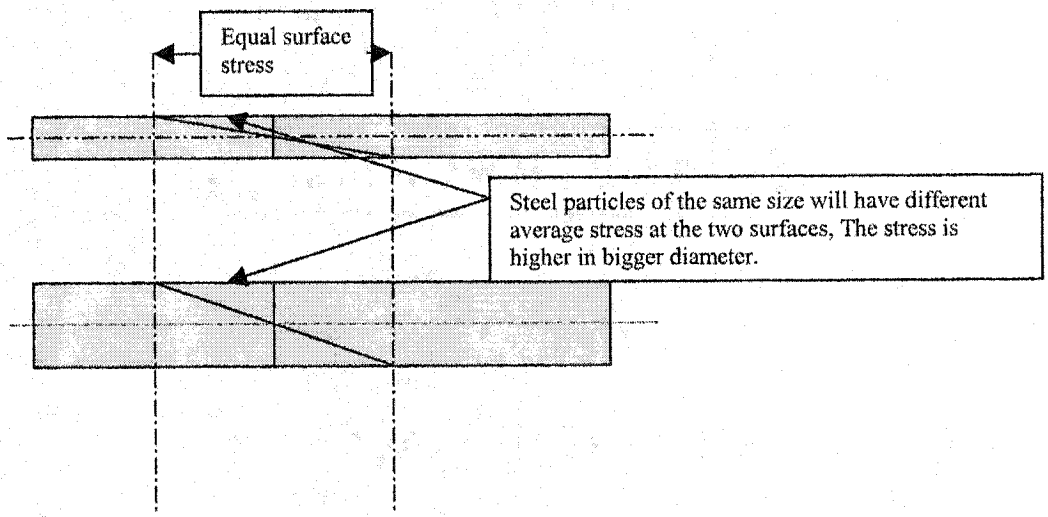


**Figure 7.1 Stress Gradients versus Diameter for Bending**

However, in the book *Fundamentals of Machine Component Design* (Juvinall,1991), it is reported that "experiments show that if the diameter increased to much more than 0.4 inch, most of the beneficial gradient effect is lost."

Hence, this effect has a big influence only on small specimens, and this should not result in a big difference between the HDD drill pipe in mini-HDD practice or in the oil industry. The typical size contrast between the drill pipe used in each industry is for a diameter from 50 mm in mini-HDD practice to 110 mm in oil field practice. Hence, this effect will not be considered further.

### 7.2.2 Statistical Size Effect

The statistical size effect is associated with the higher probability of occurrence of a large defect in an increased volume of material, resulting in lower strength for the larger part.

Kuguel (1961) developed a statistical theory of strength, giving the following relationship between stressed volume and failure stress:

$$S / S_0 = \left( \frac{V}{V_0} \right)^{-a} \tag{7.2}$$

where S and $S_0$ are the fatigue strengths at 100 million cycles.

V and $V_0$ are the volumes of surface material stressed to more than 95% of the maximum stress.

a = 0.034 is recommended for use in design of notched and unnotched parts in the Society of Automotive Engineering's guide for fatigue design. (Graham, 1968)

Applying this method to check its application for HDD pipes (Fig 7.2),

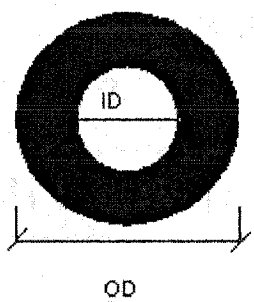


**Figure 7.2 Cross-section of Drill Pipe**

Assume the stress has a linear distribution along the diameter.

The 95% maximum stress will occur at 95% of the OD. From this assumption, the area V is calculated as

$$V = \frac{\pi}{4} * D^2 * (1 - 0.95^2) * L$$
$$V = 0.121 * D^2 * L \tag{7.3}$$

If it is assumed that all the pipes are the same length, then

$$S/S_0 = \left(\frac{V}{V_0}\right)^{-a} = \left(\frac{OD}{OD_0}\right)^{-2a} \tag{7.4}$$

Comparing the size effect of mini-HDD drill pipe with a diameter of 48.26 mm (1.9 in) which was tested at Louisiana Tech University and the oil industry pipe with a diameter of 110 mm (4.33 in) which was tested at Alberta University:

$$S/S_0 = \left(\frac{OD}{OD_0}\right)^{-2a} = \left(\frac{110}{48.33}\right)^{-0.068} = 0.9456$$

It appears that the statistical size effect would make about a 5% difference in the expected fatigue life. This result can partly explain the difference between these two tests.

### 7.2.3 Technological Size Effect

The technological size effect arises from variations in material properties caused by different processing parameters. The microstructure in a thick plate in general is characterized by large grains and unfavorably shaped inclusions, while the more heavily deformed thinner plate contains finer grains and smaller inclusions, resulting in better strength properties of the latter. Other factors related to the fabrication of the actual component such as surface quality and residual stresses may contribute significantly to the observed size effect.

Simply speaking, specimens cut from large billets are known to have lower strength than specimens from the same material rolled or forged to thinner sections. This size effect cannot be predicted by any available formula.

Thus, the main conclusion in terms of the size effect is that the smaller the pipe diameter, the higher should be the fatigue limit. Hence, this effect explains why the oil drill pipe, which is bigger than mini-HDD drill pipe, has a lower fatigue limit.

## 7.3 Consideration of Steel Grade

The steel grade used in the pipe has a strong influence on the fatigue life of the drill pipe, so the fatigue properties of various types of steel will be examined below.

If it is assumed that there are two drill pipes with identical geometry and manufacturing method, which are made of two different steels, then any difference of fatigue life between them is the result of the fatigue property of the two types of steel used in the pipes.

In this regard, the fatigue life of steel has been related to its tensile strength. Tensile strength can be estimated from a non-destructive hardness test. In mini-HDD drilling, the fatigue occurs principally as the result of bending stress caused by drill rod curvature and rotation. This means that the high strain is in a small, localized area of the cross-section. This should mean that the harder the steel, the better the fatigue performance.

In *Fundamentals of Machine Design*, an equation is provided to evaluate the fatigue endurance limit of steel. On page 262, it is pointed out that the tensile strength in psi is about 500 times the Brinell hardness.

For bending fatigue, the author of that book further points out that the basic endurance limit of steel is equal to 0.5 times the tensile strength:

$$S_n' = 0.5 S_u \tag{7.5}$$

Fatigue endurance limit can be estimated by the following equation

$$S_n = C_L C_G C_s S_n' \tag{7.6}$$

where $C_L$ is load factor, for bending, it is 1

$C_G$ is gradient factor, for diameter bigger than 0.4 mm but smaller than 2 in, it is 0.9

$C_S$ is the surface factor, for machined surface with HB is 520, it is 0.5; with HB is 467, it is about 0.56.

For ANSI 4130 steel, the endurance limit can be computed by the following:

$$S_n = 236 \times 0.5 \times 0.9 \times 0.56 = 59.47 ksi$$

This result, 59.47 ksi, is still far bigger than the test result in the TTC tests, which is only 22 ksi. The difference may be due to the stress concentration factor. That factor should be about 2.5 to 3. Table 7.1 shows the hardness and other mechanical properties for different types of steel.

**Table 7.1 Hardness and Other Mechanical Properties for Different Types of Steel**

| ANSI No. | Tempering Temperature F | Tensile Strength ksi | Yield Strength ksi | Elongation % | Reduction In area | Hardness HB |
|---|---|---|---|---|---|---|
| 4130 | 400 | 236 | 212 | 10 | 41 | 467 |
| 4150 | 400 | 280 | 250 | 10 | 39 | 530 |
| 4340 | 400 | 272 | 243 | 10 | 38 | 520 |

The test pipes in Grondin's paper are made of 4135 alloy steel; the test pipes in the TTC tests are made of steel 4130. They do not have a big difference in mechanical properties, so steel type is not a big influence in the difference between their fatigue lives.

## 7.4 Consideration of the Drill Rod Manufacturing Method

Although there is little difference in the hardness among the basic steel grades, the same steel can have different a hardness and fatigue life following different heat treatment methods. Thus, it is impossible to decide the steel fatigue property by just knowing the steel grade. Table 7.2, for example, shows that steel with ANSI grade 4130 can have very different mechanical properties under different tempering temperatures:

**Table 7.2 Mechanical Properties of ANSI Grade 4130 Steel with Varying Tempering Temperature**

| ANSI No. | Tempering Temperature F | Tensile Strength ksi | Yield Strength ksi | Elongation % | Reduction In area % | Hardness HB |
|---|---|---|---|---|---|---|
| 4130 | 400 | 236 | 212 | 10 | 41 | 467 |
| | 600 | 217 | 200 | 11 | 43 | 435 |
| | 800 | 186 | 173 | 13 | 49 | 380 |
| | 1000 | 150 | 132 | 17 | 57 | 315 |
| | 1200 | 118 | 102 | 22 | 64 | 245 |

Source: J.R. Davis (1996) (Ed.). ASTM Specialty Handbook: Carbon and Alloy Steels p21.

Further, in a normalized or annealed condition, the same steel also has different mechanical properties as shown in Table 7.3:

**Table 7.3 Mechanical Properties of ANSI Grade 4130 Steel with Varying Heat Treatment**

| ANSI No. | Treatment | Tensile Strength ksi | Yield Strength ksi | Elongation % | Reduction In Area % | Hardness HB |
|---|---|---|---|---|---|---|
| 4130 | Normalized | 97.1 | 63.3 | 25.5 | 59.5 | 197 |
| | Annealed | 81.3 | 52.3 | 28.2 | 55.6 | 156 |

The test pipes in Grondin's paper are made of 4135 alloy steel; one kind of the test pipes in the TTC tests is made of 4130 steel. It is clear that the temper method and stress concentration have an influence on the fatigue life.

# CHAPTER 8

# PIPE JOINTS AND NUMERICAL ANALYSIS

## 8.1 The Failure of Pipe Joints

Most fatigue failure of mini-HDD drill pipe used in practice is reported to occur in the joint area. In the fatigue tests in the TTC laboratory at Louisiana Tech University, more than half of the test pipes broke in the joint area.

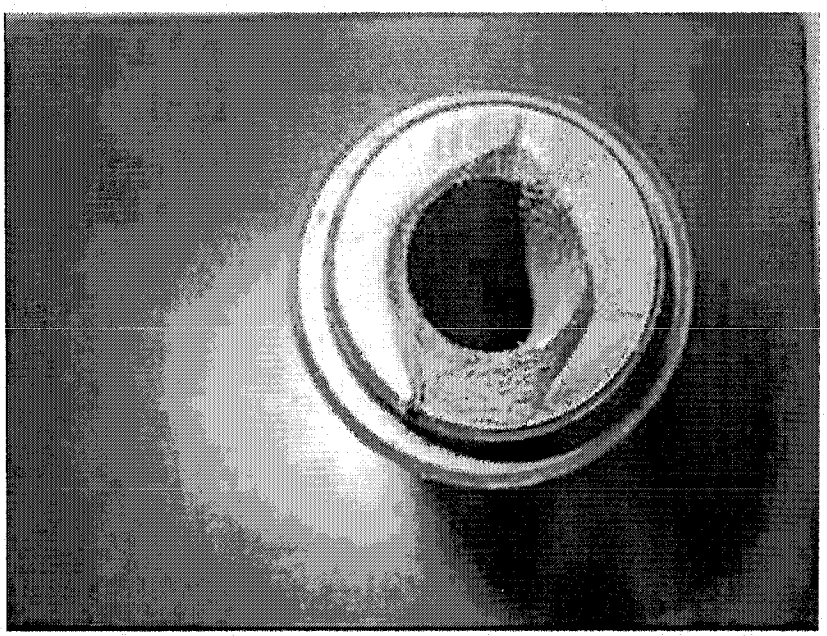

**Figure 8.1 Broken Joint Caused by Fatigue Failure Tested in the TTC Lab**

When failure occurred in the joint in the TTC tests, the failure location was always in the pin close to the last engaged thread (Fig.8.1). To investigate the stress concentration in

the joint, numerical analysis was used to simulate the stress distribution in the joint area under a bending load.

## 8.2 ANSYS Software and Contact Mechanics Analysis

ANSYS is a general purpose finite element modeling package for numerically solving a wide variety of mechanical problems. These problems include static/dynamic structural analysis (both linear and non-linear), heat transfer and fluid problems, as well as acoustic and electromagnetic problems(Table 8.1).

The stress analysis of a mini-HDD drill pipe joint includes a significant contact mechanics problem. The ANSYS software provides a strong ability to model such contacts. ANSYS supports three contact models: node-to-node, node-to-surface, and surface-to-surface. Each type of model uses a different set of ANSYS contact elements and is appropriate for specific types of problems.

### 8.2.1 Basic Contact Analysis Approach

To model the contact problem, first the parts to be analyzed for their possible interaction should be identified. If one of the interactions is at a point, the corresponding component of this model is a node. If one of the interactions is at a surface, the corresponding component of this model is an element: either a beam, shell, or solid element. The finite element model recognizes possible contact pairs by the presence of specific contact elements. These contact elements are overlaid on the parts of the model that are being analyzed for interaction.

**Table 8.1 ANSYS Contact Capabilities (Point to Surface and Surface to Surface)**

| | Point-to-Surface | | | | Surface-to-Surface | |
|---|---|---|---|---|---|---|
| | CONTAC 26 | CONTAC 48 | CONTAC 49 | CONTAC 175 | CONTAC 171,172 TARGET 169 | CONTAC 173,174 TARGET 170 |
| Point-to-Surface | Y | Y | Y | Y | | |
| 2-D | | Y | Y | Y | Y | Y |
| 3-D | | | Y | Y | | Y |
| Sliding | Large | Large | Large | Large | Large | Large |
| Augmented Lagrange Multiplier | | Y | Y | Y | Y | Y |
| Contact Stiffness | user- defined | user- defined | user- defined | semi-automatic | semi-automatic | semi-automatic |
| Auto-Meshing Tools | None | GCGEN | GCGEN | ESURF | ESURF | ESURF |
| Lower-Order | Y | Y | Y | Y | Y | Y |
| Higher- Order | Y | | | Y (2-D only) | Y | Y |
| Rigid-Flexible | Y | Y | Y | Y | Y | Y |
| Flexible-Flexible | | Y | Y | Y | Y | Y |
| Thermal Contact | | Y | Y | | Y | Y |
| Electric Contact | | | | | Y | Y |

### 8.2.2 Contact Algorithm

For surface-to-surface contact elements, ANSYS uses either the augmented Lagrangian method (default) or the penalty method.

The augmented Lagrangian method is an iterative series of penalty updates to find the exact Lagrange multipliers (i.e., contact tractions). Compared to the penalty method, the augmented Lagrangian method usually leads to better conditioning and is less sensitive to the magnitude of the contact stiffness coefficient. However, in some analyses, the augmented Lagrangian method may require additional iterations, especially if the deformed mesh becomes too distorted.

The default augmented Lagrangian method was used for this research.

## 8.3 Stress Concentration Factor for Push and Pull Conditions

### 8.3.1 Computation Model for Push and Pull Conditions

The Computation Model is based on the pipe donated by Drilltube Inc (Fig.8.2).

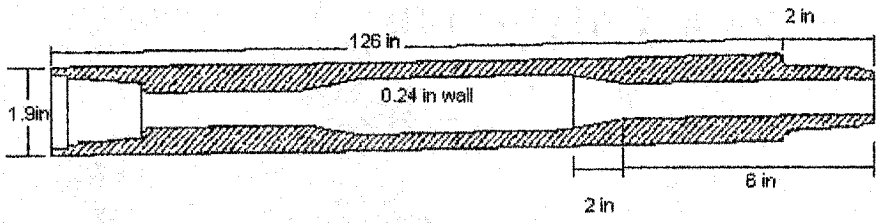


**Figure 8.2 Drill Pipe**

The computation mdel of the drill pipe joint is built using the actual size of the drill pipe (Fig 8.3)

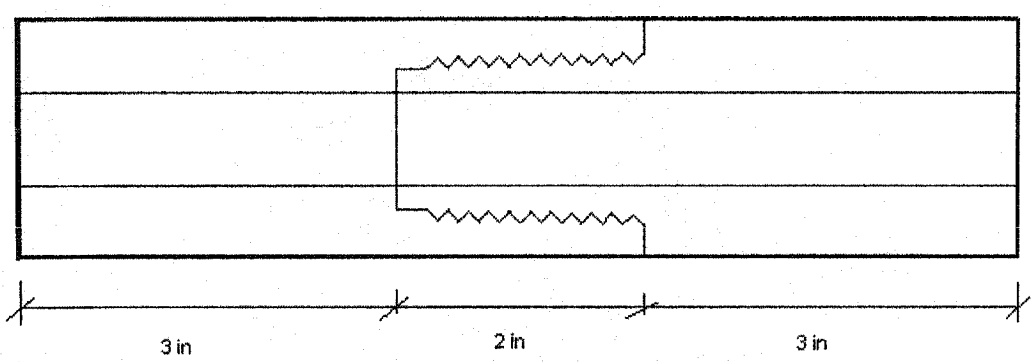


**Figure 8.3 Computation Model of the Pipe Joint**

Since pull and push conditions are axi-symmetric, the computational model can be simplified into a two-dimensional model (Fig.8.4).

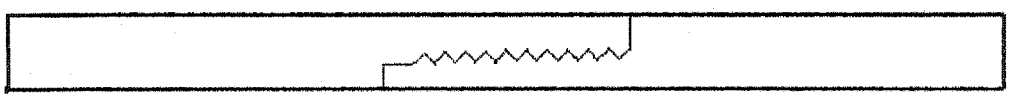

**Figure 8.4 Computational Model of the Drill Pipe Joint for Pull and Push**

The push computational model (Fig 8.5)

100lb/in is applied at one end; the other end is modeled as a fixed support.

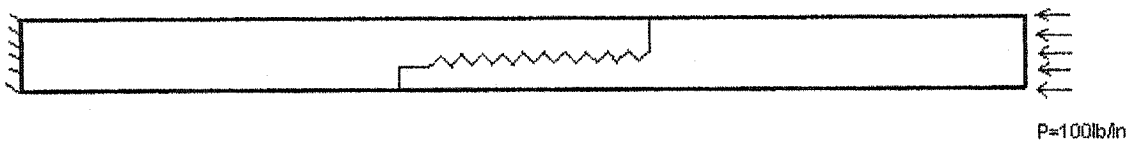


**Figure 8.5 Computational Model for Thrust under a Pressure of 100lb/in**

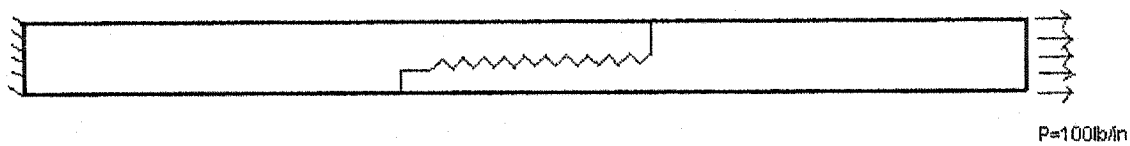


**Figure 8.6 Computational Model for Pull under a Pressure of 100lb/in**

The Finite Elements used in this model were the PLANE42 element, the CONTAC171 element, and the TARGE169 element.

### 8.3.2 Elements Used for Mesh of 2-D Model

PLANE42 is used for the mesh of 2-D modeling of solid structures. The element can be used either as a plane element (plane stress or plane strain) or as an axi-symmetric element. The element is defined by four nodes having two degrees of freedom at each node: translations in the nodal x and y directions. The element has plasticity, creep, swelling, stress stiffening, large deflection, and large strain capabilities.

CONTAC171 is used to represent contact and sliding between 2-D "target" surfaces and a deformable surface, defined by this element. This element has two degrees of freedom at each node: translations in the nodal x and y directions. This element is located on the surfaces of 2-D solid, shell, or beam elements without midside nodes. It has the same geometric characteristics as the solid, shell, or beam element face with which it is connected. Contact occurs when the element surface penetrates one of the

target segment elements on a specified target surface. Coulomb and shear stress friction is allowed.

TARGE169 is used to represent various 2-D "target" surfaces for the associated contact elements. The contact elements themselves overlay the solid elements describing the boundary of a deformable body and are potentially in contact with the target surface, defined by TARGE169. This target surface is discretized by a set of target segment elements (TARGE169) and is paired with its associated contact surface via a shared real constant set. You can impose any translational or rotational displacement, temperature, and voltage on the target segment element. You can also impose forces and moments on target elements.

The assignment of contact elements and target elements to the model follows the guidelines as discussed below:

1. If a convex surface is expected to come into contact with a flat or concave surface, the flat/concave surface should be the target surface.
2. If one surface has a fine surface mesh and, in comparison, the other has a coarse mesh, the fine mesh should be the contact surface and the coarse mesh should be the target surface.
3. If one surface is stiffer than the other, the softer surface should be the contact surface, and the stiffer surface should be the target surface.
4. If higher--order elements underlay one of the external surfaces and lower-order elements underlay the other surface, the surface with the underlying higher-order elements should be the contact surface and the other surface should be the target.

5. If one surface is markedly larger than the other surface, such as in the instance where one surface surrounds the other surface, the larger surface should be the target surface.

From the above guidelines, the pin of the joint was assigned with contact elements and the box of the joint was assigned with target elements.

Friction Coefficient:

From standard references, the static coefficient of friction for steel on steel is 0.74, but under lubrication, it can drop to only 0.06. Here, a friction coefficient of 0.06 is used since the joint is lubricated.

### 8.3.3 Analysis Result for 2-D Model

The analysis result of ANSYS 7.0 for thrust under 100 lb/in pressure is shown in Figure 8.7. The analysis result of ANSYS 7.0 for push under 100 lb/in pressure is shown in Figure 8.8.

Stress Concentration Factor

From the analysis results, the stress concentration factor can be computed as:

Stress Concentration Factor under pull stress is 3.0.

Stress Concentration Factor under push stress is 1.68.

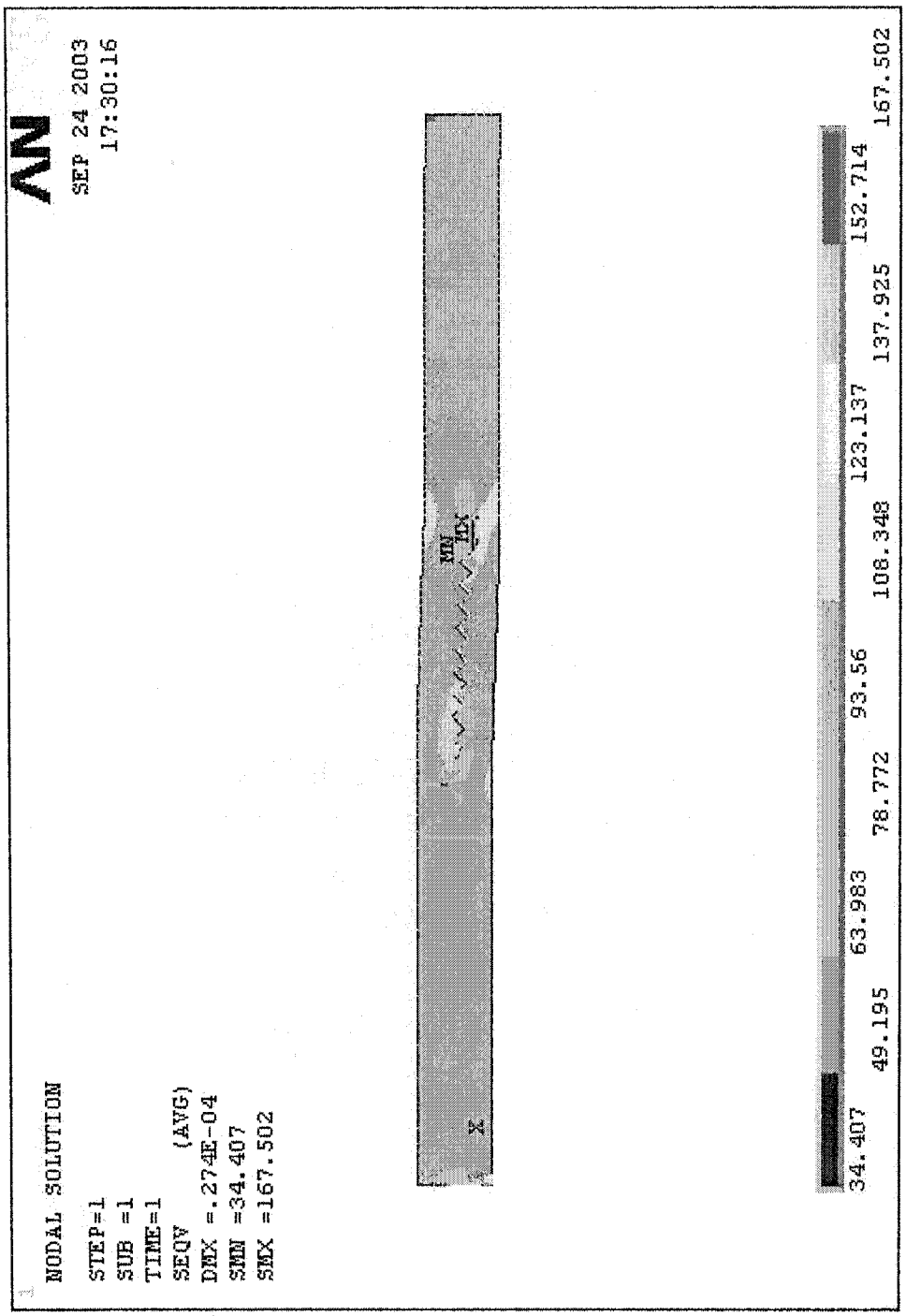


**Figure 8.7 ANSYS Analysis Result of Push under Stress of 100 lb/in**

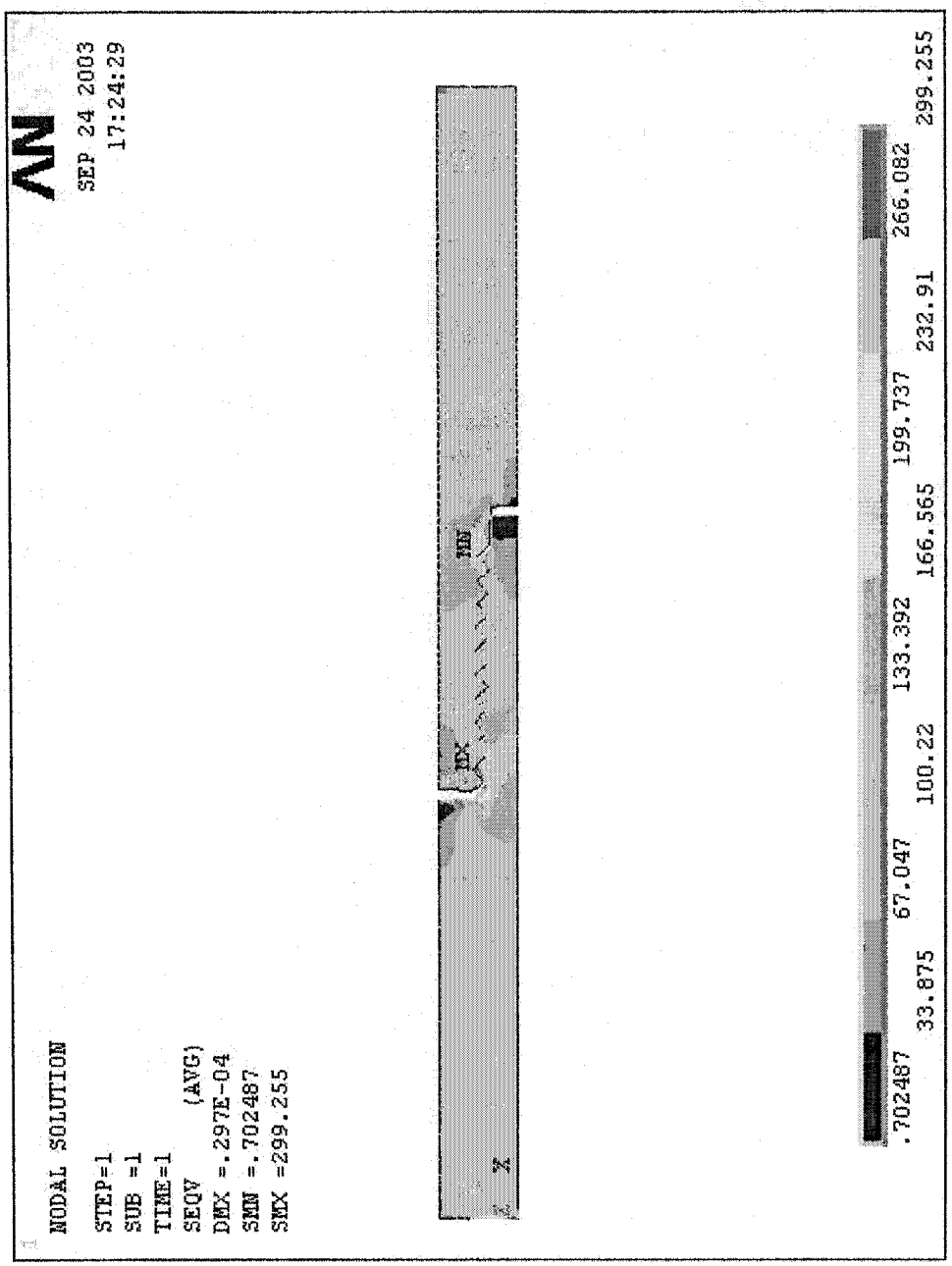


**Figure 8.8 ANSYS Analysis Result of Pull under Stress of 100 lb/in**

## 8.4 Stress Concentration Factor for Bending Conditions

### 8.4.1 Computational Model for Bending

For the bending load condition, the stresses vary across the pipe diameter. As a result, a three-dimensional finite element model, consisting of a one hundred and eighty degree segment of the pipe cross-section, is needed for a complete simulation.

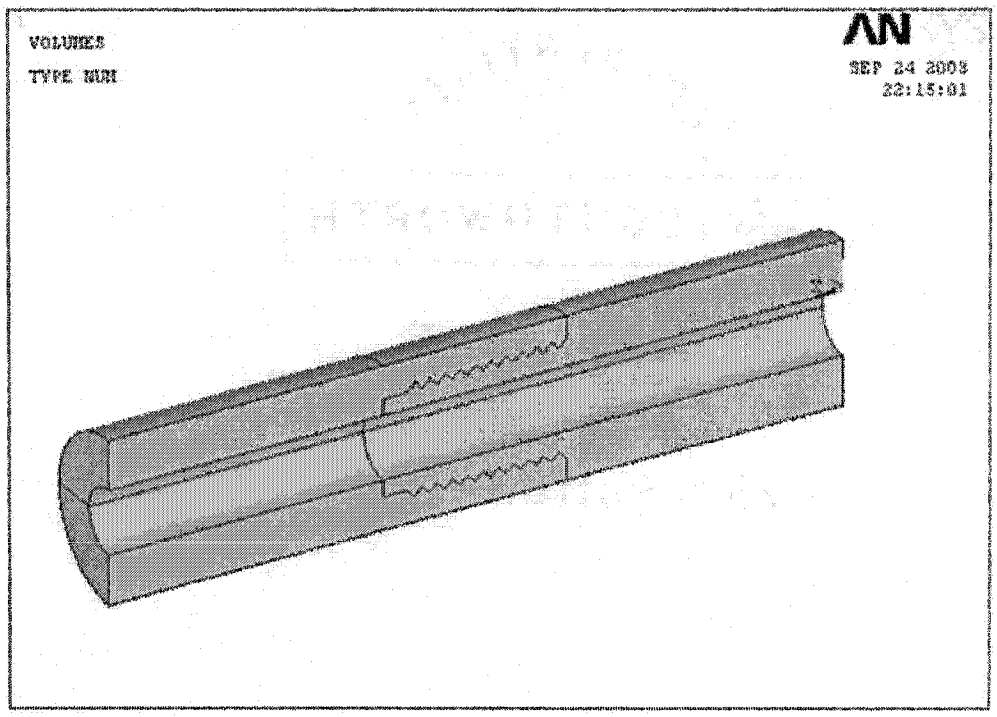


**Figure 8.9 Full Three-Dimensional Model for Drill Pipe Joint**

However, the complex geometry leads to a meshed model that exceeds the 32,000 nodes permitted in the ANSYS 7.0 (University Version) currently in use at Louisiana Tech University. Because of this limitation, a simplified model was used for the bending analysis.

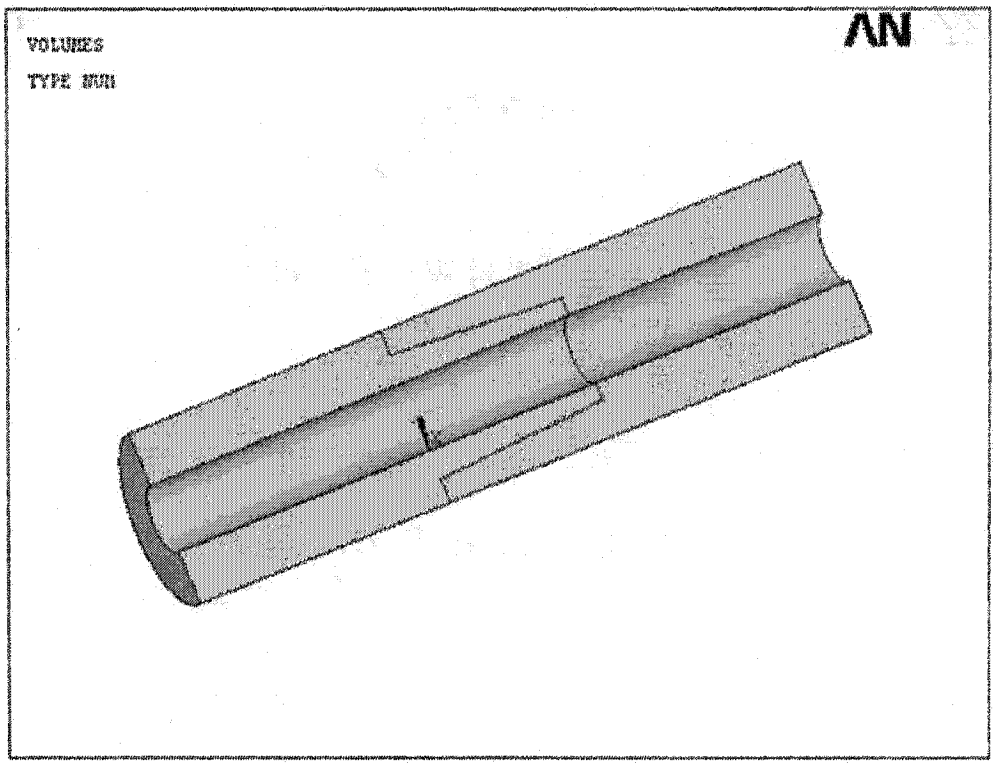


**Figure 8.10 Simplified Computational Model for Drill Pipe Joint**

The bending moment and fixed end conditions were applied as boundary conditions to this simplified model. A 190 lb-in moment was added to one side of the joint. This moment is applied as a pair of loads applied at the corner points.

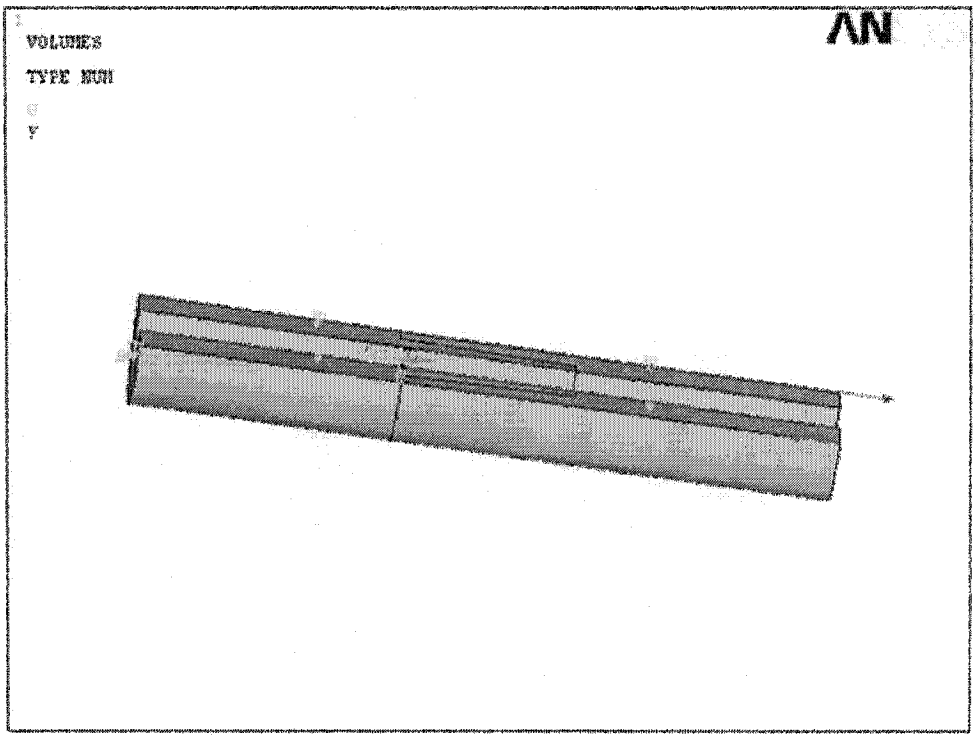


**Figure 8.11 Boundary Condition of the Simplified Model**

## 8.4.2 Elements Used for Mesh of 3-D Model

The finite elements used in this model were as follows:

SOLID186 is a higher-order 3-D 20-node structural solid element. SOLID186 has quadratic displacement behavior and is well suited to modeling irregular meshes (such as those produced by various CAD/CAM systems).

The element is defined by 20 nodes having three degrees of freedom per node: translations in the nodal x, y, and z directions. SOLID186 may have any spatial orientation. The element supports plasticity, hyperelasticity, creep, stress stiffening, large deflection, and large strain capabilities. It also has mixed formulation capability for

simulating deformations of nearly incompressible elastoplastic materials, and fully incompressible hyperelastic materials.

CONTAC174 is used to represent contact and sliding between 3-D "target" surfaces and a deformable surface, defined by this element. The element is applicable to three-dimensional structural and coupled thermal-structural contact analysis. This element is located on the surfaces of 3-D solid or shell elements with midside nodes. So, since the SOLID186 element is used here, CONTAC174 should be used as a compatible element. It has the same geometric characteristics as the solid or shell element face with which it is connected. Contact occurs when the element surface penetrates one of the target segment elements on a specified target surface. Coulomb and shear stress friction is allowed.

TARGE170 is used to represent various 3-D "target" surfaces for the associated contact elements. The contact elements themselves overlay the solid elements describing the boundary of a deformable body and are potentially in contact with the target surface, defined by TARGE170. This target surface is discretized by a set of target segment elements (TARGE170) and is paired with its associated contact surface via a shared real constant set.

As for the 2d model, the pin of the joint is assigned as contact elements and the box of the joint is assigned as target elements.

Friction Coefficient:

In order to simulate the teeth in the joint, a high friction coefficient (0.8) was assigned to the original part with teeth. For those areas without teeth, the friction coefficient was still assigned as 0.06.

### 8.4.3. Analysis Result for 3-D Model

As shown in Figure 8.9, the simulation results show that the highest stress concentration area is similar to the stress concentration area for thrust or tension, i.e., near the last engaged thread in the pin.

Stress Concentration Factor:

If the same bending moment used in the simulation is used to calculate the maximum stress in the pipe wall without a joint, the maximum stress will have the following value:

$$\sigma = \frac{My}{I} = \frac{190 * 0.95}{\frac{1}{64} * \pi * d^4} = 4517 lb/in^2$$

From the simulation, the pipe with the joint has a maximum stress of 13,540 lb/in$^2$

Thus, the stress concentration factor is:

$$SCF = \frac{13540}{4517} = 3$$

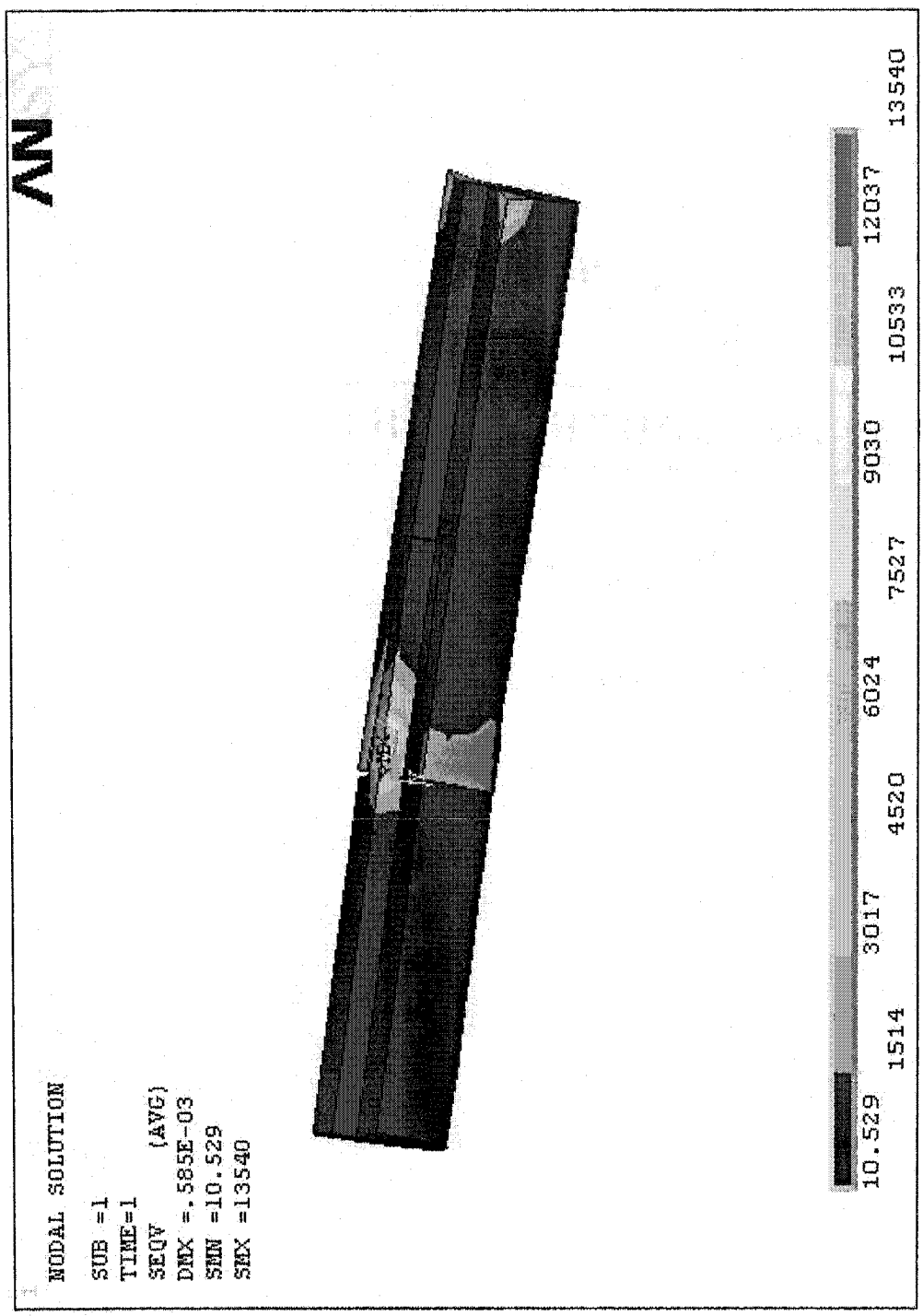


**Figure 8.12 ANSYS Analysis Result of Bending Stress Simulation**

## 8.5 Comparison of Simulation Results with Test Results

Table 8.2 shows a summary of the simulation results in terms of the stress concentration factor and stress concentration location for the simulations of bending stress, tensile stress, and compressive stress in the drill rod.

**Table 8.2 Simulation Results for Stress Concentration**

| Applied Stress Type | Stress Concentration Factor | Stress Concentration Place | Note |
|---|---|---|---|
| Bending | 3 | Last engaged thread of the pin | Simplified 3-D model |
| Thrust | 3 | Last engaged thread of the pin | 2-D model |
| Tension | 1.68 | The first engage thread of the pin | 2-D model |

The 3-dimensional simulation model used in bending is simplified, and it is expected that this may reduce the stress concentration factor, i.e. the real Stress Concentration Factor may be bigger than 3.0 in bending.

Examining the test results for comparison shows that 5 of the 6 test results involved failure at the pipe joint. The area of failure was at the pin of the last engaged thread. This is consistent with the simulation results for bending stress across a pipe joint.

One of the six test results involved failure at the pipe body. Despite the stress concentration, this can occur because of uneven curvature conditions along a drill pipe or specific conditions that accelerate fatigue failure, such as the following:

1. The joint is thicker than the pipe body, so it is stiffer in this section. This will cause the thickened section to have a lower localized curvature and the adjacent drill rod body to assume a higher curvature.

2. Defects in the surface finish, resulting from manufacture or prior use may reduce the fatigue endurance limit anywhere from 10% to 90%. The body area is bigger than the joint area, providing a greater probability of a surface fault which may influence the fatigue life heavily.
3. The drill steel may have localized defects within the body of the drill rod causing fatigue failure to occur at those locations.
4. The joint may be heat treated differently and be harder than the pipe body. Thus, the fatigue limit of the joint may higher than the pipe body because the same steel under different heat treatments can have a large difference in fatigue life.

## 8.6 Comparison of Test Results with Guidance Provided in the Atlas of Fatigue Curves

The graphs in Figures 6.3 show the S-N curves from the Atlas of Fatigue Curves (1985).

The fatigue limits range from 55 ksi (4135 cast steel) to 65 ksi (4140) for the steel types 4135 and 4140 which were normalized and tempered for one million cycles, which is very close to the steel of the drill pipe tested in TTC. The pipes donated by Drilltube, Inc. have a fatigue limit of about 25 ksi when using the nominal stress conditions in the drill pipe. The difference in fatigue limits may come from the stress concentrations of the joint in the test data. A fatigue concentration factor of over 3.0 will provide an interpreted fatigue limit of the steel of the pipe of around 75 ksi. This lies above the fatigue limit range of 55 ksi to 65 ksi, representing a reasonable fatigue life range for alloy steel. This may due to the heat treatment issue; normally the joint will be heat treated to a higher tensile strength and lower flexibility and thus has a higher fatigue limit than expected.

# CHAPTER 9

# SUMMARY AND CONCLUSIONS

## 9.1 Summary

The objective of this thesis was to understand the fatigue life of mini-horizontal directional drilling (HDD) pipes. To achieve this goal, a laboratory experimental program was planned to test the fatigue life of one kind of mini-HDD pipes.

In order to analyze the fatigue life of mini-HDD rod, a fatigue test machine was built in the laboratory of the Trenchless Technology Center. Twelve fatigue tests were conducted in this laboratory on the drill pipes donated by Drilltube, Inc. and Texas Pup, Inc. The pipes donated by Texas Pup were used as the preliminary tests to gain experience in the testing methodology. The pipes donated by Drilltube, Inc. were used to construct an S-N curve for this type of drill pipe. Those two kinds of pipes did show a difference in fatigue life behavior.

During the five preliminary tests, the strong effect of make up torque and joint lubrication was observed. In the later seven tests, six failures occurred. Five of these failures occurred at the joint area, and one failure occurred in the body area. This is consistent with the reports of field failure: the joint area is the weakest area in the whole pipe. From the test results of the second series of seven tests, an S-N curve for that type of pipe was developed. The fatigue limit for this pipe (based on a simple bending stress

approximation) is less than 22 ksi. Since the Atlas of Fatigue Curves indicates a value in the range of 55 ksi to 65 ksi for similar steels, mini-HDD rill rod fails at considerably less than the normally accepted values. The reason for this was assumed to be due to stress concentration in the joint area.

Since the stress in the joint area is very complex, numerical analysis was used to simulate the stress concentration. An ANSYS model was constructed and run for bending, tension, and thrust conditions.

After applying the stress concentration factor observed within the joint area (approximately 3.0), the fatigue limit did fall within the expected range.

In addition to the experimental and simulation results, the research investigated the theoretical stress condition in different phases of the drilling process compared to the normal stress assumptions used in practice. The S-N curve results were also used to provide an indication of the cost of drill rod fatigue according to the radius of curvature using some illustrative assumptions about curved drilling and drill rod usage.

## 9.2 Conclusions

From the tests carried out at the Trenchless Technology Center, the following conclusions are drawn:

1. The fatigue failure of mini-HDD drill pipe can occur either at the joint or at the body of mini-HDD drill pipes. For the drill pipe donated by Drilltube, Inc, 5 out of 6 failures occurred at the joint.
2. The fatigue failure prediction equation developed for the oil industry by Grondin at University of Alberta provides a conservative prediction if used to predict the fatigue life for the mini-HDD drill pipes donated by Drilltube, Inc.

3. The stress concentration factor at the drill joint has an important influence on the fatigue failure of mini-HDD drill pipes. The FEA analyses show that the stress concentration factor for bending in the drill joint is about 3.0.
4. Bending fatigue is the key factor in deciding the fatigue life of mini-HDD drill pipes.

## 9.3 Recommendations

In studying the fatigue life of mini-HDD drill pipes, the following recommendations are made for future study in this area.

1. More test data is critical in determining the fatigue life of mini-HDD drill pipes. In this test, all the data used to build the regression equation came from only one manufacturer of drill pipe. The fatigue behavior of other makes of drill rod and the effects of different joint designs need to be understood.
2. All the tests were conducted on one size and a single grade of mini-HDD drill pipe. Although the size of drill pipe is not believed to have a significant influence on the fatigue resistance, the grade of steel could be a significant factor. Therefore, different grades of drill pipe should be investigated.
3. The computation of the stress concentration factor for bending was carried out using a simplified model because of the limit of the version of the Finite Element Analysis software used. A more precise analysis should be done on this topic. The comparison of different joint designs is also an interesting future research topic.
4. The heat treatment method and the manufacturing method used in making mini-HDD drill pipes may have an influence in the fatigue resistance ability of mini-HDD drill pipes; this should be analyzed in the future.

5. The interaction between cyclic bending and mean stress was not studied here because of the limit of the fatigue test machine. Although the interaction between cyclic bending, cyclic torsion, and cyclic axial tension was determined to be a less important factor in deciding the fatigue life of mini-HDD drill pipes, it still will have some influence. These issues should also be studied.
6. The misuse of mini-HDD drill pipes in the field has a great influence in determining the fatigue life of mini-HDD drill pipes. Also, the drill pipes tested in the test program were new drill pipes with their joints made up only once in the whole test process. However, in the field, the joints are connected and disconnected every time. Further study of these issues would be useful.

# APPENDIX

# SAS PROGRAM

**SAS Input Program for Regression**
**of Fatigue Test Results of Drill Pipe Donated by Drilltube, Inc.**

```
00001 // EXEC SAS
00002 //SAS.SYSIN DD *
00003 DATA YYY;
00004 INPUT STRESS REVOLUTION @@;
00005 X=LOG10(STRESS); Y=LOG10(REVOLUTION);
00006 LINES;
00007 21955 2277031
00008 41218 255214
00009 25119 1425460
00010 25119 1341415
00011 58112 70138
00012 41218 383846
00013 ;
00014 PROC REG;
00015 MODEL Y=X;
00016 PROC PLOT;
00017 PLOT Y*X / VREF=0 VPOS=19 HPOS=50;
```

# REFERENCES AND BIBLIOGRAPHY


Amro, Mohammed M. (2000). "Equations Predict Drill-pipe Fatigue" *Oil & Gas Journal*, July 10, 2000. pp 36-42.

Bachman, W.S. (1951). "Fatigue Testing and Development of Drill Pipe to Tool Joint Connections." *World Oil*, Vol. 132, No.1, pp 104-116

Beer, Ferdinand P, and E. Russell Johnston, Jr. (1992). *Mechanics of Materials*. 2nd ed. McGraw-Hill, Inc. New York.

Boresi, A.P., R. J. Schomidt, O.M.Sidebottom (1993). *Advanced Mechanics of Materials*, 5th Edition, John Wiley & Sons Company, New York.

Boyer, Howard E. (1986). *Atlas of Fatigue Curves*, American Society for Metals, Metals Park, Ohio 44073.

Callister, William D. Jr. (1994). *Materials Science and Engineering, An Introduction.* 3rd ed. John Wiley & Sons, Inc. New York.

Engineering, (1967) "Wohler's experiments on the Strength of Metals," *Engineering*, August 23, 1967, p 60.

Forrest, P G. (1962). *Fatigue of Metals*. Pergamon, Press Inc. New York.

Gnyp, I. P., I. S. Babyuk, and B. O. Chernov (1990). "Optimizing the Service Life of Drill-Collar Joints on the Basis of Fracture Mechanics Criteria," *Soviet Materials Science*, Vol.26, No.6 706-710.

Graham, J.A. (1968) *Fatigue Design Handbook* Society of Automotive Engineering, Warrendale, PA.

Gregory Fehr and Edmond I. Bailey (1994). "Developing Standardized Connection Analysis Techniques For Slim Holm Core Rod Designs." *Drill Technology*, 1994; Presented at the Energy-Sources Technology Conference, New Orleans, Louisiana, January 23-26, 1994.

Grondin, G.Y. and G.L. Kulak (1991). "Fatigue of Drill Pipe" *Structural Engineering Report No.171*, Department of Civil Engineering The University of Alberta, Edmonton , Alberta.

Haagensen, P.J. (1990). "Size Effects in Fatigue of Non-Welded Components." *Proc. of the Ninth International Conference on Offshore Mechanics and Arctic Engineering*, Houston, Texas February 18-23, 1990. pp 689-699.

Hadala, Paul, Robert A. McKim and Aziz V. Saber (2001). *Evaluation of Drill Pipe in Mini-Horizontal Directional Drilling Construction: Development of a Fatigue Testing Machine and Analysis of Severely Bent Drill Rods* A Report on LEQSF Project No (1998-99)-RD-B-14, TTC Report, Louisiana Tech University.

Hill, T.H., P.V. Seshadri, and K.S. Durham (1991). "A Unified Approach to Drill Stem Failure Prevention," *Proc. Drilling Conference*, 11-14 March 1991, Amsterdam, The Netherlands.

Irwin, G.R., (1957). "Analysis of Stresses and Strains Near the End of a Crack Traversing a Plate" *Trans ASME, Journal of Applied Mechanics*, Vol 24, p 361.

Joosten, M.W., J. Shute, and R.A. Ferguson (1985). "New Study Shows How to Predict Accumulated Drill Pipe Fatigue". *World Oil*, Vol.201, No. 5, PP 65-70

Juvinall, Robert C. and Kurt M. Marshek (1991). *Fundamentals of Machine Component Design*. Second Edition, John Wiley & Sons Company, New York.

Kuguel, R (1961). "A Relation Between Theoretical Stress Concentration Factor and Fatigue Notch Factor Deduced from the Concept of Highly Stressed Volume," *Proc. ASTM*, Vol.61, 1961, pp732-748.

Lubinski, A. (1961). "Maximum Permissible Dog-Legs in Rotary Boreholes" *Journal of Petroleum Technology*, Vol. 13, No.2, pp. 175-194.

Malik, Omesh (1995). *Analysis of a Steel Pipe Joint with No Welds for Trenchless Construction*, M.S. Thesis, Louisiana Tech University, Ruston, LA.

Manson, S.S. (1962) "Discussion of Experimental Support for Generalized Equation Predicting Low Cycle Fatigue" *Trans ASME, Journal of Basic Engineering*, Vol.84, No.4, Dec 1962, p537

McKelvie, S.A., Cayton, C., and Tyhurst,C. (1992). "Design criteria for directional drilling projects" *Proceedings: North American No-Dig'92*, North American Society for Trenchless Technology, Chicago, IL.

Miner, M.A. (1945) "Cumulative Damage in Fatigue" *Transaction ASME, Journal of Applied Mechanics*, Vol 67, September 1945, p 159.

Moore, H.F. and Kommers, J.B (1927) *The Fatigue of Metals.* Scott, Greenwood and Son, London.

Neuber, H. (1946), *Theory of Notches,* Springer-Verlag, Berlin.

Paris, P.C. and Erdogan, F.(1963) "A Critical Analysis of Crack Propagation Law" *Trans ASME, Journal of Basic Engineering*, Vol.85, No.4, 1963, p528.

Peterson R.E.(1950), "Discussion of a Century Ago Concerning the Nature of Fatigue, and Review of Some of the Subsequent Research Concerning the Mechanics of Fatigue" *ASTM Bull.*, No. 164, Feb. p50

Reed-Hill, R. E, and Reza Abbaschian. (1994). *Physical Metallurgy Principles.* 3rd ed. PWS Publishing Company, Boston.

Severinchik, N.A.and B.V.Kopei, (1977) "Inhibitive Protection of Steel Drill Pipes From Corrosion Fatigue." *Soviet Materials Science*, Vol.13, n 3, May-Jun, pp 318-321

U.S. Army Corps of Engineers, Trenchless Technology Center and American Public Works Association. (1999). *Trenchless Technology Applications in Public Works.* American Public Works Association, Kansas City.

Wu, X.J. Akid, R. (1994) "Frequency effects on the fatigue crack initiation and propagation in an offshore steel" *Proceedings of the International Offshore and Polar Engineering Conference*, 10-15 April,1994, Osaka, Japan, Vol.4, pp 142-147

Yasushi Tsukano, Shunji Nishi, Hisamitus Miyoshi, Eizoh Takeuchi, and Yasuo Sogo (1990). "Optimum Design of Internal Upset Geometry of Drill Pipe for Longer Fatigue Life," *Nippon Steel Technical Report*, Nippon Steel Corp. Tokyo, Japan.

Zhou, Junshu (1998), *Dynamic analysis of mini-HDD drillstrings using finite element method*, M.S. thesis, Louisiana Tech University, Ruston, Louisiana